



National Technical University of Athens
School of Mechanical Engineering
Fluids Section
Parallel CFD & Optimization Unit

Heat Transfer Studies in Power Electronics using Triply Periodic Minimal Surfaces

Diploma Thesis

Katsarelos Athanasios

Advisor: Kyriakos C. Giannakoglou, Professor NTUA

Athens, 2025

Acknowledgements

First and foremost, I would like to express my sincere gratitude to my supervisor, Professor K. Giannakoglou, for giving me the opportunity to work on such an interesting topic. Throughout my studies at NTUA, his teaching and guidance have shaped a distinctive way of thinking, for which I am truly grateful.

Furthermore, I would like to thank all the staff of the Computational Fluid Dynamics and Optimization Unit, and in particular Dr. N. Galanos, for the time he devoted to guiding me, which greatly facilitated the writing of this thesis.

And last but not least, I would like to thank my friends and family for their continuous psychological support throughout the course of my studies.



National Technical University of Athens
School of Mechanical Engineering
Fluids Section
Parallel CFD & Optimization Unit

Heat Transfer Studies in Power Electronics using Triply Periodic Minimal Surfaces

Diploma Thesis

Katsarelos Athanasios

Advisor: Kyriakos C. Giannakoglou, Professor NTUA

Athens 2025

Abstract

The subject of this diploma thesis is a feasibility study of the use of Triply Periodic Minimal Surfaces (TPMS), to design heat sinks for power-electronics applications. All these geometries are examined and compared to traditional geometries promoting heat exchange through a series of parametric studies. The flow is considered turbulent, incompressible, and is solved using the conjugate heat transfer algorithm (chtMultiRegion-SimpleFoam solver), which is based on the finite volume approach.

Triply Periodic Minimal Surfaces (TPMS) are defined surfaces that repeat periodically in all directions and have zero mean curvature everywhere, dividing space into two continuous and interpenetrating regions.

The problem to be studied consists of a heat source at a constant temperature (assuming this to simulate power electronics) on its lower surface, with the geometry that enhances heat transfer to be placed above it, within the air flow.

The diploma thesis includes two main categories of parametric studies. The first parameters to be investigated are related to the construction of a TPMS or the thickness distribution over the mathematically defined mean surface. Then, the use of hybrid TPMS, which are interpolated from two TPMS linearly or gradually, is investigated.

The effectiveness of the tested devices promoting heat transfer is assessed primarily in terms of their ability to increase the average outlet temperature of the coolant, and also

in terms of whether it can be achieved without excessive total pressure losses. Through this analysis, the critical design parameters that lead to the development of a cooling geometry, which can be used as initialization in future optimizations, are identified. An optimization loop, which is beyond the scope of this diploma thesis, may refine them.



Εθνικό Μετσόβιο Πολυτεχνείο
Σχολή Μηχανολόγων Μηχανικών
Μονάδα Παράλληλης Υπολογιστικής Ρευστοδυναμικής &
Βελτιστοποίησης

Μελέτες Μεταφοράς Θερμότητας σε Ηλεκτροικά Ισχύος με χρήση Τριπλά Περιοδικών Ελάχιστων Επιφανειών

Διπλωματική Εργασία

Κατσαρέλος Αθανάσιος

Επιβλέπων: Κυριάκος Χ. Γιαννάκογλου, Καθηγητής ΕΜΠ

Αθήνα 2025

Περίληψη

Η διπλωματική εργασία αυτή εξετάζει τη μελέτη τριπλά περιοδικών ελάχιστων επιφανειών (ΤΠΕΕ), με σκοπό την δημιουργία ψηκτρών με εφαρμογή στα ηλεκτρονικά. Όλες οι γεωμετρίες εξετάστηκαν και συγκρίθηκαν με παραδοσιακές γεωμετρίες μέσω παραμετρικών μελετών. Η ροή θεωρείται τυρβώδης και ασυμπίεστη και επιλύεται με τη μέθοδο της συζευγμένης μεταφοράς θερμότητας (επιλύτης chtMultiRegionSimpleFoam), η οποία είναι βασισμένη στην τεχνική των πεπερασμένων όγκων.

Οι ΤΠΕΕ ορίζονται ως επιφάνειες που επαναλαμβάνονται περιοδικά προς όλες τις κατευνήσεις και έχουν μηδενική μέση καμπυλότητα, χωρίζοντας τον σε δύο συνεχείς περιοχές.

Ο σχεδιασμός του συστήματος μεταφοράς θερμότητας περιλαμβάνει τη θερμική πηγή η οποία έχει σταθερή θερμοκρασία στην κάτω επιφάνεια της (επέχει θέση συνιστώσας ηλεκτρονικών ισχύος) με την ψυκτική γεωμετρία που τοποθετείται στο πάνω μέρος της. Το εργαζόμενο μέσο είναι αέρας.

Η διπλωματική εργασία περιλαμβάνει δύο κύριες κατηγορίες παραμετρικών μελετών. Οι πρώτες παράμετροι που πρέπει να ερευνηθούν σχετίζονται με την κατασκευή του πραγματικού σώματος της ΤΠΕΕ ή τη μέθοδο με την οποία θα προσδοθεί πάχος στη γεωμετρία. Έπειτα διερευνάται η χρήση υβριδικών ΤΠΕΕ οι οποίες παρεμβάλλονται από δυο ΤΠΕΕ, είτε γραμμικά είτε σταδιακά.

Η αποτελεσματικότητα των ψυκτικών γεωμετριών ενίσχυσης της μεταφοράς θερμότητας αξιολογείται κυρίως ως προς την ικανότητά τους να αυξάνουν τη μέση θερμοκρασία εξόδου του ρέοντος ρευστού και, στη συνέχεια, ως προς το αν οι βελτιώσεις αυτές μπορούν να

επιτευχθούν χωρίς να προκαλέσουν πρόσθετες συνολικές απώλειες ολικής πίεσης στη ροή. Μέσω αυτής της ανάλυσης, εντοπίζονται οι κρίσιμες παράμετροι σχεδιασμού που οδηγούν στην ανάπτυξη μιας γεωμετρίας ενίσχυσης της μεταφοράς θερμότητας προς το εργαζόμενο μέσο, η οποία θα χρησιμοποιηθεί ως αρχικοποίηση για μελλοντικές βελτιστοποιήσεις.

Abbreviations

CFD Computational Fluid Dynamics.

CHT Conjugate Heat Transfer.

IWP I-graph Wrapped Package.

PCOpt/NTUA Parallel CFD Optimization Unit of the National Technical University of Athens.

RANS Reynolds-Averaged Navier–Stokes equations.

TPMS Triply Periodic Minimal Surfaces.

Contents

1	Introduction	8
1.1	The importance of cooling in Engineering	8
1.2	Triply Periodic Minimal Surfaces	10
1.3	The OpenFOAM software	12
1.4	Purpose of this thesis	13
2	Generation of geometries promoting heat exchange from TPMS	15
2.1	Design space boundaries	15
2.2	Cell unit surface equation	15
2.3	Extrusion methods	16
3	Design of the Heat Exchange System	20
3.1	Thermal Source	20
3.2	Cooling Channel	20
3.3	Geometries promoting heat exchange	20
3.3.1	Heat sink	21
3.3.2	TPMS-Shaped geometries promoting heat exchange	22
4	CHT modeling	23
4.1	Flow equations	23
4.2	Turbulence Model	24
4.3	Boundary conditions	24
4.4	Grid generation	25
4.5	Case and solver properties	26
4.6	Performance metrics	27
5	Results of conventional geometries	28
5.1	Conventional geometries promoting heat exchange	28
5.2	Geometries' efficiency	30
6	Parametric studies	33
6.1	Parametric Study 1: Periodicity pattern	33
6.1.1	Gyroid patterns	34
6.1.2	IWP patterns	35
6.1.3	Primitive patterns	36
6.1.4	Analysis of Results	38

6.2	Parametric Study 2: Thickness	39
6.2.1	Non-uniform thickness Gyroid	39
6.2.2	Non-constant thickness IWP	41
6.2.3	Non-constant thickness Primitive	41
6.2.4	Analysis of Results	43
6.3	Parametric Study 3: Solid network TPMS geometries	44
6.3.1	Solid Network Gyroid, IWP, Primitive	44
6.3.2	Solid network Gyroid Patterns	46
6.3.3	Solid Network IWP Patterns.	48
6.3.4	Solid Network Primitive Patterns	49
6.3.5	Analysis of Results	51
7	Hybrid TPMS	53
7.1	Theoretical background	53
7.1.1	Linear interpolation	53
7.1.2	Gradual interpolation	55
7.2	Hybrid Gyroid - IWP	56
7.3	Hybrid Primitive-Gyroid	56
7.4	Hybrid Primitive-IWP	57
7.5	Gradually transformed geometries	59
7.6	Analysis of Results	60
8	Conclusions	62

Chapter 1

Introduction

1.1 The importance of cooling in Engineering

Modern mechanical systems across various industries, such as automotive, aerospace, and electronics are becoming increasingly power-intensive [1], [2]. As a result, the need for effective thermal management has increased significantly. Since a large fraction of electrical power is converted into thermal power, the use of cooling mechanisms (in general, devices enhancing heat transfer) becomes essential. Excess heat raises the temperature, which can cause materials to expand, leading to deformations and mechanical failures. Incorporating a cooling mechanism into a system not only protects it from possible malfunctions but also increases its efficiency and performance [3].

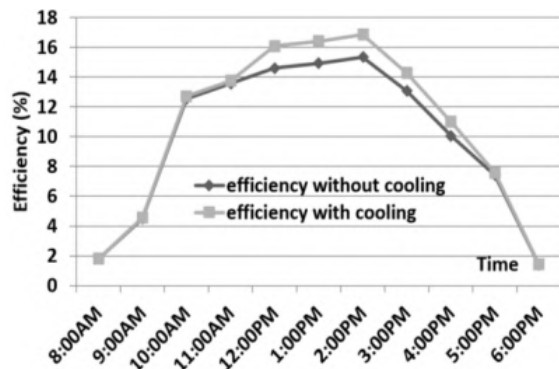


Figure 1.1: Effects of Photovoltaics' (PV) efficiency with or without cooling from reference [3].

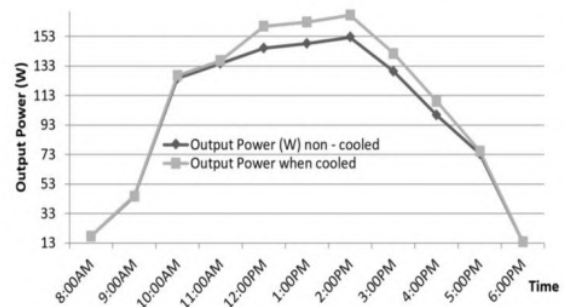


Figure 1.2: Effects of Photovoltaics' (PV) output power with or without cooling from reference [3].

Cooling mechanisms can be categorized based on whether they operate passively or actively [4]. The main attribute of passive cooling is that it occurs without mechanical devices such as fans, pumps, and compressors. The primary advantage of passive cooling is that it requires little energy because it is based only on the phenomena of conduction, convection, and radiation.

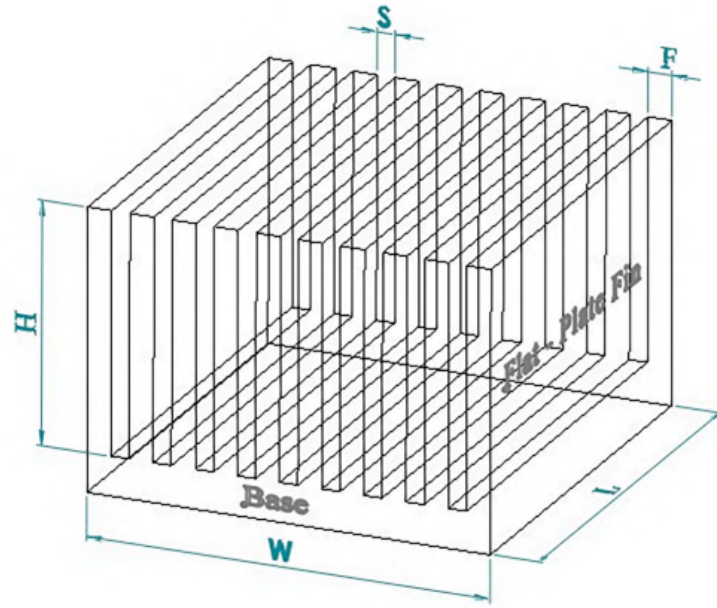


Figure 1.3: Heat sink design parameters. Fin thickness (F), base thickness (W), space (S), heat sink length (L), fin height (H) from reference [5].

Heat sinks are the most popular passive cooling solutions in mechanical and electronic systems. This solution is based on convective heat transfer between the solid cooling geometry and the cooling fluid. The basic parameters that define the geometry of a heat sink are the thickness of the fin, the thickness of the base, the fin spacing, the heat-sink length of the heat sink, and the height of the fin [5]. Figure (1.3) shows all these dimensional parameters. Additionally, microchannels are another cooling geometry based on heat sink geometry. Microchannels consist of many low cross-sectional canals, which offer a huge surface-to-volume ratio. As a result, the cooling efficiency is improved, but these small canals significantly increase total pressure losses. Another common geometries promoting heat exchange are cylindrical pins, which can be of equal size and equidistant or not. A large number of small cylinders enhances convection. Their cylindrical shape decreases the total pressure drop, making them a cost-effective and widely used option.

A significant parameter that plays a crucial role in heat transfer efficiency is the wet surface. Wet surface is the area of the cooling geometry that is in contact with the cooling fluid. A comparison between low-height (lower wetted area) and high-height heat sinks shows that a larger wetted area generally improves the heat-transfer potential. As a result, surfaces with high wet areas are preferable for heat transfer applications. However, higher wet areas also increase fluid–solid friction, and thus, total pressure losses.

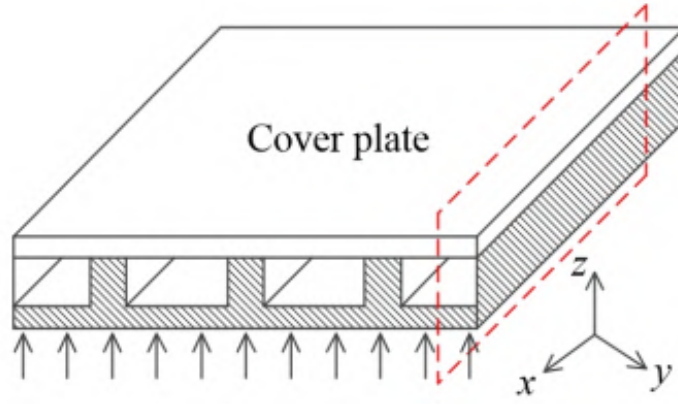


Figure 1.4: Microchannel from reference [6].

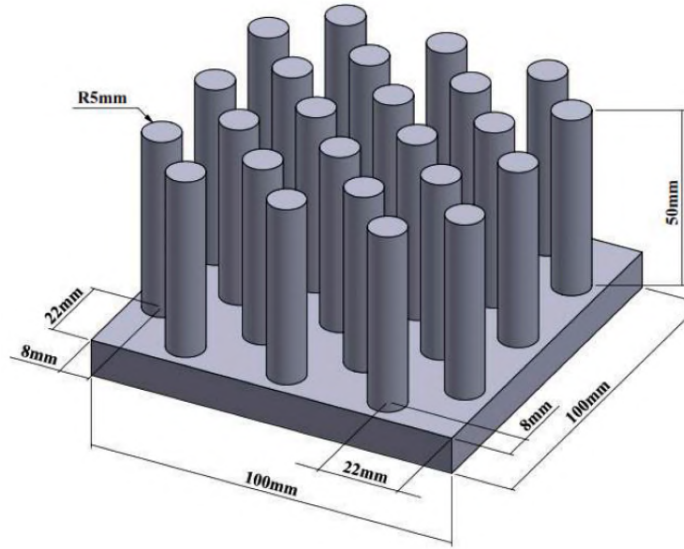


Figure 1.5: Cylindrical heat sinks from reference [7].

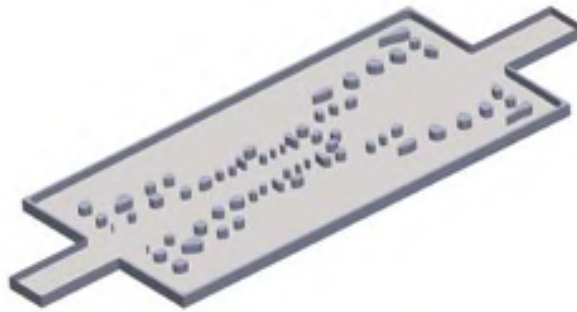


Figure 1.6: Cylindrical heat sinks with non-uniform distribution from reference [8].

1.2 Triply Periodic Minimal Surfaces

The selection of the appropriate cooling geometry is a key factor in heat transfer problems. Geometries with a high surface-to-volume ratio represent an interesting category for further investigation. Among these, Triply Periodic Minimal Surfaces (TPMS), in ad-

dition to the high surface-to-volume ratio, also offer a set of design parameters, providing various cases for parametric studies in cooling applications.

Minimal surfaces can be defined as surfaces that minimize the total surface area subject to some constraint. The mean curvature of those surfaces is zero. The concept was first introduced by Joseph-Louis Lagrange in the 18th century, who formulated the problem mathematically. However, it was Jean-Baptiste-Marie Meusnier who provided the first explicit solutions, including classical geometries such as the helicoid and the catenoid.

TPMS [9], [10], [11] are a special class of minimal surfaces characterized by their periodicity in all three spatial dimensions. Due to their structural complexity and tunable properties, TPMS have found applications across a wide range of disciplines, including materials science [12], automotive [13], and biomedical engineering [14]. Even though, there are many TPMS geometries, this thesis is solely concerned with the Gyroid, the I-graph wrapped package, and the Primitive TPMS (fig (1.7)).

The complexity of TPMS requires high-fidelity simulation tools, as experimental evaluation can be costly and time-consuming. For that reason, Computational Fluid Dynamics (CFD) tools are able to analyze fluid flows and heat transfer problems which involve Conjugate Heat Transfer (CHT). For this purpose, OpenFOAM is suitable since it can solve cases with complex geometries, providing accurate solutions.

In addition, the design and configuration of heat dissipation surfaces play a critical role

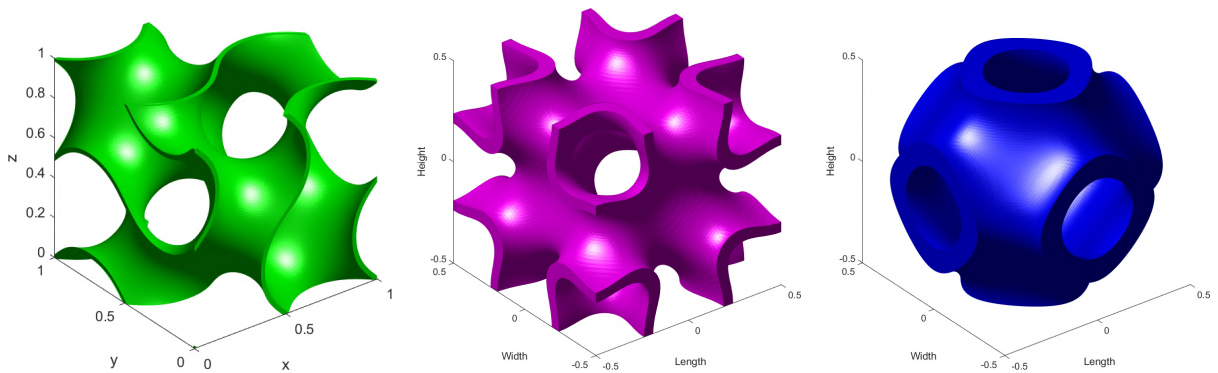


Figure 1.7: Basic Triply Periodic Minimal Surfaces. Gyroid cell unit (left). IWP cell unit (mid). Primitive cell unit (right).

in enhancing thermal management. Geometries with a high surface area in contact with the cooling fluid, under fixed volume constraints, offer an effective solution to this challenge. That happens because the heat flux is distributed better and over a larger interface area. TPMS certainly belong to this type of surface [15].

Given that these surfaces exhibit a high surface-area-to-volume ratio, it is of particular interest to further investigate their geometric properties and assess how such geometries can contribute to enhanced thermal management. Similar geometries have been used

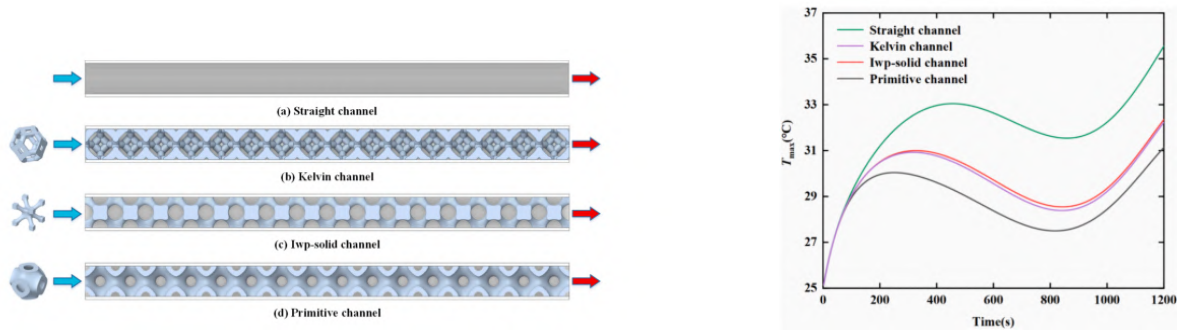


Figure 1.8: Different channels made by geometries with high interface area (left). Maximum temperature recorded on each channel (right) from reference [15].

in a previous diploma thesis [16] at PCOpt/NTUA. The objective of the aforementioned study was to analyze the construction of these geometries and examine their performance for mixing applications. Figure (1.9) illustrates a static mixer featuring two inlets for distinct fluids, with the primary objective of achieving efficient mixing.

This diploma thesis applies TPMS to CHT cases. The complexity of these geometries is expected to promote mixing between the cold fluid near the heat transfer geometry and high-temperature regions, thus increasing heat transfer to the fluid.



Figure 1.9: Static mixing device with a Gyroid geometry. Fluid enters from the left side and there is a common outlet on the right side, [16].

1.3 The OpenFOAM software

OpenFOAM [17], [18] (Open Field Operation and Manipulation) was released in 2004 by the OpenCFD company. It is a software written in C++ and can solve fluid flow, heat transfer, structural, and electromagnetic problems. The software uses the finite volume method for discretization and allows the handling of complex geometries.

OpenFOAM's is freely available, and its source code is open for developers to customize the software to their needs. Additionally, OpenFOAM supports parallel computation, significantly reducing the processing time required. For CHT problems, solver chtMultiRegionSimpleFoam [19], [20], [21], [22] is available. CHT algorithms can simulate cases with repeated solid and liquid domains, considering conduction and convection phenomena.

All cases simulated in OpenFOAM follow a similar configuration. Specifically, the cooling geometry is placed on top of a heat source, while cold air flows along the channel. The objective is for the fluid to exit at the highest possible temperature (\bar{T}_{out}^F), with low total pressure losses. Figure (1.10) visualizes the general setup of all subsequent simulations.

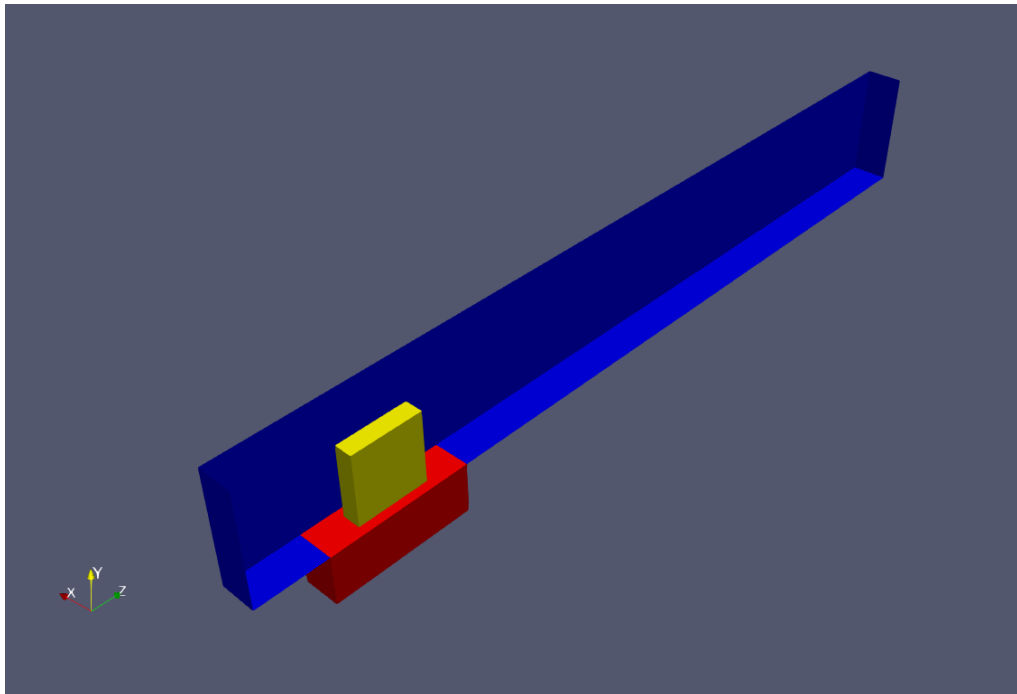


Figure 1.10: Flow domain with heat source underneath. Fluid regions are presented with blue color, heat source with a metallic body (the heat source stands for its lower surface) and red color, and with yellow color is the volume that includes any tested cooling device, where a TPMS will be placed. Fluid flow direction is along the positive z-axis.

1.4 Purpose of this thesis

This thesis investigates add-on geometries for power electronics applications using CHT, enhancing the heat transfer between the solid and the fluid. Cooling devices and a case without such a device are used as references to compare them with TPMS. In addition, a series of parametric studies are conducted to detect the most influential design parameters. The outcomes of these parametric studies will serve as a preliminary basis for future research employing advanced optimization methods.

To achieve this, the theoretical background of these geometries is presented first. Then, the details about the design of the cooling system, the fluid and flow properties, and the objective functions are presented. A comparison of the conventional and TPMS geometries promoting heat exchange follows. Subsequently, some parameters are examined for the TPMS and, then, different TPMS are combined.

It is mentioned that the main purpose is to enhance the heat transfer of the system,

but for simplification, the term cooler or geometries promoting heat exchange is used. The outline of this diploma thesis is:

- Chapter 2 explains the theoretical background of TPMS and how they can be extruded into 3D geometries with thickness, promoting heat exchange.
- Chapter 3 describes the heat exchange system, providing details on the thermal source, the channel, and the geometries promoting heat exchange.
- Chapter 4 reports on the generation of the computational grid, the discretization schemes used in the CHT solver, and the objective functions used to evaluate the cooling performance.
- Chapter 5 includes the results of conventional geometries promoting heat exchange and the basic units of TPMS.
- Chapter 6 discusses parametric studies focusing on TPMS periodicity, thickness, and extrusion method and proceeds with their application in the CHT problem.
- Chapter 7 explains the concept of hybrid TPMS and compares them with the non-hybrid geometries.
- Chapter 8 concludes the thesis with some conclusions and lessons learned.

Chapter 2

Generation of geometries promoting heat exchange from TPMS

In this chapter, the theoretical background for the generation of geometries promoting heat exchange based on TPMS is explained. It is essential to present their mathematical description that defines their surface. Then, the two methods that lead to the creation of a 3D cooling geometry from a TPMS are introduced. This background is important because all these geometries are later incorporated into the CHT problem under consideration.

2.1 Design space boundaries

Since all TPMS consist of periodic functions, their patterns can be continuously extended. Thus, the first step of their generation is to define a hypothetical parallelepiped that bounds a single TPMS geometry. For example, figures (2.1) and (2.2) have been designed for $x, y, z \in [-0.5, 0.5]$, and parameters a, b, c are equal to 1 to depict the cell unit, which can be repeated along the axis and create more complex patterns.

2.2 Cell unit surface equation

Before the generation of a 3D cooling geometry, a zero-thickness TPMS surface has to be designed inside the parallelepiped. This, practically, corresponds to the mean surface of the cooling device to be designed. The bounding parallelepiped is chosen for a fair comparison among various candidate solutions. The zero-thickness surface equations [23] of TPMS such as Gyroid, Primitive, and IWP are:

$$f(x, y, z) = \sin(2a\pi x) \cos(2b\pi y) + \sin(2b\pi y) \cos(2c\pi z) + \sin(2c\pi z) \cos(2a\pi x) = 0, \quad (2.1)$$

$$\begin{aligned} f(x, y, z) = & 2(\sin(2a\pi x) \cos(2b\pi y) + \sin(2b\pi y) \cos(2c\pi z) + \sin(2c\pi z) \cos(2a\pi x)) \\ & - (\cos(4a\pi x) + \cos(4b\pi y) + \cos(4c\pi z)) = 0 \end{aligned} \quad (2.2)$$

$$f(x, y, z) = \cos(2a\pi x) + \cos(2b\pi y) + \cos(2c\pi z) = 0, \quad (2.3)$$

where a, b, c are constants that define how frequently a surface is repeated across the axis, which is related to. Given that the design space is $x, y, z \in [-0.5, 0.5]$, in figure (2.3), the z -axis pattern is repeated twice across the domain, but along the other axes, the pattern inside the design space appears only once. Another example is shown in figure (2.4), where the cell unit of IWP is repeated three times along each axis within its boundary box. As a result, TPMS can increase its surface inside a boundary space. Thus, the surface-to-volume ratio increases, making TPMS a suitable geometry for heat exchange applications.

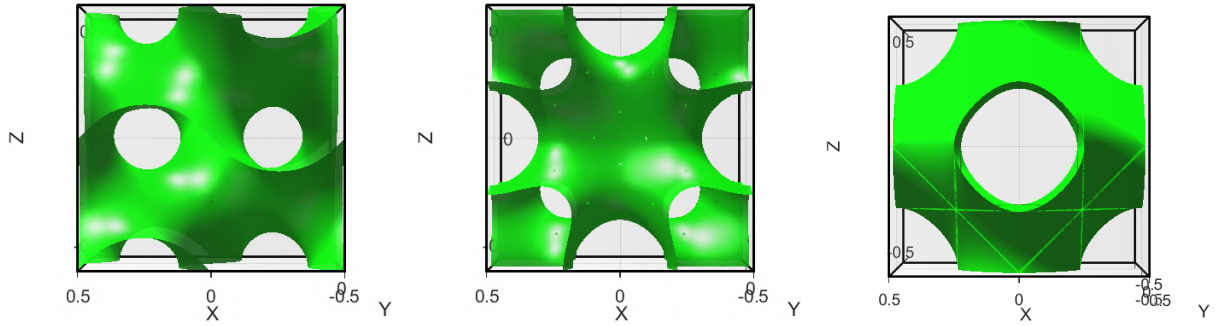


Figure 2.1: Front view of basic TPMS. Gyroid (left). IWP (mid). Primitive (right).

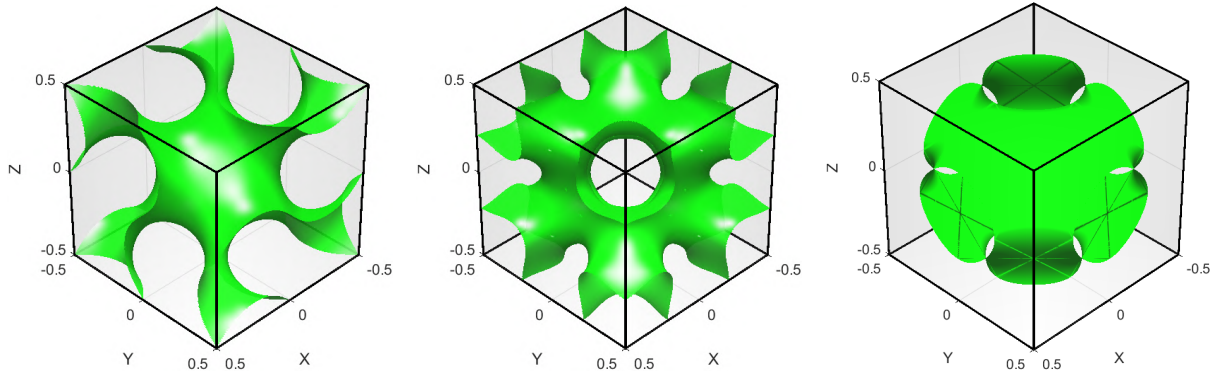


Figure 2.2: Isometric view of basic TPMS. Gyroid (left). IWP (mid). Primitive (right).

2.3 Extrusion methods

After the surface is fully defined, it has to be thickened along the normal to the surface direction to create a 3D object [24]. There are two different ways of extrusion (i.e. ways of adding thickness):

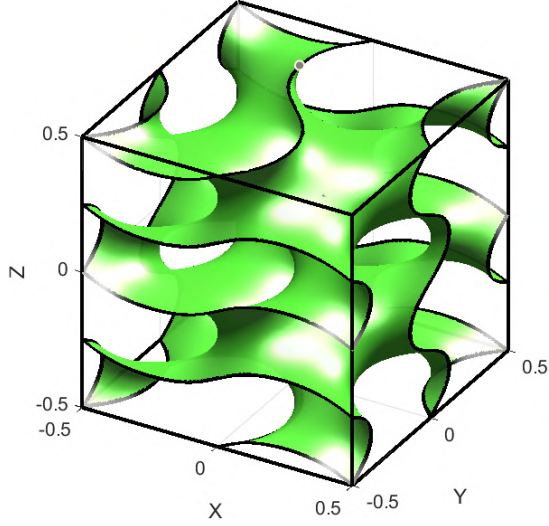


Figure 2.3: Gyroid zero thickness surface with parameters $a = 1, b = 1, c = 2$, enclosed in a unit cube.

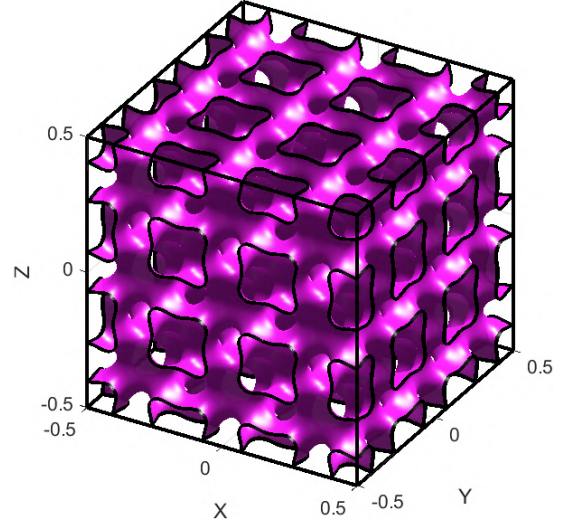


Figure 2.4: IWP zero thickness surface with parameters $a = 3, b = 3, c = 3$, enclosed in a unit cube.

- Solid sheet extrusion
- Solid network extrusion

For solid sheet extrusion, given that there is a surface $f(x,y,z) = 0$, the 3D object is formed by extruding the surface equation at both sides, and the new solid object is formed between these surfaces. The solid-sheet extruded object is defined by the following double inequality:

$$-\frac{t}{2} \leq f(x, y, z) \leq \frac{t}{2} \quad (2.4)$$

where t is the desired thickness. On the other hand, in solid network extrusion, the object is extruded in one direction and the new solid object is formed between the zero-mean surface and the transposed surface, which is formulated by the following double inequality:

$$f(x, y, z) \leq t \quad (2.5)$$

The zero-thickness IWP surface and the sheet extruded surface are presented in Figure (2.5). On the other hand, solid network extruded IWP geometry is also presented in figure (2.6). The last important parameter that MSLattice uses to convert a surface into an object is the relative density [25]. Relative density is the ratio of 3D TPMS object's volume and the volume of the cell in which the geometry is enclosed. Additionally, a sheet-network IWP and a solid network IWP of the same relative density are showed in figure (2.7).

It is noted that these extrusion methods lead to different geometries. The case of sheet-solid extrusion is preferred because of its high wet area and the different flow channels

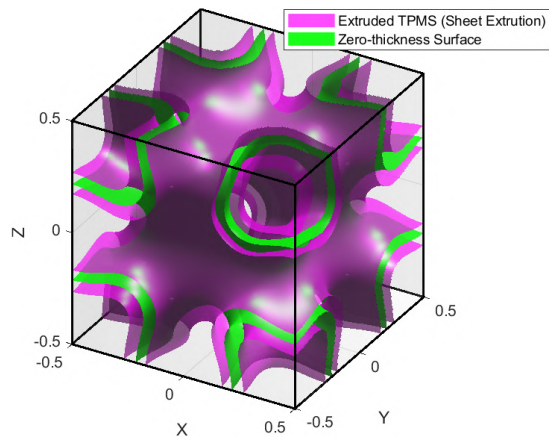


Figure 2.5: Sheet extruded surface in both directions.

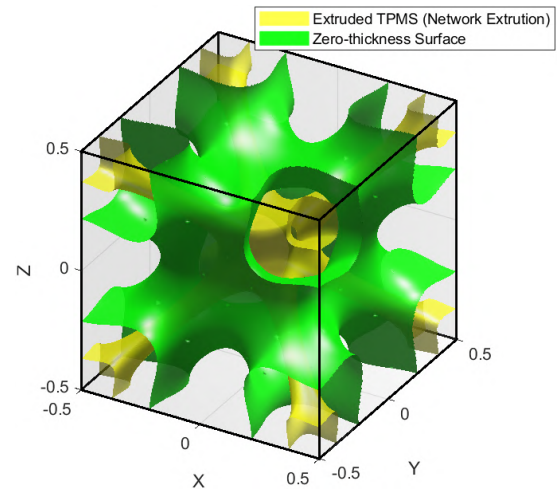


Figure 2.6: Network extruded surface in both directions.

that are created. The solid network extraction will be used in the parametric study to compare it with the solid sheet extrusion.

Next step is to describe the system promoting heat exchange with more dimensional details and explain how these geometries promoting heat exchange are incorporated into it.

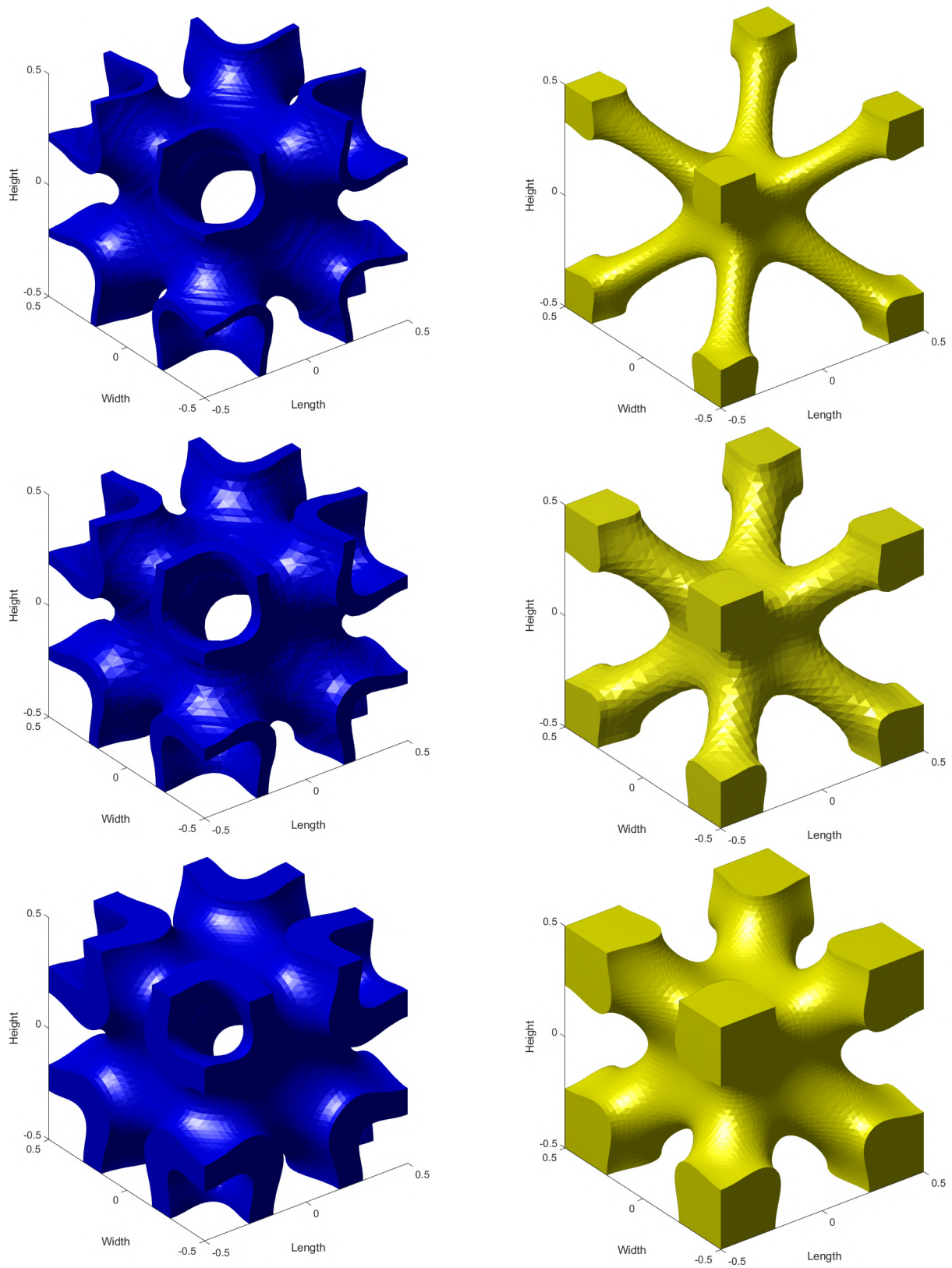


Figure 2.7: Solid sheet and solid network extruded IWP surface with different relative density. Solid sheet extruded surfaces (on left) and network extruded surfaces (on right).

Chapter 3

Design of the Heat Exchange System

The heat exchange system simulates a power electronics board on which TPMS-based geometries are incorporated as the cooling structures. First, the thermal source and the flow channel are introduced, followed by the different geometries promoting heat exchange considered, including conventional heat sinks, basic TPMS structures, and hybrid combinations. The reason for using various TPMS is that optimization methods might have a high computational cost and, depending on the selected method, the optimized solution might seriously be affected by the initialization. Thus, a parametric study is preferred to "clean" the design space and find promising configurations that will likely be used as good initializations in future optimization runs.

3.1 Thermal Source

The thermal source is modeled as a rectangular parallelepiped with dimensions $x = 1$ cm, $y = 1.2$ cm, $z = 4$ cm (figure (3.1)). This component represents a heated metal element exposed to a high temperature on one side and an air stream on the other side. Within the simulation, it acts as a constant-temperature heat source.

3.2 Cooling Channel

The canal also has a rectangular parallelepiped shape (figure (3.1)) with dimensions of $x = 1$ cm, $y = 10$ cm, and $z = 12$ cm. The direction of flow of the fluid is parallel to the z -axis. The length and the height of the field of flow extends far beyond the thermal source to better capture the development of the flow.

3.3 Geometries promoting heat exchange

In this section, every heat exchange geometry in each case has some common properties. All of them are made of aluminum, are placed in the center of the thermal source, and must fit in a box with external dimensions of: $x = 0.25$ cm, $y = 1$ cm, and $z = 1$ cm. The main purpose of those geometries is to dissipate as much heat flux as possible from

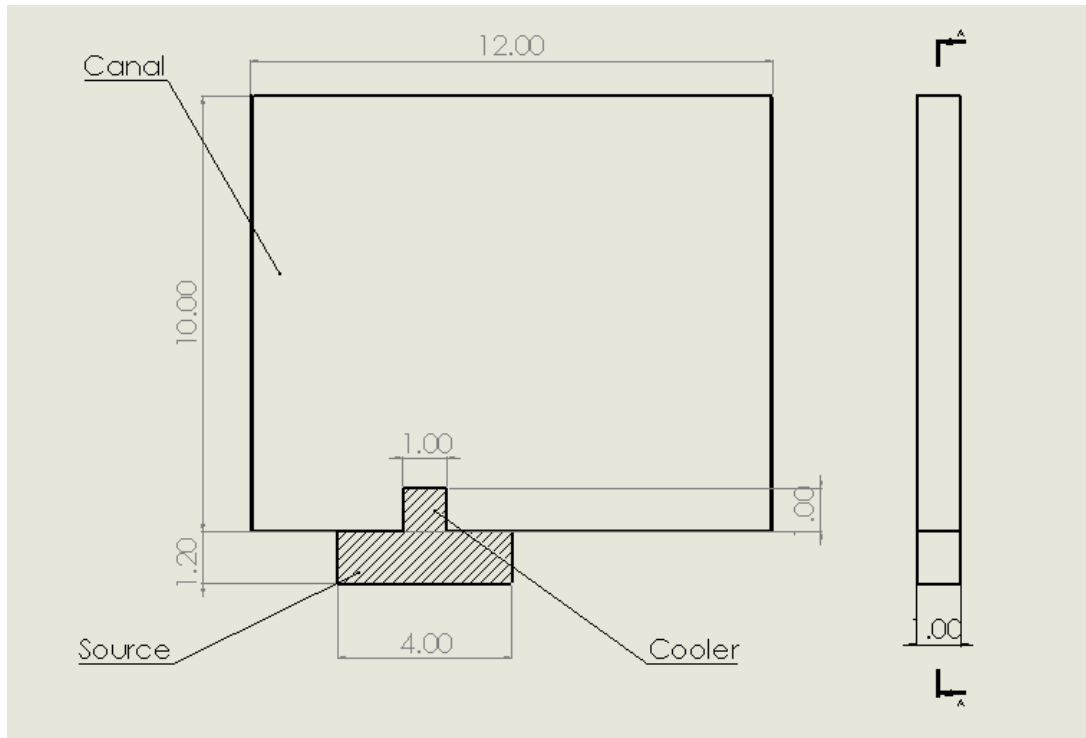


Figure 3.1: Drawing of the cooling system.

the thermal source, and then the airflow that passes through these geometries cools the surface. In detail, the geometries that to be used include heat sinks, Gyroid, IWP, and Primitive.

3.3.1 Heat sink

Heat sinks [26] are widely used in electronics cooling, making them an interesting option for comparison with TPMS. This geometry includes a pattern of small rectangular cuboids that cover all the available space. Instead of simulating a full heat sink is preferable to exploit periodicity, as periodicity is also one of TPMS's main properties.

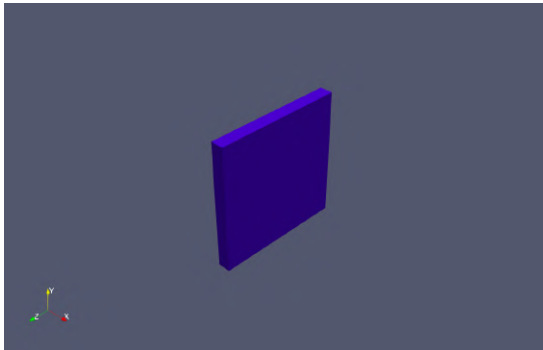


Figure 3.2: Heat sink geometry.



Figure 3.3: Microchip heat sink from reference [27].

3.3.2 TPMS-Shaped geometries promoting heat exchange

To define the geometry of all TPMS it is necessary to know the design parallelepiped that TPMS has to be enclosed, the coefficients a , b , c that were defined in the previous chapter, and the relative density. For these cases, the boundary limits are 0.25 cm for the x-axis, 1 cm for the y-axis, and 1 cm for the z-axis. In equations (2.1),(2.2),(2.3) the parameters $a=8\pi$, $b=2\pi$, and $c=2\pi$ are used. The relative density for all geometries is 30%. All these geometries are shown in figure (3.4).

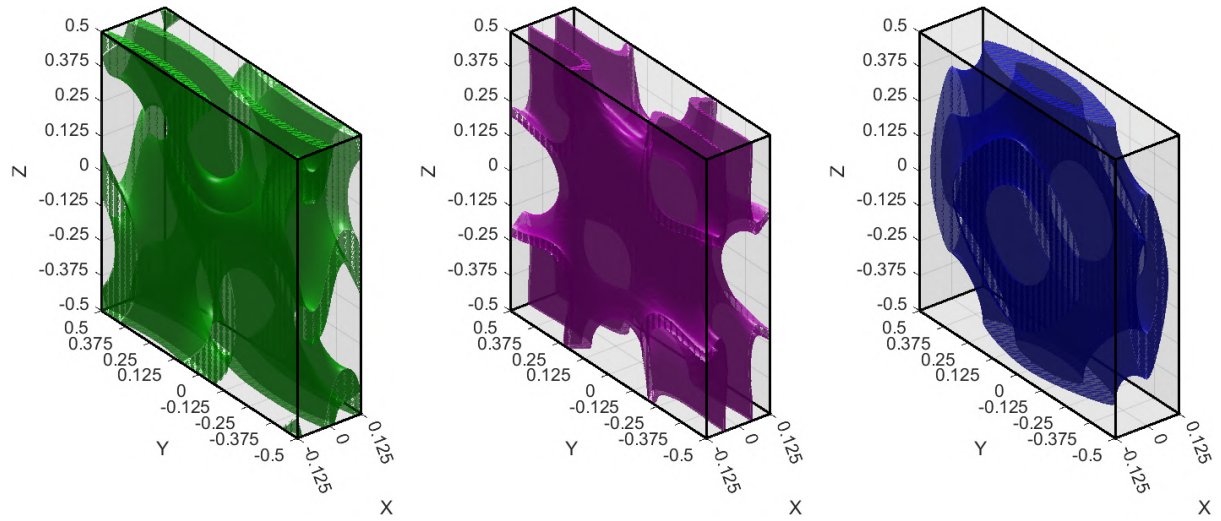


Figure 3.4: Geometries of Gyroid (left), IWP (mid), Primitive (right), promoting heat exchange.

Chapter 4

CHT modeling

As described in chapter 3, the selected software is OpenFOAM and specifically the cht-MultiRegionSimpleFoam solver for CHT cases. CHT is necessary for these cases since the source and the heat exchange geometry are solids, and the working fluid is air; all of them must simultaneously be resolved.

4.1 Flow equations

The Reynolds-averaged Navier–Stokes (RANS) [28] equations are time-averaged equations that describe turbulent flows. These partial differential equations express the conservation of mass, momentum, and energy. For an incompressible fluid flow, these are written as:

$$R^p = -\frac{\partial u_i}{\partial x_i} = 0 \quad (4.1)$$

$$R_i^p = u_j \frac{\partial u_i}{\partial x_j} + \frac{1}{\rho^F} \frac{\partial p}{\partial x_i} - \frac{\partial \tau_{ij}}{\partial x_j} = 0 \quad (4.2)$$

$$R_T^F = u_j C_p \frac{\partial T^F}{\partial x_j} + \frac{u_j}{2} \frac{\partial u_k^2}{\partial x_j} - \frac{\partial}{\partial x_j} \left(\frac{k^F}{\rho^F} \frac{\partial T^F}{\partial x_j} \right) = 0 \quad (4.3)$$

where

u_i : cartesian velocity components

p : static pressure

$\tau_{ij} = (\nu + \nu_t) \left(\frac{\partial u_i}{\partial x_j} + \frac{\partial u_j}{\partial x_i} \right)$: stress tensor

ρ^F : fluid's density

c_p : specific heat transfer coefficient under constant pressure

T^F : fluid's temperature

k^F : fluid's thermal conductivity for which:

$$\frac{k^F}{\rho^F} = c_p \alpha = c_p \frac{\nu + \nu_t}{Pr} \quad (4.4)$$

where Pr is the Prandtl number, α the thermal diffusivity, ν the kinematic viscosity and ν_t the turbulent kinematic viscosity.

Heat conduction in the solid regions is described by :

$$R_T^S = -\frac{\partial}{\partial x_i} \left(k^S \frac{\partial T^s}{\partial x_i} \right) = 0 \quad (4.5)$$

where k_s is solid's thermal conductivity. Equation (4.1) refers to the conservation of mass. Equation (4.2) expresses the conservation of momentum in each direction of the flow, and equation (4.3) expresses the conservation of energy to compute the temperature field in the fluid domain and equation (4.5) computes the temperature field in the solid domain.

4.2 Turbulence Model

Turbulence is a fluid motion that includes stochastic changes in the fluid pressure and velocity. Visually, it appears as randomly shaped small-sized vortices, that are developed through the fluid. To be able to model turbulence, the Spalart–Allmaras [29] is used. This is a one-equation model which is expressed:

$$R^{\tilde{\nu}} = u_j \frac{\partial \tilde{\nu}}{\partial x_j} - C_{b1} (1 - f_{t2}) \tilde{S} \tilde{\nu} + \left(C_{w1} f_w + \frac{C_{b1}}{\kappa^2} f_{t2} \right) \left(\frac{\tilde{\nu}}{d} \right)^2 - \frac{1}{\sigma} \left[\frac{\partial}{\partial x_j} \left[(\nu + \tilde{\nu}) \frac{\partial \tilde{\nu}}{\partial x_j} \right] + C_{b2} \frac{\partial^2 \tilde{\nu}}{\partial x_i^2} \right] = 0 \quad (4.6)$$

where: $\nu_t = \tilde{\nu} f_{v1}, f_{v1} = \frac{X^3}{X^3 + C_{v1}^3}$ and $X = \frac{\tilde{\nu}}{\nu}$.

The other equations of the model are:

$$\tilde{S} = S + \frac{\tilde{\nu}}{\kappa^2 d^2} \quad (4.7)$$

$$S = \sqrt{2 \Omega_{ij} \Omega_{ij}} \quad (4.8)$$

$$\Omega_{ij} = \frac{1}{2} \left(\frac{\partial u_i}{\partial x_j} - \frac{\partial u_j}{\partial x_i} \right) \quad (4.9)$$

$$f_{v2} = 1 - \frac{X}{1 + X f_{v1}} \quad (4.10)$$

$$f_w = g \left(\frac{1 + C_{w3}^6}{g^6 + C_{w3}^6} \right) \quad (4.11)$$

$$g = r + C_{w2} (r^6 - r) \quad (4.12)$$

and also the constants: $\sigma = \frac{2}{3}$, $C_{b1} = 0.1355$, $C_{b2} = 0.622$, $\chi = 0.41$, $C_{w1} = 3.239$, $C_{w2} = 0.3$, $C_{w3} = 2$, $C_{v1} = 7.1$, $C_{t3} = 1.2$, $C_{t4} = 0.5$.

4.3 Boundary conditions

The boundary conditions for the problem are the following:

- Inlet: Dirichlet conditions are imposed on the velocity, fluid temperature (300 K), and the Spalart–Allmaras variable $\tilde{\nu}$, while a zero Neumann condition is imposed

on the static pressure.

- **Outlet:** Zero Neumann conditions are imposed on the velocity, fluid temperature, $\tilde{\nu}$, while a zero Dirichlet condition is imposed on pressure, which is also the reference pressure.
- **External walls¹:** The velocity on the walls is set to zero (no-slip condition), $\tilde{\nu}$ is set to zero, and a zero Neumann condition is imposed on pressure. All external walls are considered adiabatic. Thus, a zero Neumann condition is imposed on solid temperature, apart from the bottom face of the heat source which has Dirichlet temperature conditions (400 K).
- **Internal walls²:** For internal walls, the boundary conditions for velocity, pressure, and the turbulence model are the same as the external walls, but for the temperature, internal walls are interfaces in which the common nodes will take heat transfer phenomena at both the fluid and solid sides into account.

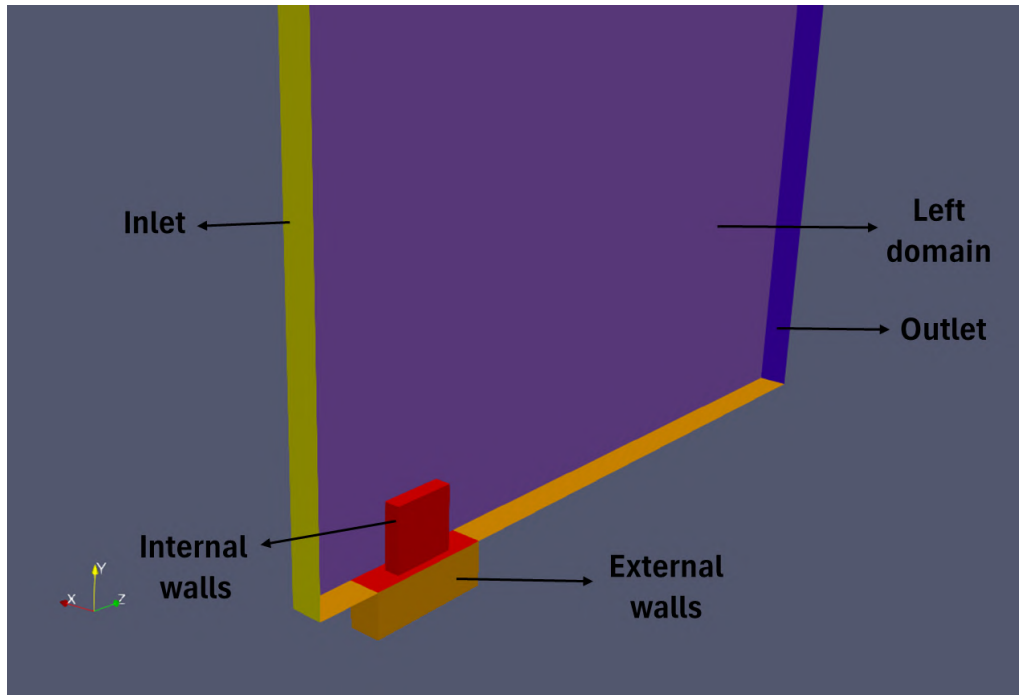


Figure 4.1: Flow domain with heat source underneath.

4.4 Grid generation

Given that all the TPMS geometries are complex, an unstructured grid of pyramids and hexahedra is used. For that purpose, Fidelity Pointwise software generates the computational grid, emphasizing the minimization of cell non-orthogonality. Table (4.1) includes

¹Walls that have no borders with solid

²Walls that have borders with solid

the number of grid cells used for each geometry and the corresponding grid element counts of the geometries promoting heat exchange.

Geometry	Gyroid	IWP	Primitive	Parallelepiped Fin	Rounded Fin
Number of cells	550,000	250,000	100,000	250,000	300,000

Table 4.1: Number of cells inside each cooling geometry.

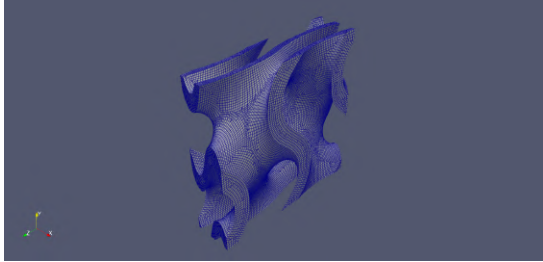


Figure 4.2: Gyroid grid.

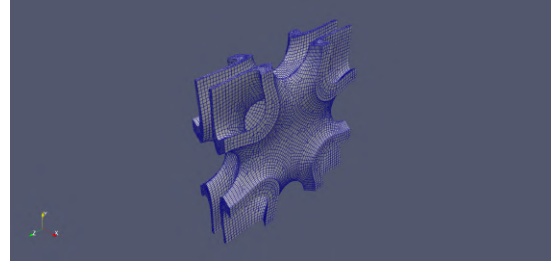


Figure 4.3: IWP grid.

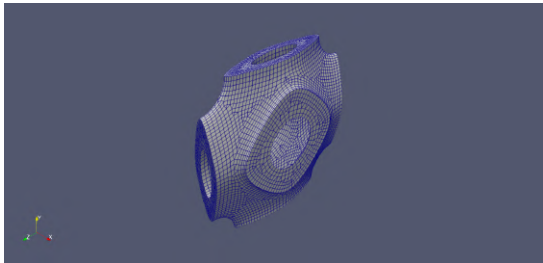


Figure 4.4: Primitive grid.

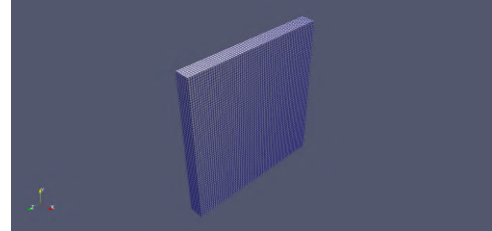


Figure 4.5: Conventional parallelepiped fin grid.

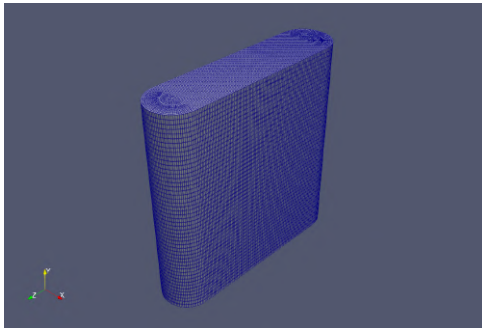


Figure 4.6: Conventional parallelepiped fin grid.

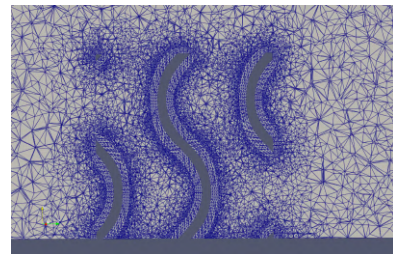


Figure 4.7: Gyroid computational grid.

For the gyroid case, the total number of cells of the whole grid is 2,100,000. The computational grid of the canal region consists of 1,400,000 cells, the Source region has 150,000 cells, and the Gyroid contains 550,000. Figure (4.7) depicts a section of the computation grid near the gyroid.

4.5 Case and solver properties

For all the cases to be simulated, the inlet air velocity is equal to 2 m/s, directed parallel to the z-axis. Table (4.2) contains the properties of the fluid, and the solid used in the

simulation, and table (4.3) contains the solver details. According to Table (4.2), the Reynolds number is equal to 2420 and, to be on the safe side, it was decided to model the flow as turbulent.

Property	Value	Unit
Solid density	2719	kg/m ³
Solid thermal conductivity	202.4	W/(m · K)
Solid specific heat (C_p)	871	J/(kg · K)
Air density	1.225	kg/m ³
Air specific heat (C_p)	1006.43	J/(kg · K)
Air dynamic viscosity	1.846×10^{-5}	Pa · s
Hydraulic diameter	0.0182	m
Reynolds number	2420	-
Prandtl number	0.726414	-

Table 4.2: Material and fluid properties.

Parameter	Value
Maximum iterations	3000
Velocity relaxation	0.5
Pressure relaxation	0.5
Fluid energy equation relaxation	0.7
Solid energy equation relaxation	0.9
$\tilde{\nu}$ relaxation	0.5

Table 4.3: Solver settings.

4.6 Performance metrics

The objective functions that evaluate the effectiveness of the cooling, in the present study, are:

$$T_{out}^{\bar{F}} = \frac{\int_{A_{outlet}} Tu_z dA}{\int_{A_{outlet}} u_z dA} \quad (4.13)$$

$$\omega_{total,losses} = \frac{\int_{A_{outlet}} \left(p + \frac{1}{2}\rho u_i^2\right) dA - \int_{A_{inlet}} \left(p + \frac{1}{2}\rho u_i^2\right) dA}{\frac{A_{inlet}\rho v_{inlet}^2}{2}} \quad (4.14)$$

The first one refers to the total pressure losses across the field, which are calculated by equation (4.14). Equation (4.13) refers to the quality of the cooling, calculated as the mass-averaged temperature at the outlet face. The objective is to maximize \bar{T}_{out}^F , while the pressure loss coefficient is treated as a constraint.

Chapter 5

Results of conventional geometries

In this chapter, all the geometries presented in Chapter 3 are simulated. These geometries are separated into two groups. The first is the group of conventional geometries promoting heat exchange, which include cases without a cooling geometry, with a rectangular fin, and with a fin with rounded corners. The second group consists of single unit cells of TPMS. It should be noted that the first group will be considered as reference solutions to compare with.

5.1 Conventional geometries promoting heat exchange

Figure (5.1) presents the convergence of the solved equations. Since the add-on heat exchange promoting body and source geometries are modeled as different regions, each is expected to have different residuals. As all residuals of equations are lower than 10^{-6} , the results are considered to be converged.

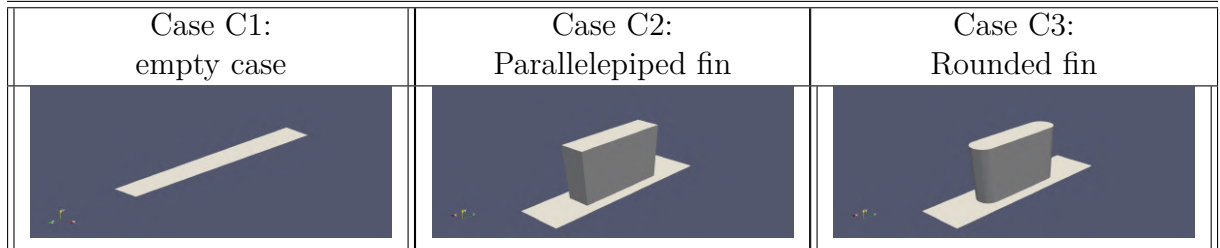


Table 5.1: Geometries of conventional cases.

Case name	C1	C2	C3
$\omega_{t,losses}[-]$	0.01215	0.1675	0.146
$T_{outlet}[K]$	303.3	312.57	315.49

Table 5.2: Performance of conventional cases.

In figure (5.2), all the conventional geometries that are widely used in similar applications are presented. As expected, case C1 has the minimum total pressure losses without a significant increase in \bar{T}_{out}^F ; this was expected as there is no solid obstacle to generate losses

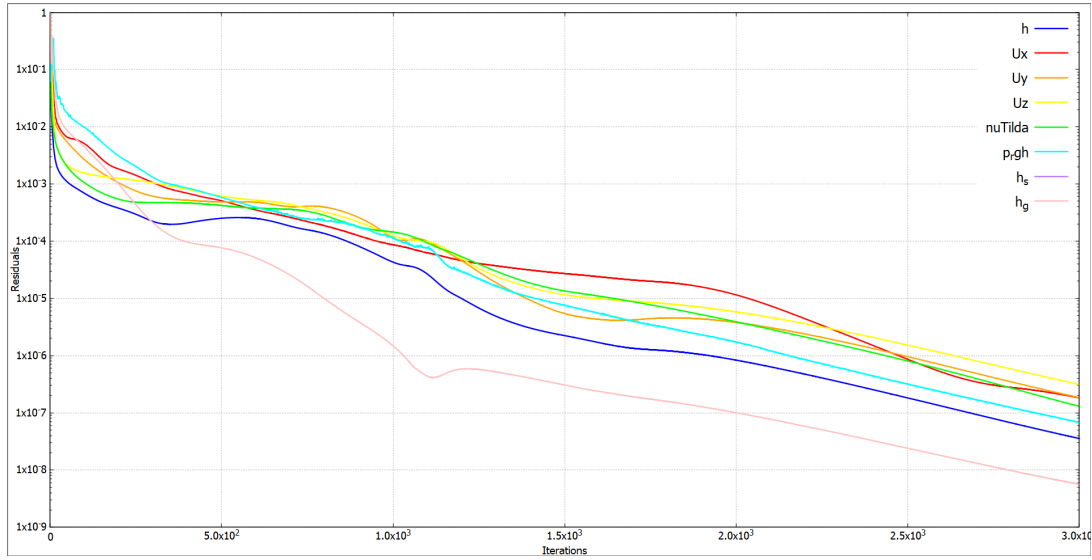


Figure 5.1: Residuals of the Navier-Stokes and energy equations of case C2.

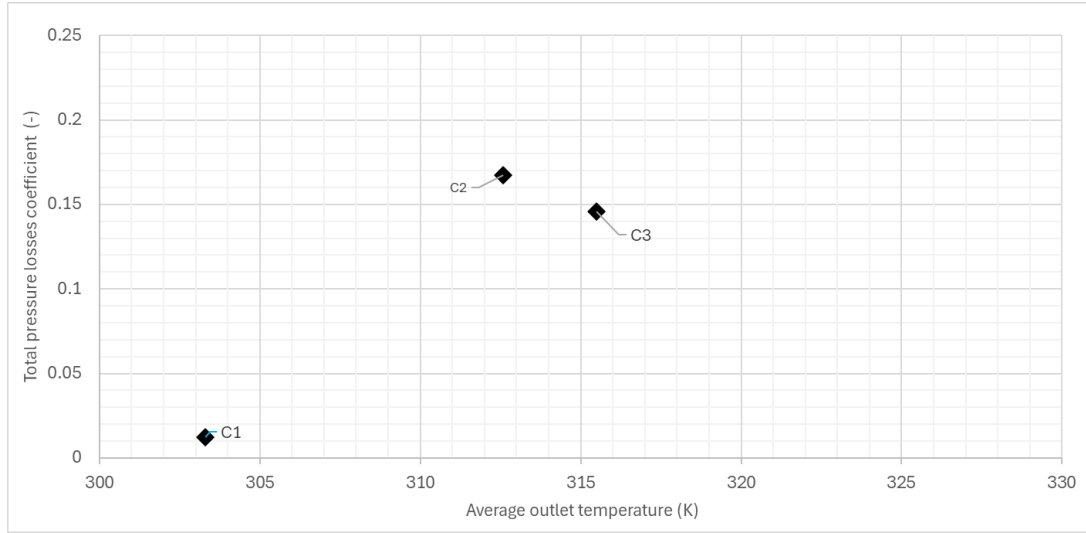


Figure 5.2: Performance of the convective geometries.

and increase heat transfer. On the other hand, case C2 shows increased losses, while \bar{T}_{out}^F is also higher than in case C1. In addition, case C3 represents a more aerodynamic form than that of case C2 and demonstrates better performance metrics than the latter. The purpose of the following cases is to further increase performance at the expense of using more complicated heat exchange-promoting devices. Figure (5.3) shows that the placement of a heat exchange-promoting geometry enhances diffusion, depicting a higher thermal trail.

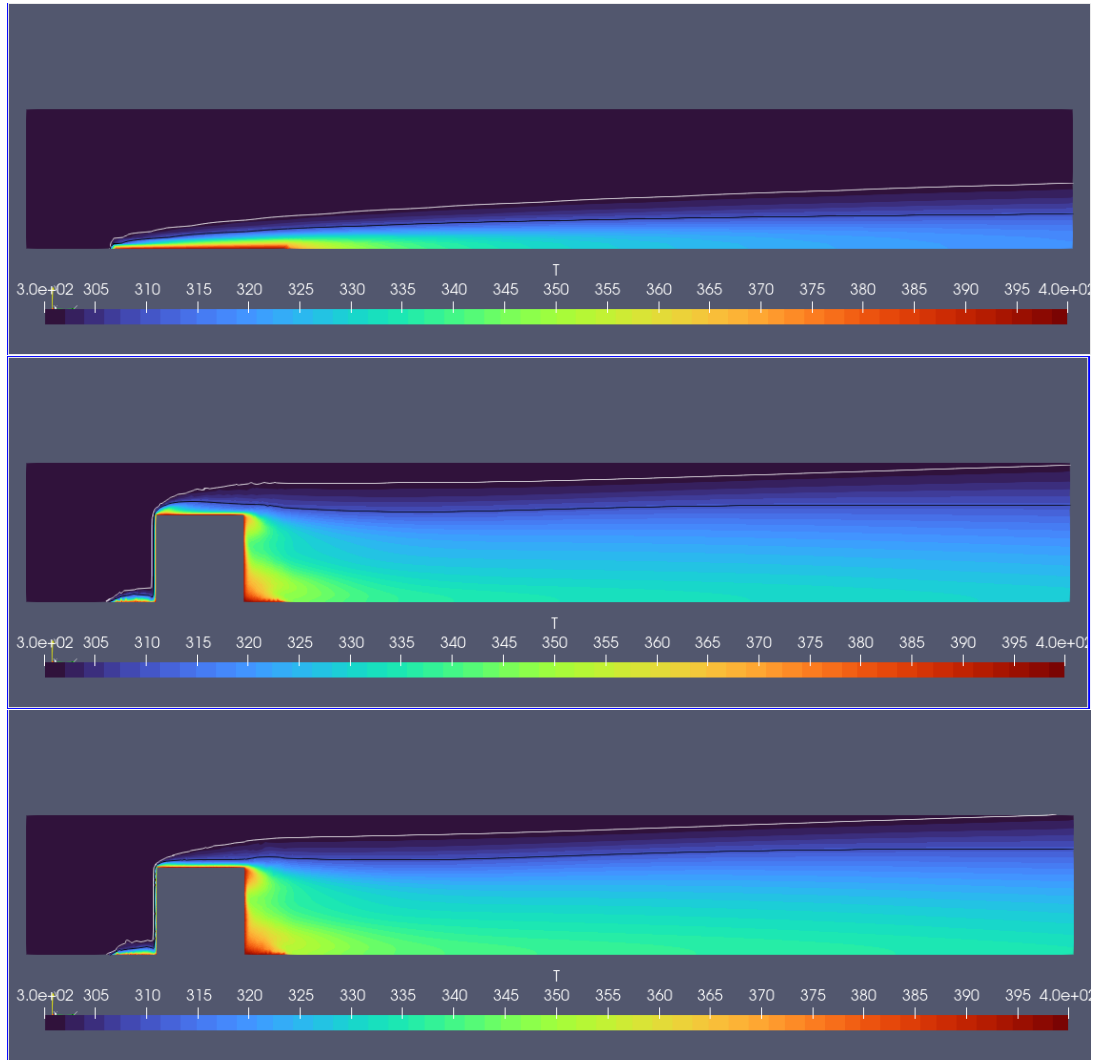


Figure 5.3: Temperature iso-areas at midplane of x-direction for cases C1(up), C2(mid), and C3(down). The white lines indicate the 301 K iso-line, while the black lines correspond to the 310 K iso-line.

5.2 Geometries' efficiency

As all reference geometries have been set, it is important to examine the efficiency of the simple unit cells of TPMS. In table (6.10), all these geometries are presented. Com-

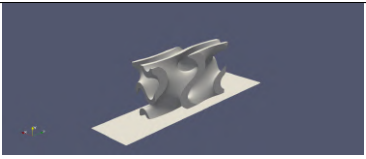
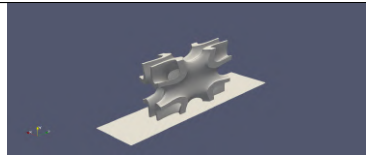
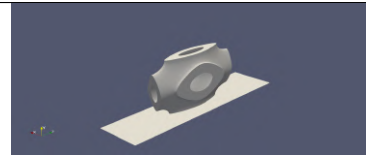
Case T1: Gyroid	Case T2: IWP	Case T3: Primitive
		

Table 5.3: Geometries of TPMS of single cell units.

paring the iso-lines of 301 K and 310 K between figures (5.3) and (5.4), it is clear that the isothermal lines of TPMS are located much higher(on the y-axis) than conventional

geometries. This means that the outlet average temperature has increased. Gathering the

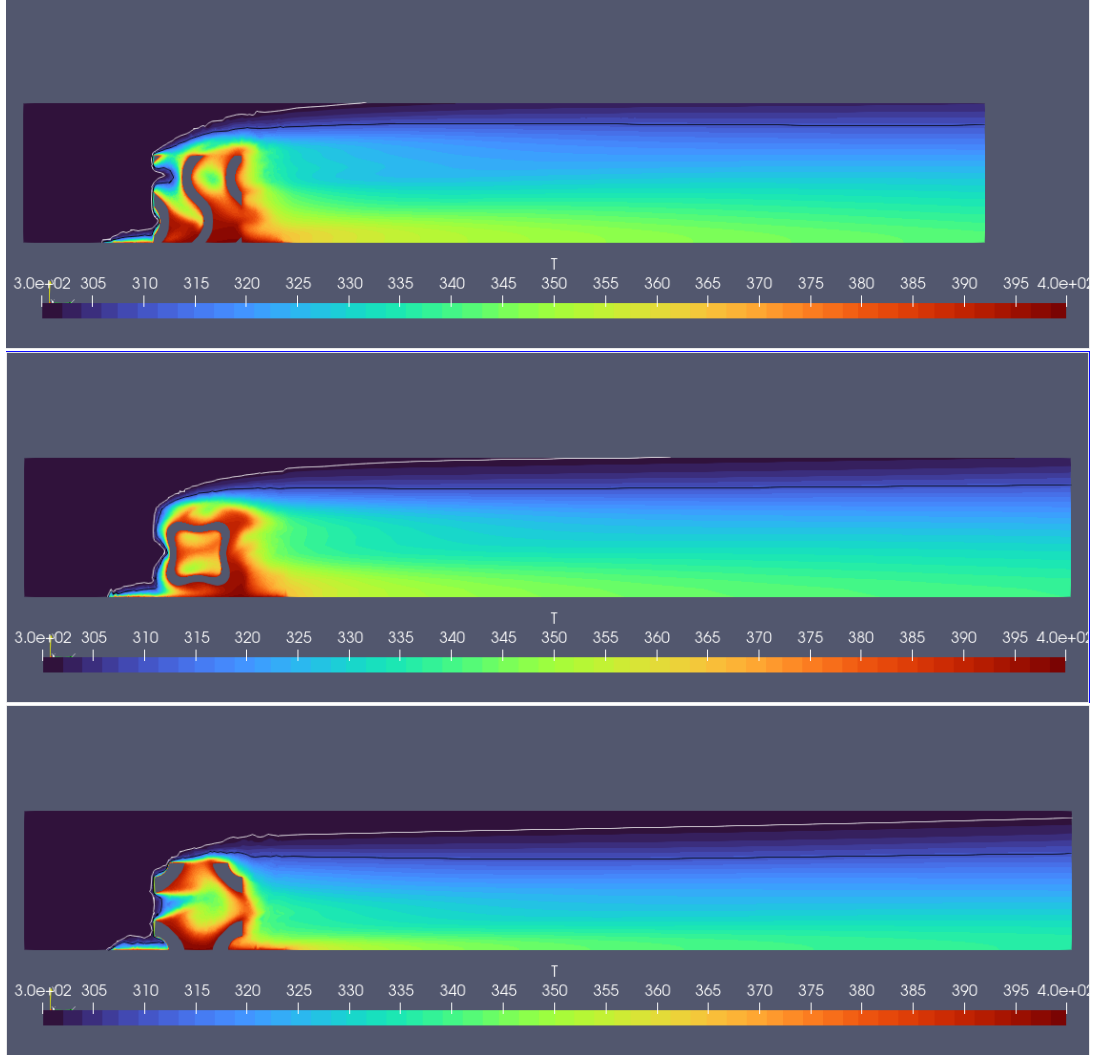


Figure 5.4: Temperature iso-areas at midplane of x-direction for cases T1, T2, and T3. The white lines indicate the 301 K iso-line, while the black lines correspond to the 310 K iso-line.

results of all CFD cases, these are plotted in figure (5.5). Considering that the optimal solution has to be on the bottom right side of the chart, all solutions, except C2, are considered non-dominated [30]. Furthermore, the gyroid was expected to exhibit higher total pressure losses due to its non-aerodynamic shape. In addition, case T3 does not have higher \bar{T}_{out}^F , like the other TPMS, and behaves similarly to case C3.

In table (5.4) the data of figure (5.5), are presented. Given that the TPMS geome-

Geometry	C1	C3	T3	T2	T1
$\omega_{t,losses}[-]$	0.01215	0.146	0.1453	0.1578	0.17318
$T_{outlet}[K]$	303.3	315.49	314.37	318.74	319.78

Table 5.4: Performance of the so-far non-dominated solutions of figure (5.5)

tries are more effective than the heat sink cooler, it would be more interesting to analyze

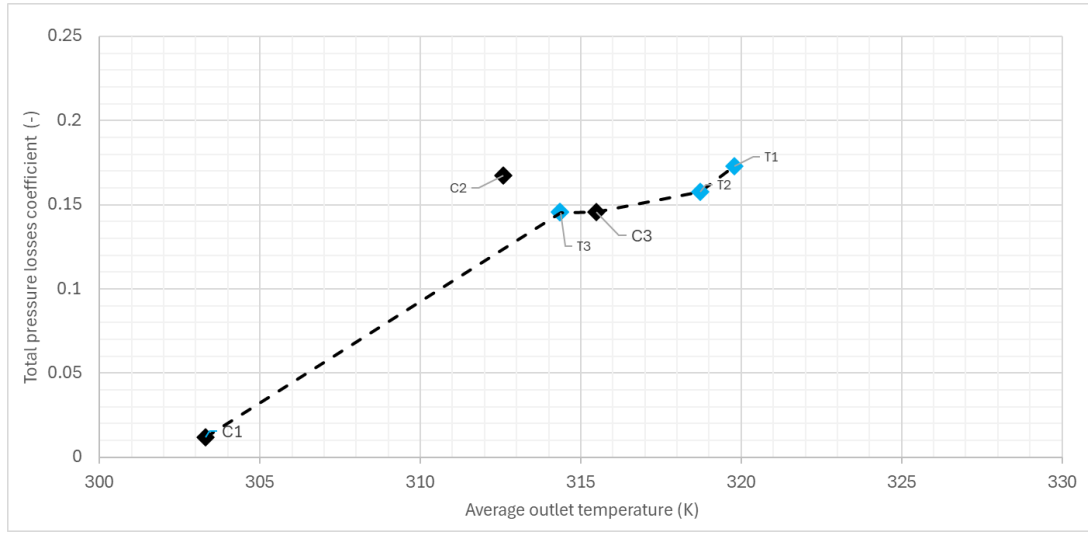


Figure 5.5: Study of basic geometries. The front of the so-far non-dominated solutions is displayed with the non-continuous line.

how the parameters that constitute a TPMS geometry influence heat exchange. As a result, the introduction of single-unit TPMS cells offers more satisfying solutions, as T2 has similar pressure losses to the C3 case, but increases the average outlet temperature from 315.49 to 318.74 K. Additionally, T1 yields the highest temperature increase, but also has the highest total pressure losses.

Chapter 6

Parametric studies

In this chapter, parametric studies are conducted to investigate the performance of TPMS, considering the periodic property and the thickness distribution. All tested geometries are encapsulated into the same boundary box as the previous ones.

6.1 Parametric Study 1: Periodicity pattern

In this section, the nature of the TPMS geometries will be exploited by replacing a single cell with its double or quadruple replicate. The new heat exchange promoting geometries will become more complex by increasing the surface area in contact with the cooling fluid. However, by doing so, the area of heat exchange promoting geometries which is in contact with the source is reducing as the patterns repeat.

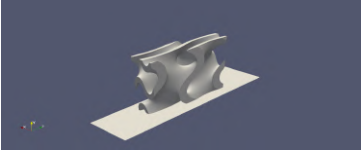
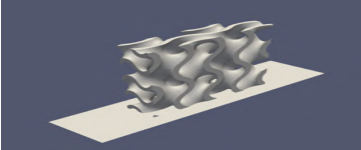
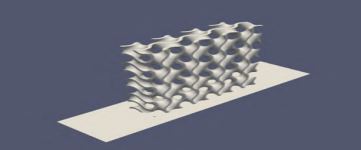
Case T1: Gyroid	Case S1a: Dual Gyroid	Case S1b: Quadruple Gyroid
		

Table 6.1: Patterns of Gyroid geometry.

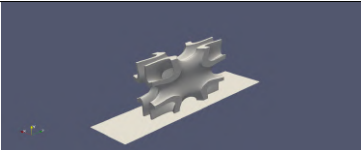
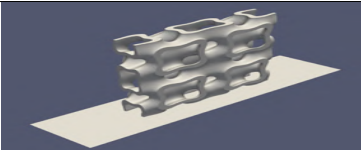
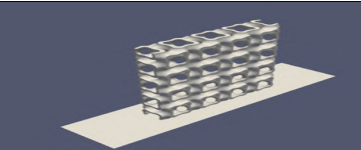
Case T2: IWP	Case S1c: Dual IWP	Case S1d: Quadruple IWP
		

Table 6.2: Patterns of IWP geometry.

In tables (6.1),(6.2),(6.3), the gyroid, IWP, and Primitive geometry encapsulated into the same box with a double and a quadruple periodicity pattern are illustrated. It is noted

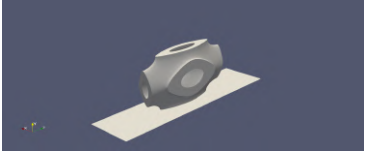
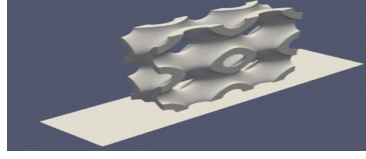
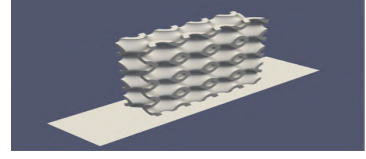
Case T3: Primitive	Case S1e: Dual Primitive	Case S1f: Quadruple Primitive
		

Table 6.3: Patterns of Primitive geometry.

that the more times the single cell of a TPMS is repeated, the finer the grid is needed to capture the flow details.

6.1.1 Gyroid patterns

In figure (6.1) temperature iso-areas are presented. The thickness of the thermal boundary layer is higher than in case T1. That leads to higher \bar{T}_{out}^F . All repeated gyroids have

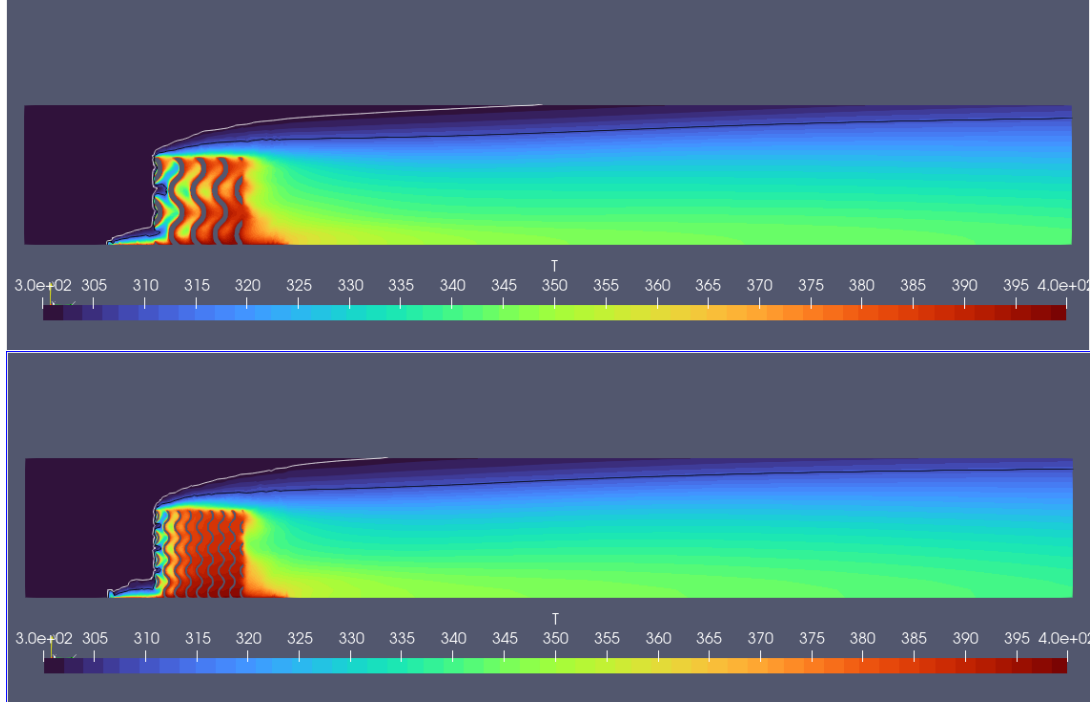


Figure 6.1: Temperature iso-areas at midplane of x-direction for cases S1a (up), S1b (down). The white lines indicate the 301 K iso-line, while the black lines correspond to the 310 K. iso-line.

been placed in figure (6.2). As the geometry becomes more complicated, the surface that comes in contact with the cooling fluid becomes larger. The total pressure loss coefficient increases due to the higher friction. Even though complicated surfaces enhance heat exchange between the fluid and the metal, heat transfer inside the solid geometry becomes more difficult. As a result, there is an upper limit to the \bar{T}_{out}^F . For that reason, the dual pattern of the gyroid has a higher \bar{T}_{out}^F than the quadruple one. The results shown in figure (6.2) are also presented in table (6.4).

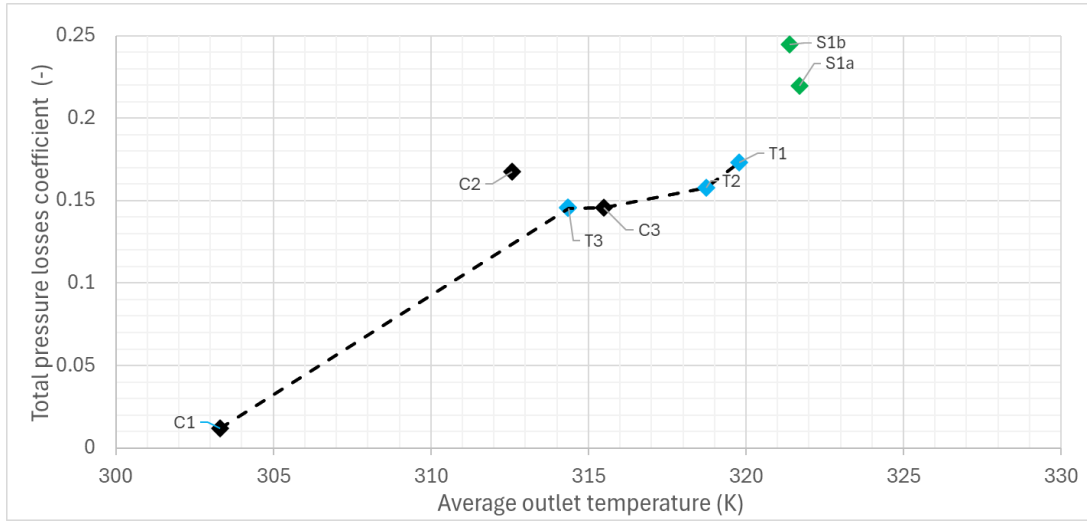


Figure 6.2: Comparison of repeated gyroid geometries (green colored) with conventional (black colored) and basic TPMS (blue colored) geometries.

Geometry	T1	S1a	S1b
$\omega_{t,losses}[-]$	0.1731	0.2195	0.2445
$T_{outlet}[K]$	319.78	321.69	321.39

Table 6.4: Performance metrics of the repated cell Gyroid geometries of figure (6.2).

6.1.2 IWP patterns

In figure (6.3), the temperature iso-areas of IWP patterns that are presented in figure (6.2) with temperature iso-lines are shown. It is obvious, from figure (6.4) and table (6.4), that the behavior of the IWP is not different from that of the gyroid. Specifically, there is an efficiency improvement for the double IWP, but the quadruple IWP decreases the average outlet temperature. Thus, the total pressure loss coefficient is increased. The empty case and the heat sink geometry are included to make the benefits of TPMS more visible.

Geometry	T2	S1c	S1d
$\omega_{t,losses}[-]$	0.1578	0.2156	0.2384
$T_{outlet}[K]$	318.74	320.87	320.96

Table 6.5: Performance metrics of repeatedIWP geometries of figure (6.4).

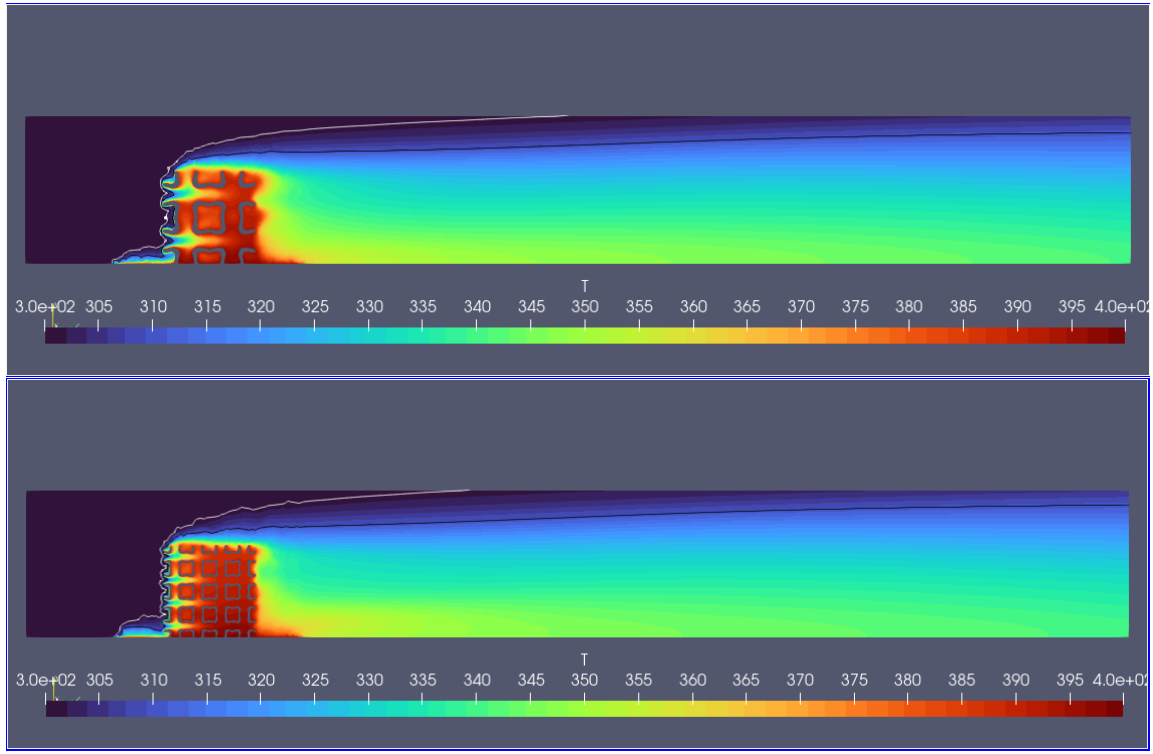


Figure 6.3: Temperature iso-areas at midplane of x-direction for cases S1c (up), S1d (down). The white lines indicate the 301 K iso-line, while the black lines correspond to the 300 K iso-line.

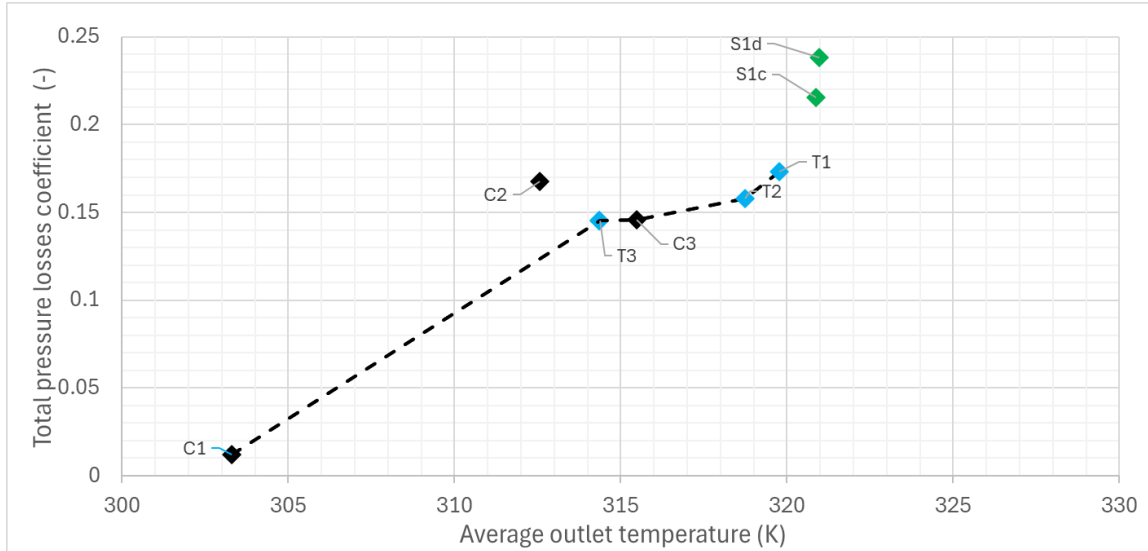


Figure 6.4: Comparison of repeated IWP geometries (green colored) with conventional (black colored) and basic TPMS (blue colored) geometries. The front of the so-far non-dominated solutions is displayed with the non-continuous line.

6.1.3 Primitive patterns

The last repeated TPMS geometries to be examined are the geometries of table (6.3). Figure (6.5) shows a similar profile.

However, it is remarkable that the performance of the dual Primitive is similar to that

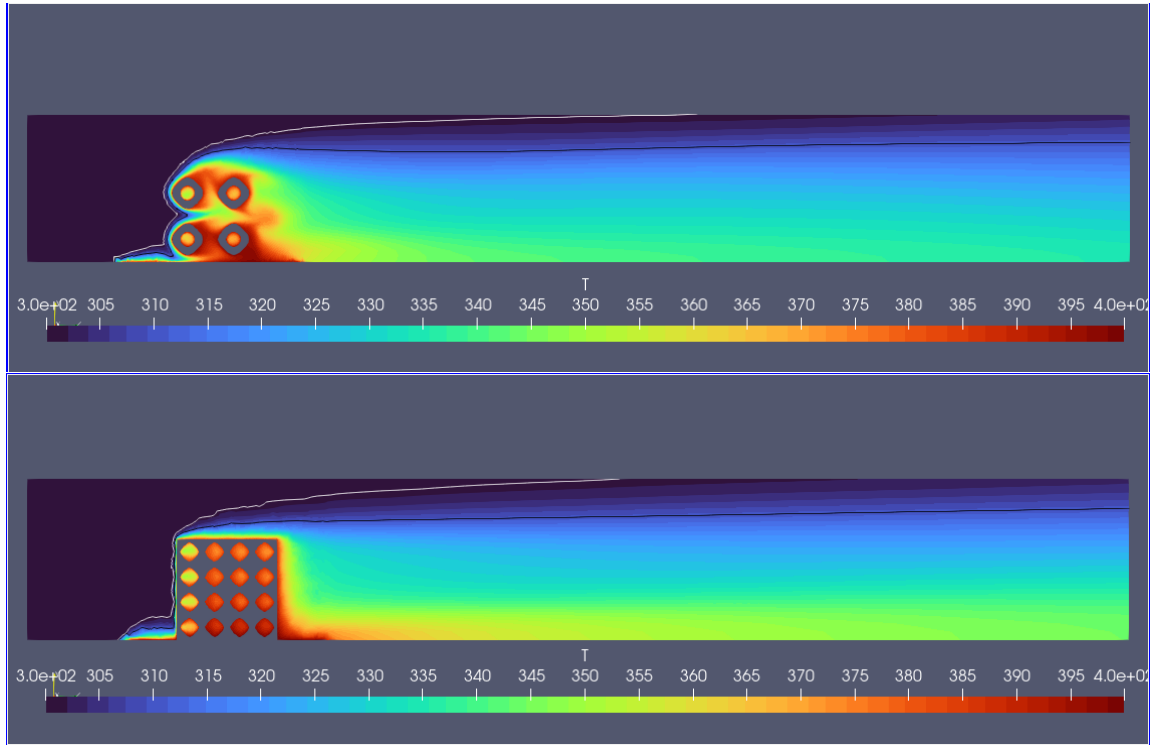


Figure 6.5: Temperature iso-areas at midplane of x-direction for cases S1e (up), S1f(down). The white lines indicate the 301 K iso-line, while the black lines correspond to the 310 K iso-line.

of the quadruple case. Figure (6.6) and table (6.6) compares the Primitive with the heat-sink geometry and the empty case, in detail.

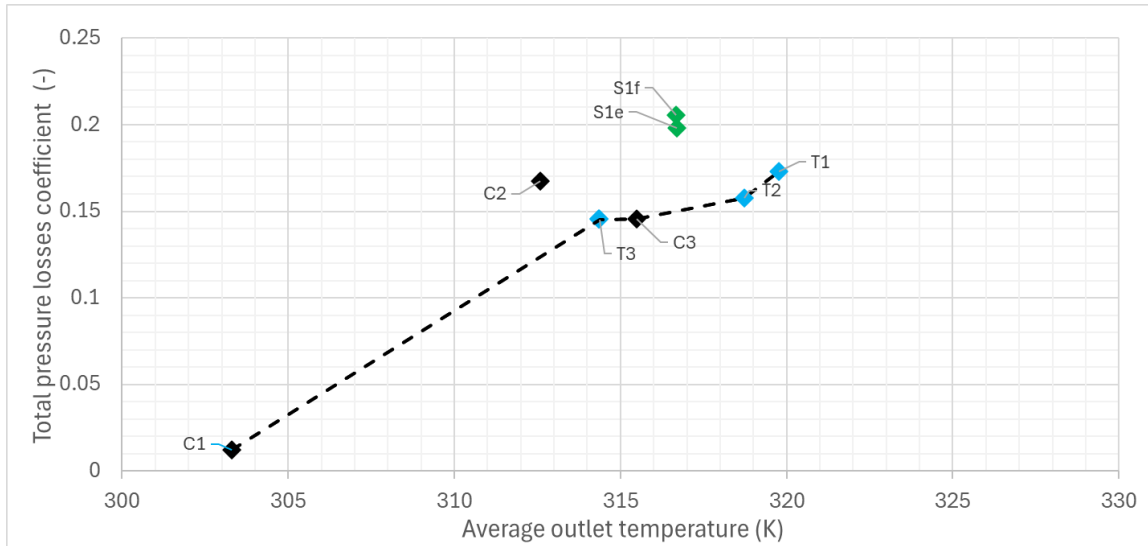


Figure 6.6: Comparison of repeated Primitive geometries (green colored) with conventional (black colored) and basic TPMS (blue colored) geometries. The front of the so-far non-dominated solutions is displayed with the non-continuous line.

Geometry	T3	S1e	S1f
$\omega_{t,losses}[-]$	0.1453	0.1980	0.2053
$T_{outlet}[K]$	314.37	316.70	316.67

Table 6.6: Performance of repeated Primitive geometries of figure (6.6).

6.1.4 Analysis of Results

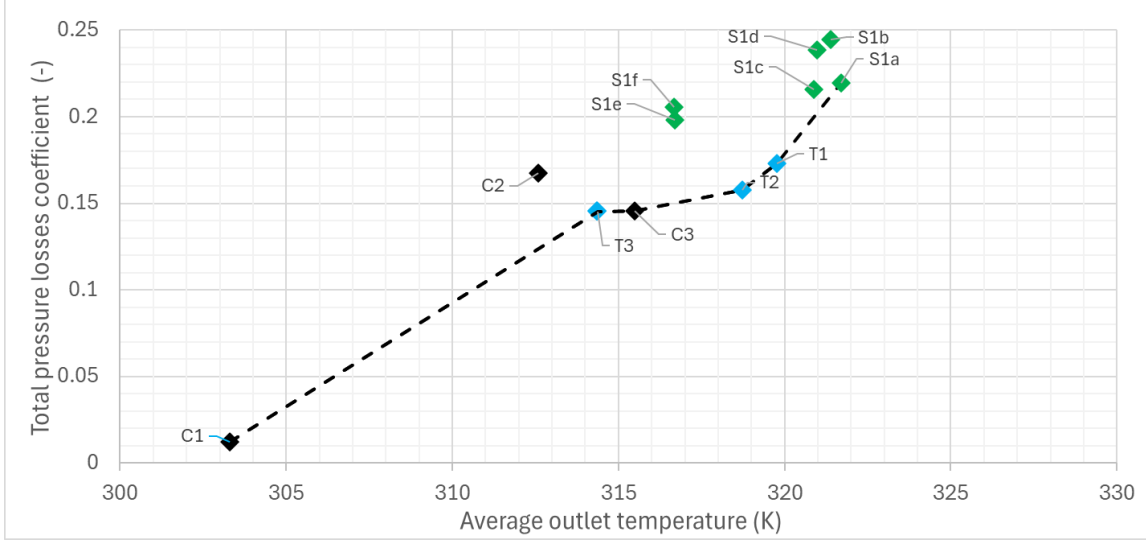


Figure 6.7: Summary of results of the first parametric study (green colored), conventional (black colored), and basic TPMS (blue colored) geometries. The front of the so-far non-dominated solutions is displayed with the non-continuous line.

Geometry	C1	T3	C3	T2	T1	S1a
$\omega_{t,losses}[-]$	0.01215	0.1453	0.146	0.1578	0.17318	0.2195
$T_{outlet}[K]$	303.3	314.37	315.49	318.74	319.78	321.69

Table 6.7: Current optimal front of figure (6.7).

In figure (6.7) and table(6.7) all the simulated geometries are presented. The dual geometries promote heat transfer because the wet area increases. However, all quadruple geometries have higher total pressure losses and similar thermal performance to the double-pattern geometries, and for that reason, all the quadruple-patterned geometries do not belong to the front of the so-far non-dominated solutions. As a result, geometry S1a, which is not dominated by any other, is included in the front.

6.2 Parametric Study 2: Thickness

This section examines non-uniform thickness distributions along the flow direction (z-axis). Specifically, the cases of the single cell¹ of a gyroid, IWP, and a Primitive will be used with either increasing or decreasing thickness along the z-axis. For example, at figure (6.8) is the section of the fluid channel where the fluid enters the cooling geometry, the relative density is equal to 10%, while where fluid exits the cooling geometry (figure (6.10)), relative density is 90%.



Figure 6.8: Inlet Gyroid section.

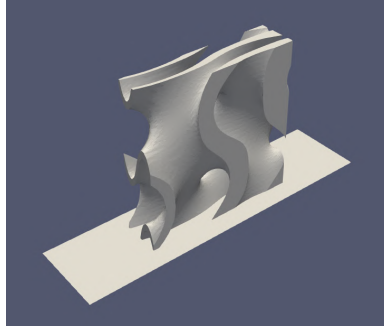


Figure 6.9: Non-constant thickness Gyroid.



Figure 6.10: Outlet gyroid section.

6.2.1 Non-uniform thickness Gyroid

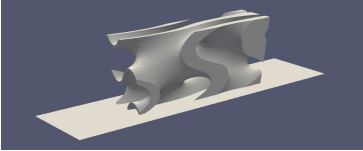
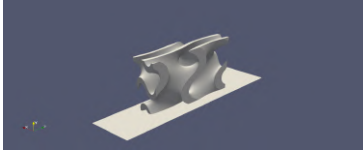
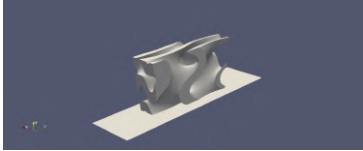
Case S2a: Increasing Thickness Gyroid	Case T1: Gyroid	Case S2b: Decreasing Thickness Gyroid
		

Table 6.8: Geometries of non-uniform thickness for Gyroid geometry.

In figure (6.11), temperature iso-areas of increasing and decreasing thickness are presented. The thermal boundary layer is thicker in case S2a than S2b.

Geometry	S2a	T1	S2b
$\omega_{t, \text{losses}} [-]$	0.1943	0.1732	0.1907
$T_{\text{outlet}} [K]$	320.15	319.78	320.77

Table 6.9: Performance metrics of non-uniform Gyroid geometries of figure (6.14).

¹Minimal of a TPMS

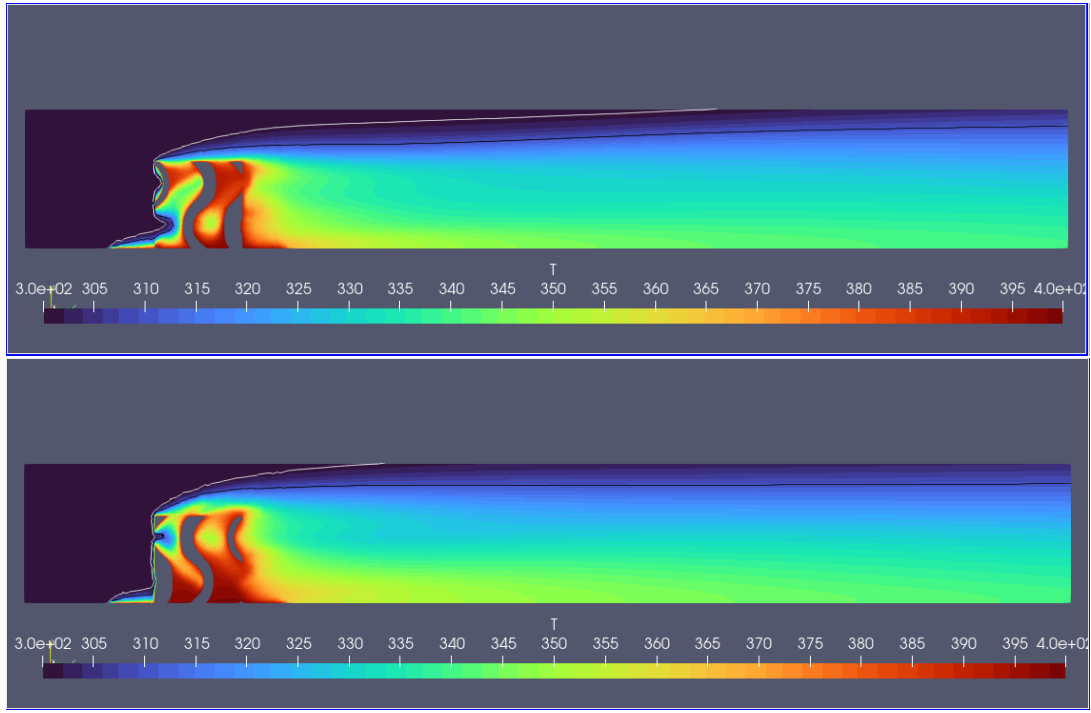


Figure 6.11: Temperature iso-areas at midplane of x-direction for cases S2a (up), S2b(down). The white lines indicate the 301 K iso-line, while the black lines correspond to the 310 K iso-line.

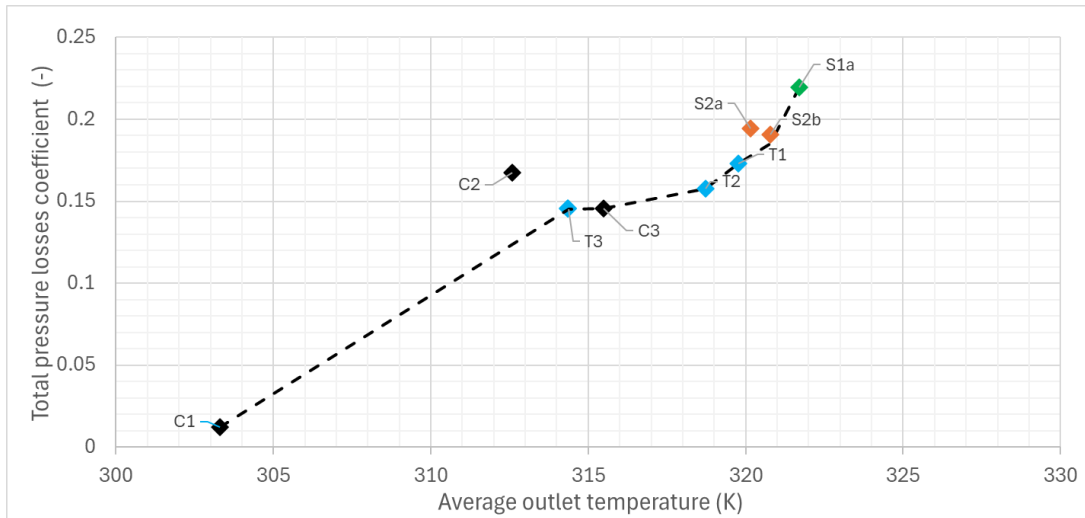


Figure 6.12: Comparison of so-far non-dominated geometries with non-uniform thickness Gyroid geometries(orange colored). The front of the so-far non-dominated solutions is displayed with the non-continuous line.

Varying the thickness increases the total-pressure-loss coefficient. Both increasing and decreasing thickness Gyroids have a higher \bar{T}_{out}^F than the normal gyroid. From figure (6.14), for similar total-pressure losses, TPMS geometries achieve an outlet temperature higher by 8 K.

6.2.2 Non-constant thickness IWP

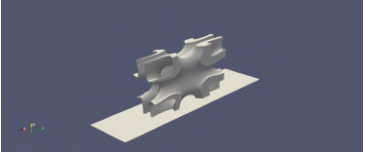
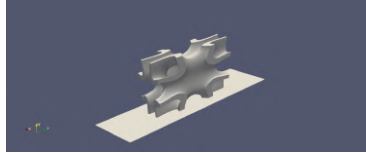
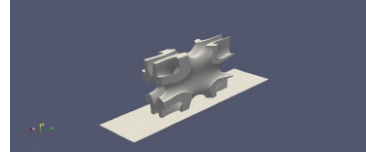
Case S2c: Increasing Thickness IWP	Case T2: IWP	Case S2d: Decreasing Thickness IWP
		

Table 6.10: Geometries of non-constant thickness for IWP geometry.

Different thickness distributions for the geometry IWP are examined. In figure (6.14), the coefficient of total pressure losses is higher than in the case of the heat sink, but \bar{T}_{out}^F at the outlet is almost higher by 6 K. Moreover, the IWP, which increases its thickness, has better thermal behavior than the Gyroid geometry.

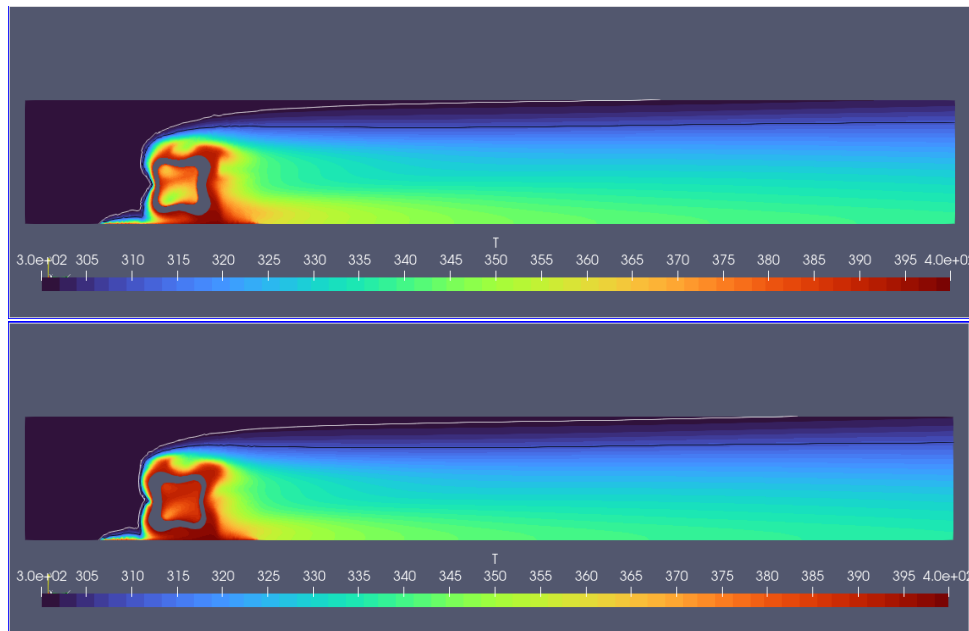


Figure 6.13: Temperature iso-areas at midplane of x-direction for cases S2c (up), S2d(down). The white lines indicate the 301 K iso-line, while the black lines correspond to the 310 K iso-line.

Geometry	S2c	T2	S2d
$\omega_{t,losses}[-]$	0.17381	0.158	0.17429
$T_{outlet}[K]$	318.92	318.74	316.87

Table 6.11: Performance metrics of non-uniform IWP geometries of figure (6.14).

6.2.3 Non-constant thickness Primitive

Figure (6.15) depicts the temperature field of the increasing and decreasing thickness of the Primitive geometry.

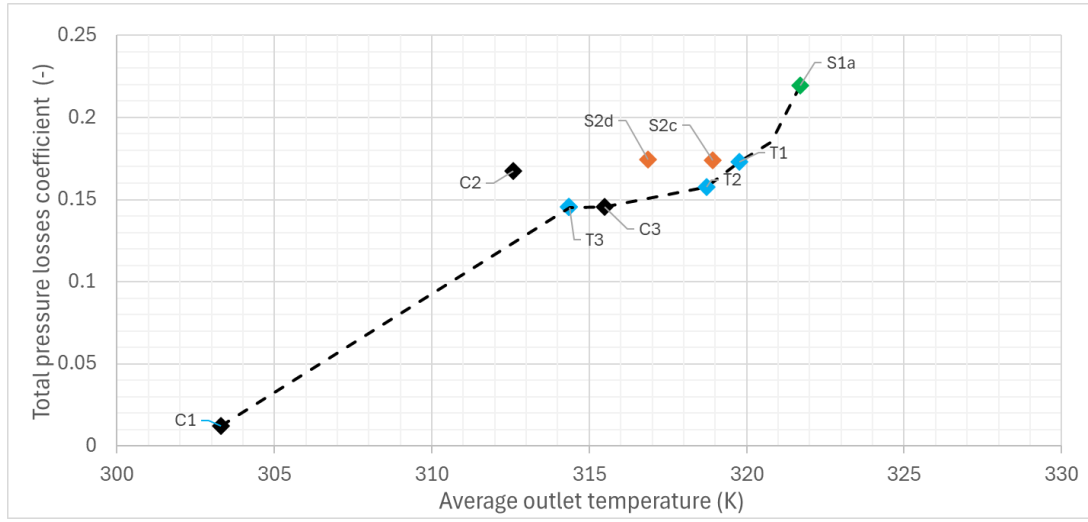


Figure 6.14: Comparison of so-far non-dominated geometries with non-uniform thickness IWP geometries (orange colored).

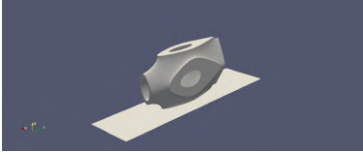
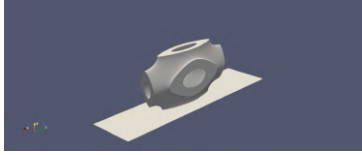
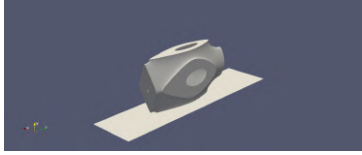
Case S2e: Increasing Thickness Primitive	Case C3: Primitive	Case S2f: Decreasing Thickness Primitive
		

Table 6.12: Geometries of variable thickness for Primitive geometry.

According to table (6.13), decreasing the thickness Primitive geometry has a similar average outlet temperature but increased total pressure losses due to the bigger recirculation regions inside. The increasing thickness Primitive has better heat efficiency but much more total pressure losses. In general, all the cases of that section have better performance than the traditional heat sink. Considering the slight enhancement demonstrated by the Primitive case, it is reasonable to expect that its alternative configurations will not offer significant improvement compared to the other TPMS geometries.

Geometry	S2e	Primitive	S2f
$\omega_{t,losses}[-]$	0.166	0.1453	0.1541
$T_{outlet}[K]$	315.51	314.37	314.34

Table 6.13: Performance of the non-dominated solutions figure (6.16).

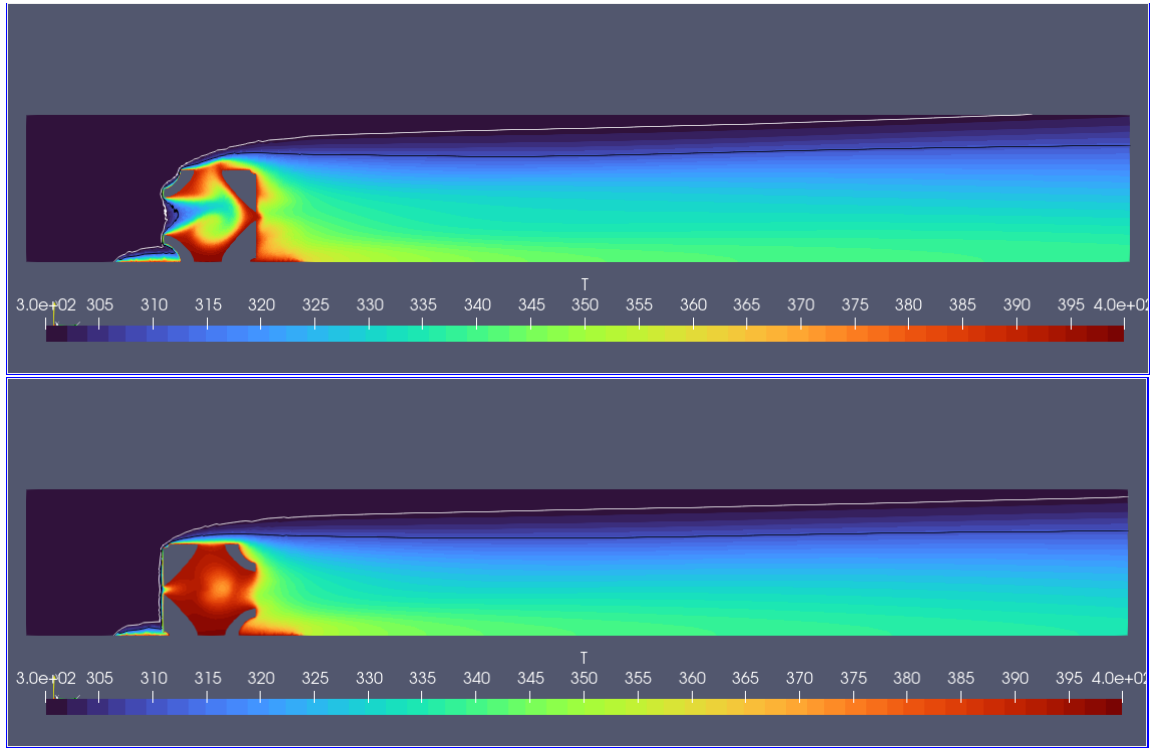


Figure 6.15: Temperature iso-areas at midplane of x-direction for cases S2e (up), S2f (down).

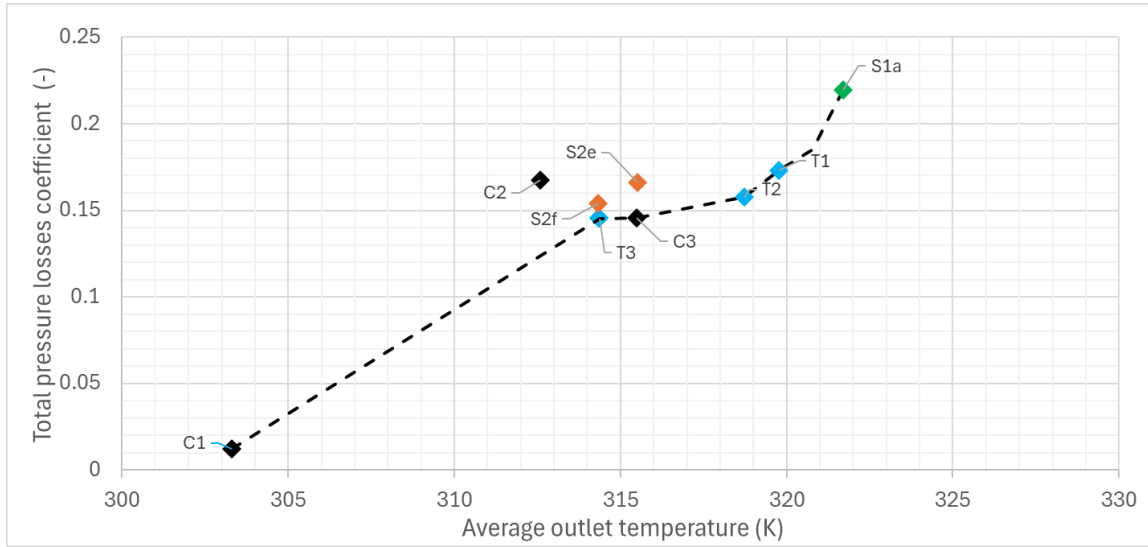


Figure 6.16: Comparison of so-far non-dominated geometries with non-uniform thickness Primitive geometries (orange colored).

6.2.4 Analysis of Results

Geometry	C1	T3	C3	T2	T1	S2b	S1a
$\omega_{t,losses}[-]$	0.0122	0.1453	0.1457	0.1578	0.1732	0.1851	0.2195
$T_{outlet}[K]$	303.30	314.37	315.49	318.74	319.78	320.77	321.69

Table 6.14: Performance metrics of non-uniform Primitive geometries of figure (6.17).

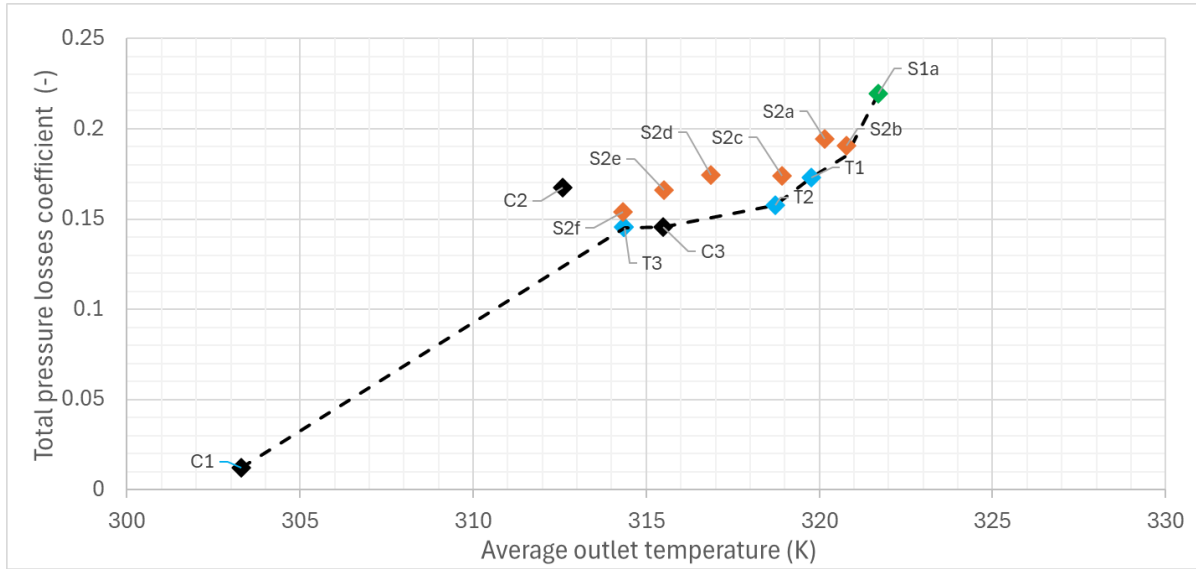


Figure 6.17: Summary results of the second parametric study (orange colored), conventional (black colored), basic TPMS (blue colored) geometries, and the first parametric study (green colored).

Having a non-constant thickness in all cases increases the total pressure losses coefficient because of recirculation regions or the local small canals which are created inside the heat exchange geometry. From all the non-uniform thickness geometries that have been examined, only the decreasing thickness Gyroid was incorporated into the front of non-dominated solutions.

Each TPMS behaves differently under thickness variation. For example, some cases increased the \bar{T}_{out}^F while others reduced it. However, the total pressure losses make this parameter unreliable for the thermal efficiency, and will not be used in subsequent studies.

6.3 Parametric Study 3: Solid network TPMS geometries

An alternative concept of TPMS is to use their Solid Network geometry. All Network Solid geometries can be created from the extrusion method presented in Chapter 3. Solid-network TPMS form a single, interconnected flow channel, unlike solid-sheet extrusions, which create two disconnected sub-channels (figure (6.18)); merging sub-channels occurs only downstream of the geometry. Apart from the single-cell heat transfer enhancing geometries promoting heat exchange, repeated patterns will be tested too.

6.3.1 Solid Network Gyroid, IWP, Primitive

Using MsLattice is the Solid Network TPMS are generated. From figure (6.19), it is obvious that the thermal boundary layer is thicker than the geometries examined in previous chapters.

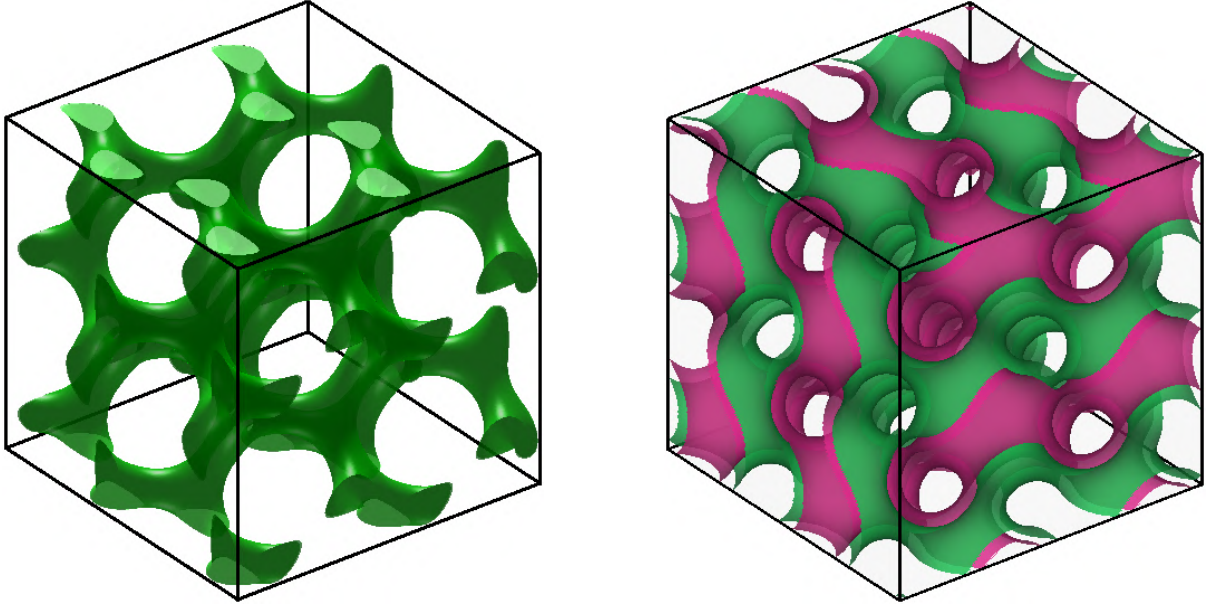


Figure 6.18: Double (pink and green color) sub-channel inside a solid sheet geometry (left) and single channel in a network solid geometry.

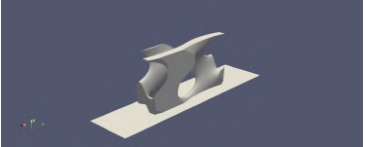


Case S3a: Solid Network Gyroid	Case S3b: Solid Network IWP	Case S3c: Solid Network Primitive
		

Table 6.15: Geometries of network sheet extrusions.

Geometry	S3c	S3b	S3a
$\omega_{t,losses}[-]$	0.0315	0.0412	0.052
$T_{outlet}[K]$	315.81	321.63	325.72

Table 6.16: Performance of solid network extruded geometries of figure (6.20).

According to figure (6.20), solid network geometries have higher efficiency. The \bar{T}_{out}^F is higher, and the solid network Gyroid has the highest one of all the previous cases. The total pressure losses are lower than all the previous cases, and it is also close to the total pressure losses of the empty case scenario. Additionally, heat exchange efficiency (Primitive, IWP, Gyroid) remains the same for their Network Solid form. These three new solutions completely dominate all the others. Thus, only network solid extrusions are used in the forthcoming studies.

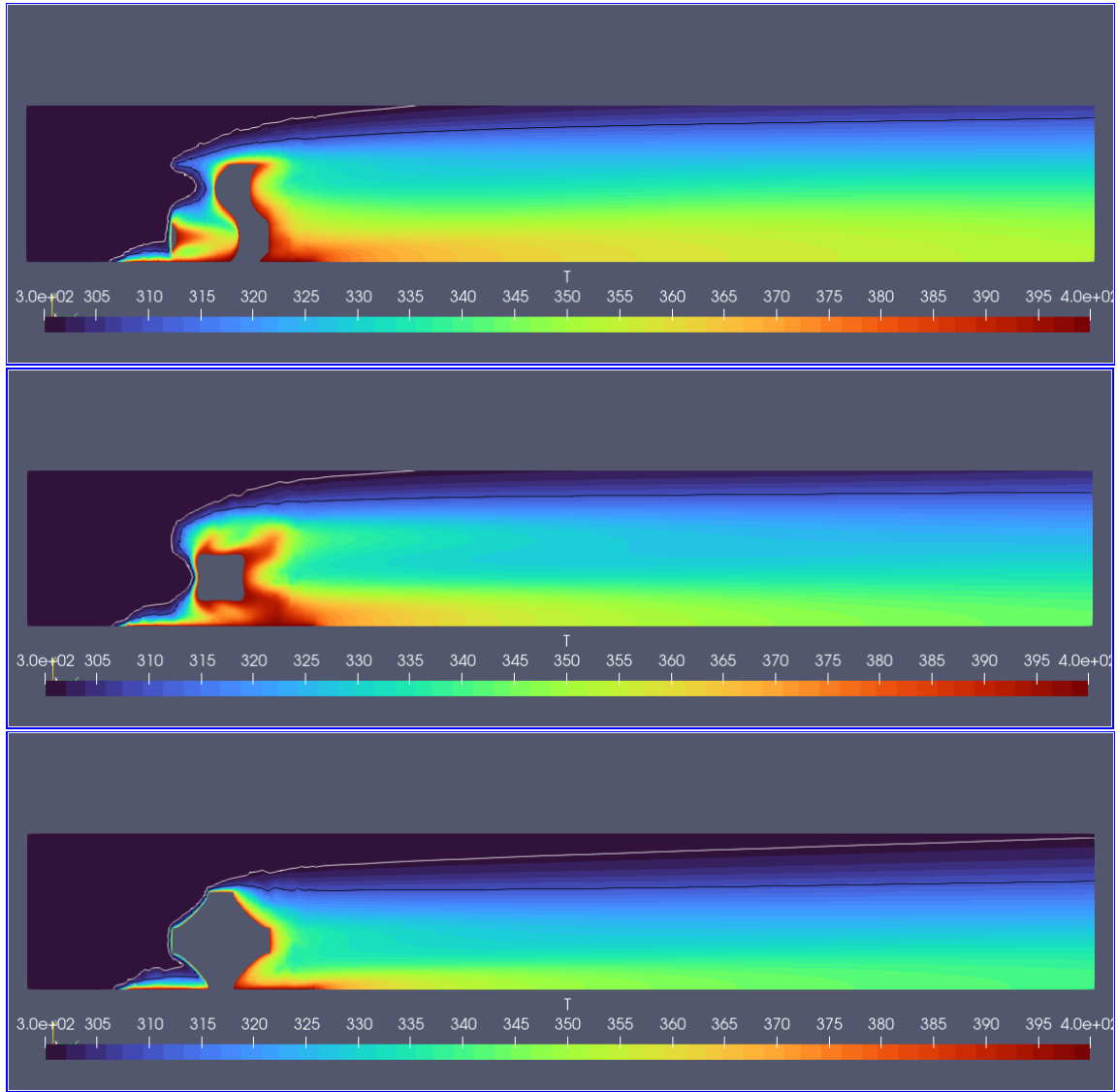


Figure 6.19: Temperature iso-areas at midplane of x-direction for cases S3a (up), S3b (mid), S3c (low).

6.3.2 Solid network Gyroid Patterns

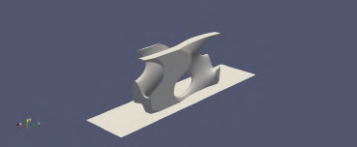
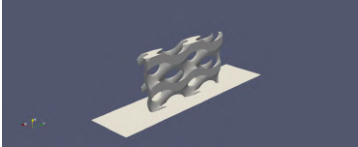
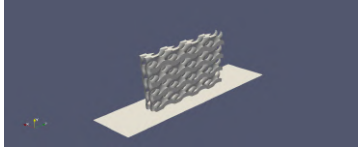
Case S3a: Solid Network Gyroid	Case S3d: Dual Solid Network Gyroid	Case S3e: Quadruple Solid Network Gyroid
		

Table 6.17: Patterns of network sheet Gyroid geometries promoting heat exchange.

Using the solid network Gyroid geometry and increasing the number of the repeats of Gyroid's unit cell, the dual and quadruple Gyroid are created (table (6.17)). According to figure(6.21) and table (6.18), the total pressure losses coefficient increased, as expected,

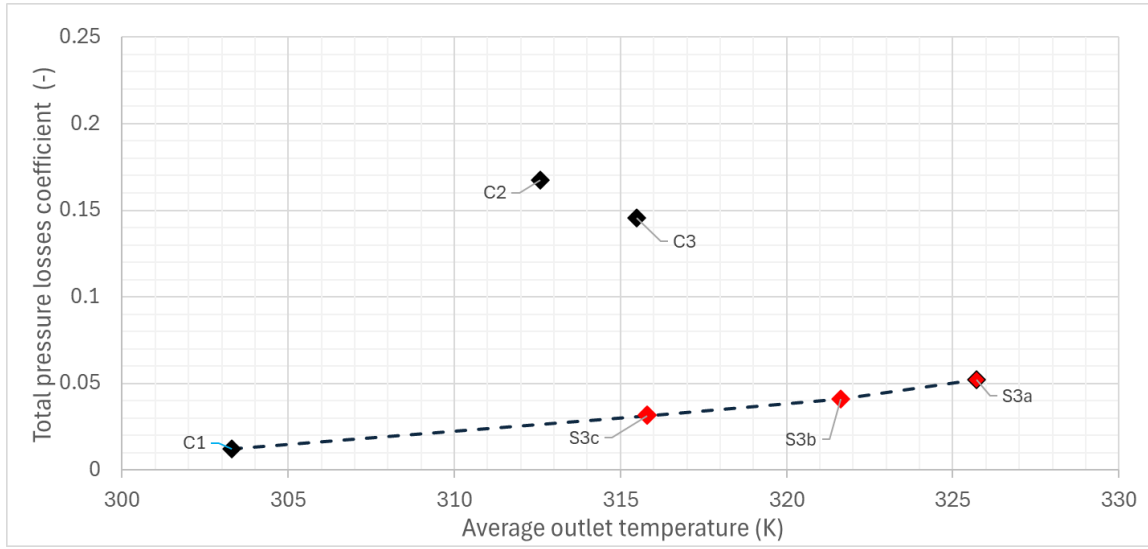


Figure 6.20: Comparison of so-far non-dominated geometries with solid network extruded basic TPMS (red colored).

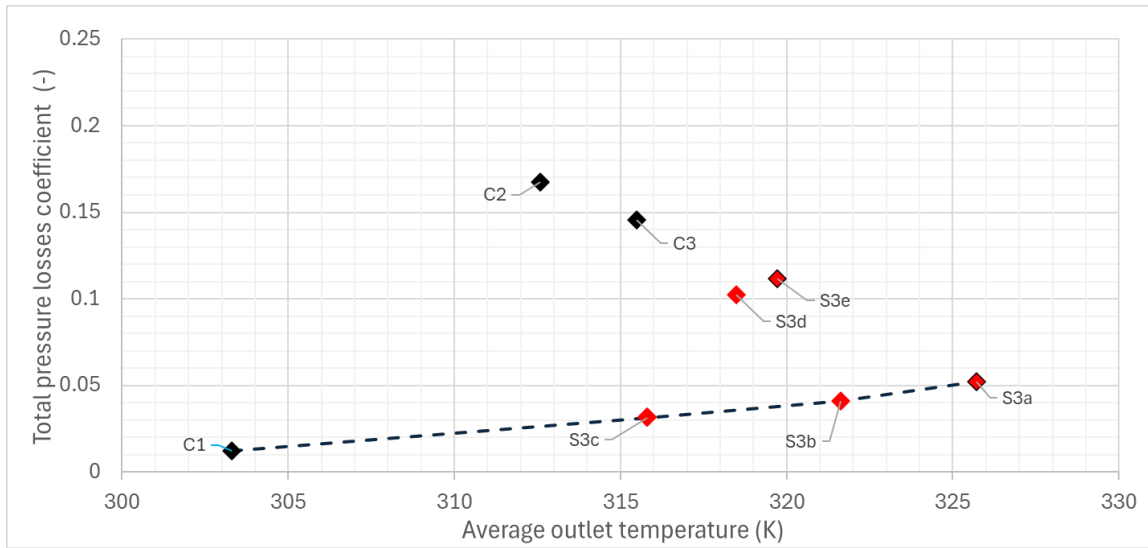


Figure 6.21: Comparison of so-far non-dominated geometries with solid network Gyroid patterns (red colored).

but \bar{T}_{out}^F reduced. However, these cases perform better than cases C2 and C3.

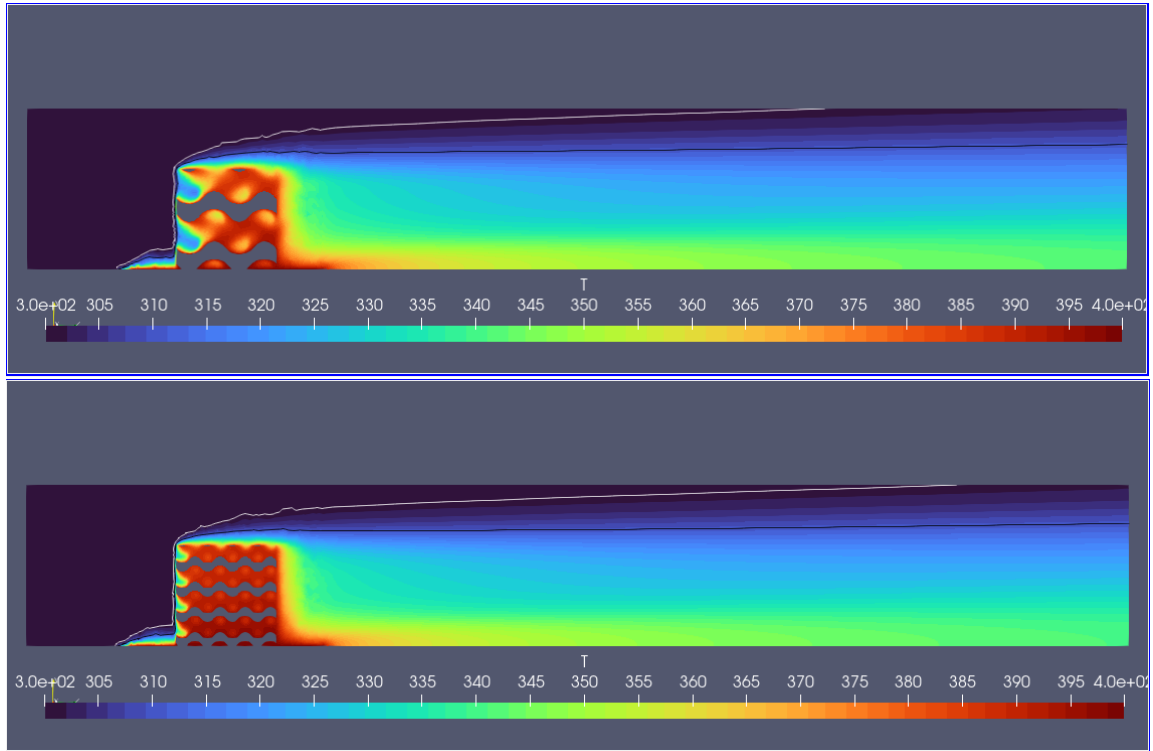


Figure 6.22: Temperature iso-areas at midplane of x-direction for cases S3d (up), S3e (down).

Geometry	S3a	S3d	S3e
$\omega_{t,losses}[-]$	0.052	0.102	0.112
$T_{outlet}[K]$	325.72	318.48	319.71

Table 6.18: Performance metrics of solid network extruded Gyroid patterns of figure (6.21).

6.3.3 Solid Network IWP Patterns.

In figure (6.19), the dual and quadruple IWP are presented. Solid Network IWP geome-

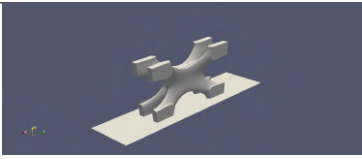
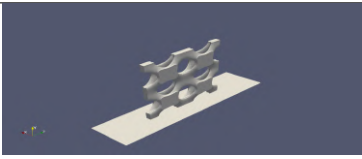
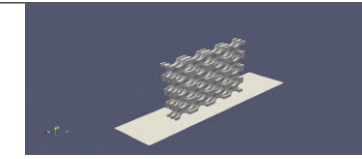
Case S3b: Solid Network IWP	Case S3f: Dual Solid Network IWP	Case S3g: Quadruple Solid Network IWP
		

Table 6.19: Patterns of network sheet IWP geometries promoting heat exchange.

tries also increase the total pressure loss coefficient. In addition, the \bar{T}_{out} of IWP and its patterns are between the temperatures of the solid sheet gyroid and the Primitive unit cells.

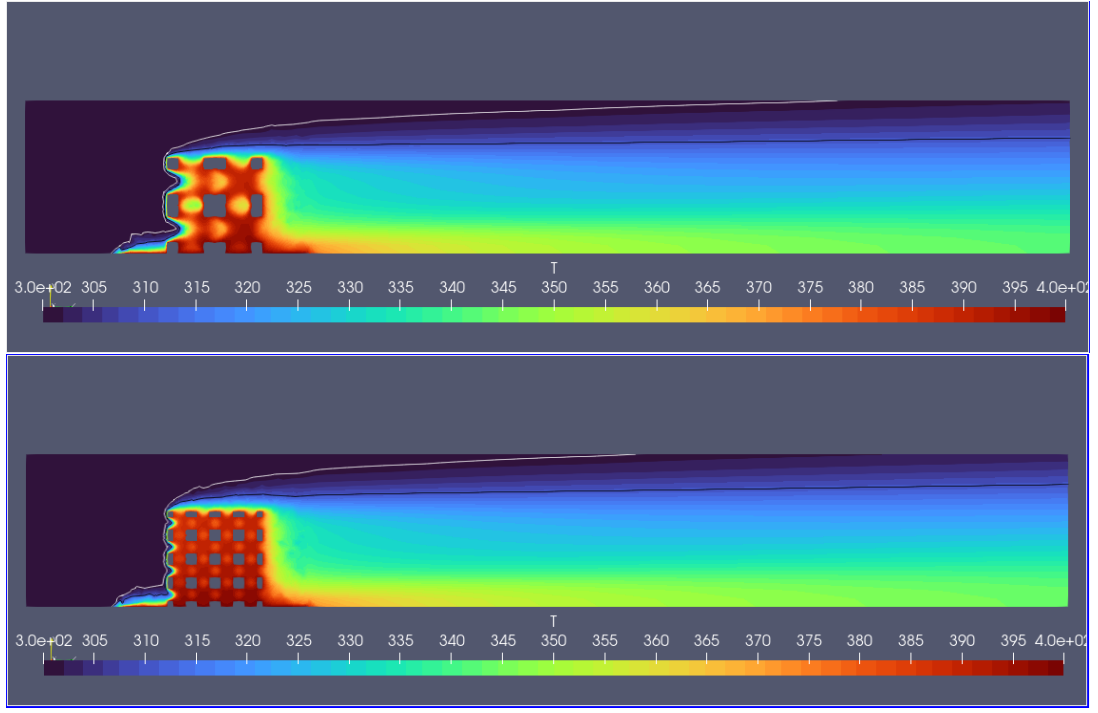


Figure 6.23: Temperature iso-areas at midplane of x-direction for cases S3f (up), S3g (down) .

Geometry	S3b	S3f	S3g
$\omega_{t,losses}[-]$	0.0411	0.0999	0.1161
$T_{outlet}[K]$	321.63	317.69	319.51

Table 6.20: Performance of solid network extruded IWP patterns of figure (6.24).

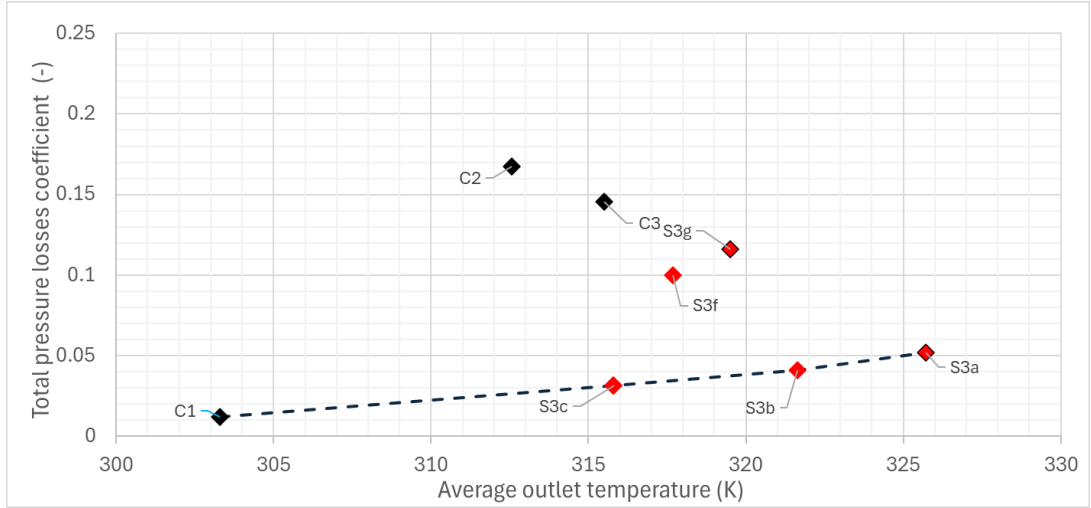


Figure 6.24: Comparison of so-far non-dominated geometries with solid network IWP patterns (red colored).

6.3.4 Solid Network Primitive Patterns

The Solid Network Primitive patterns perform differently since their thermal efficiency becomes even better. However, they are unable to achieve better performance than the Solid Network Gyroid and Solid Network IWP but the total pressure losses coefficient

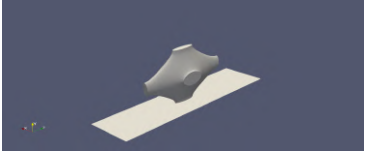
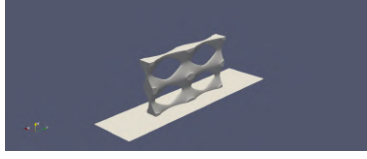
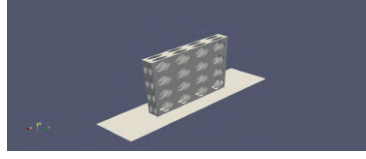
Case S3c: Solid Network Primitive	Case S3h: Dual Solid Network Primitive	Case S3i: Quadruple Solid Network Primitive
		

Table 6.21: Geometries of network prim extrusions.

Geometry	S3c	S3h	S3i
$\omega_{t,losses}[-]$	0.0315	0.0906	0.1262
$T_{outlet}[K]$	315.81	315.65	320.04

Table 6.22: Performance metrics of solid network extruded Primitive patterns of figure (6.26).

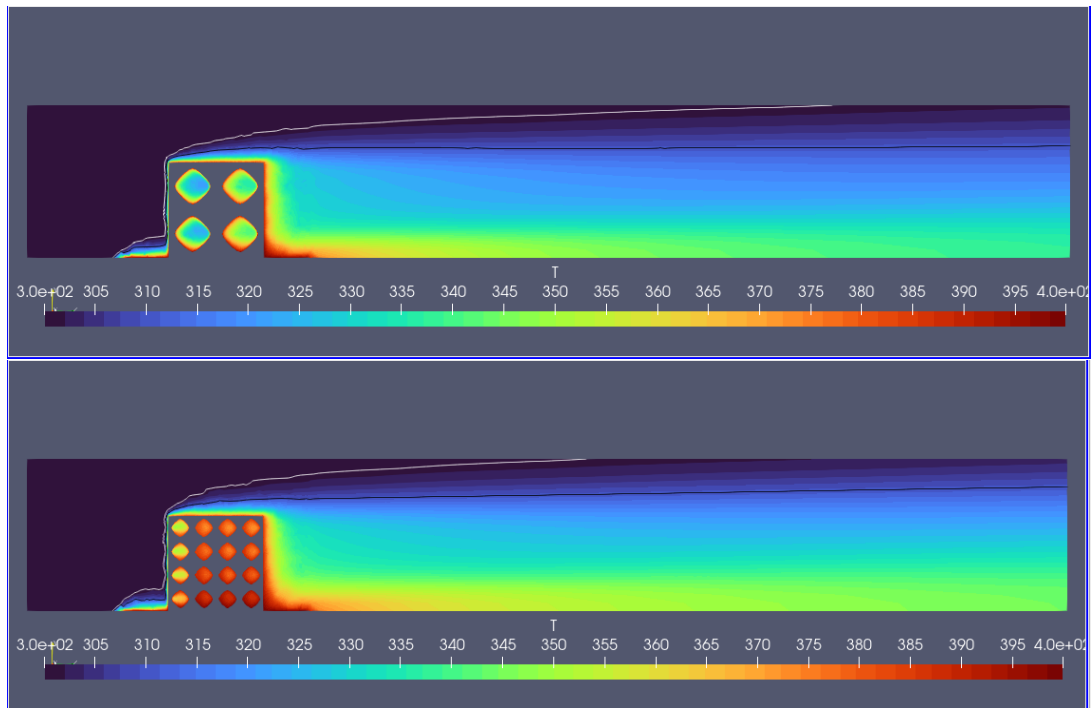


Figure 6.25: Temperature iso-areas at midplane of x-direction for cases S3h (up), S3i (down) .

takes on similar values.

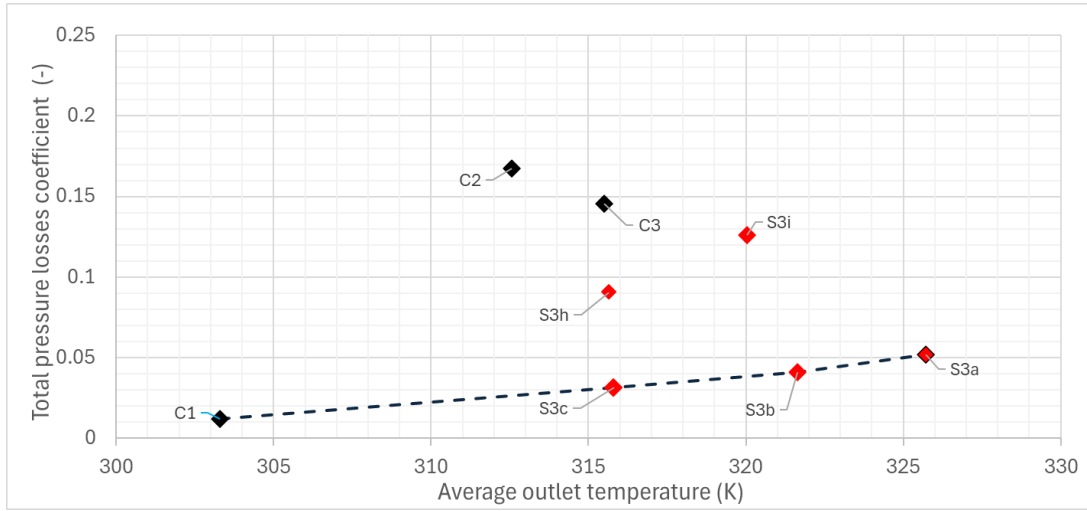


Figure 6.26: Comparison of so-far non-dominated geometries with solid network Primitive patterns (red colored).

6.3.5 Analysis of Results

The introduction of the solid network TPMS geometries offers more efficient solutions compared to the previous ones. Solutions S3a, S3b, and S3c not only reduces total pressure losses by about 50%, but increases \bar{T}_{out}^F even more (figure (6.27)). However, the repeated geometries did not manage to increase the average outlet temperature of the working fluid, and their pressure losses were, on the one hand, better than all the sheet solid geometries promoting heat exchange, but on the other hand, less efficient in comparison with the single-cell network extruded surfaces. Therefore, pattern geometries will not be used in further studies, which all include geometries generated through network solid extrusion.

Among all examined solutions, S3a and S3b reduce the total pressure losses to almost 1/3 of those of the traditional geometries and significantly increase the heat exchange profit (the \bar{T}_{out}^F when a cooling geometry is placed) by almost 10 K.

Geometry	C1	S3c	S3b	S3a
$\omega_{t,losses}[-]$	0.01214	0.1453	0.0412	0.052
$T_{outlet}[K]$	303.31	314.37	321.63	325.72

Table 6.23: Performance of solid network extruded Gyroid patterns of figure (6.27).

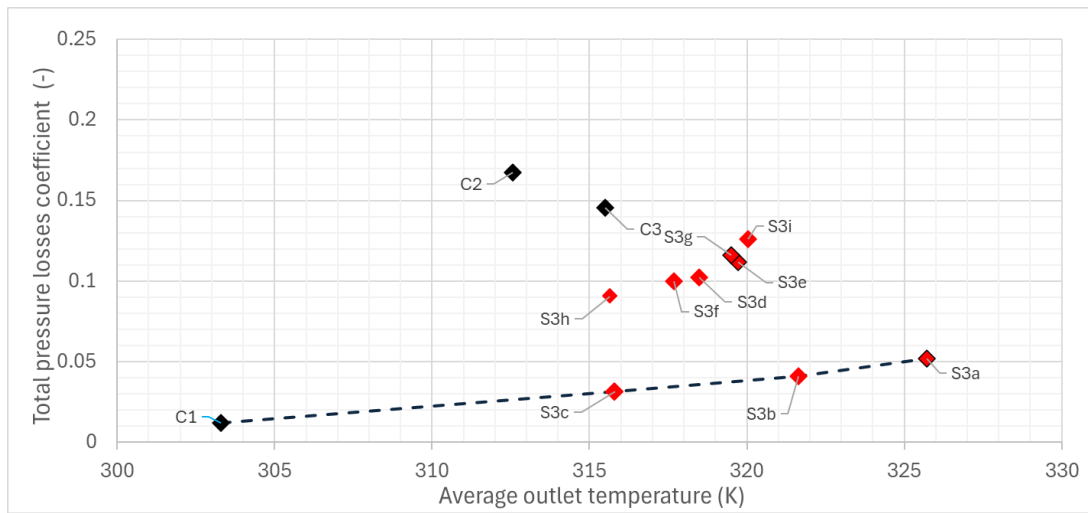


Figure 6.27: Summary results of the third parametric study (red colored), conventional (black colored), basic TPMS (blue colored) geometries, the first parametric study (green colored), and the second parametric study (orange colored).

Chapter 7

Hybrid TPMS

7.1 Theoretical background

This parametric study is concerned with the evaluation of mixed TPMS. There are many ways in which mixed TPMS can be generated, but two of them are used. The first one is the linear interpolation between the surface equations, and the second one will involve a gradual transition from one TPMS surface to another across the flow axis.

7.1.1 Linear interpolation

Given that equations 2.1 to 2.3 represent a TPMS, they can be interpolated into a single surface using a parameter t , which defines the proportion of each original geometry. For example, the equation that combines the Gyroid (figure (2.1)) with the IWP geometry (figure (2.2)) is:

$$\begin{aligned} F(x, y, z, t) = & t \left(\sin(X) \cos(Y) + \sin(Y) \cos(Z) + \sin(Z) \cos(X) \right) \\ & + (1 - t) \left(2 \left(\sin(X) \cos(Y) + \sin(Y) \cos(Z) + \sin(Z) \cos(X) \right) \right. \\ & \left. - \left(\cos(2(X)) + \cos(2(Y)) + \cos(2(Z)) \right) \right) = 0. \end{aligned} \quad (7.1)$$

Figure (7.1) presents the hybrid TPMS of equation 7.1 for three different values of parameter t . The geometries with t near to zero tend to resemble a Gyroid and near 1 an IWP. Another example is the mixture of Gyroid geometry with Primitive. This is expressed by the following equation equation 7.2 and figure (7.2):

$$\begin{aligned} F(x, y, z, t) = & t \left(\sin(2a\pi x) \cos(2b\pi y) + \sin(2b\pi y) \cos(2c\pi z) + \sin(2c\pi z) \cos(2a\pi x) \right) \\ & + (1 - t) (\cos(2a\pi x) + \cos(2b\pi y) + \cos(2c\pi z)) = 0. \end{aligned} \quad (7.2)$$

The last combination is the equation of IWP(2.2) with the equation of Primitive (2.3),

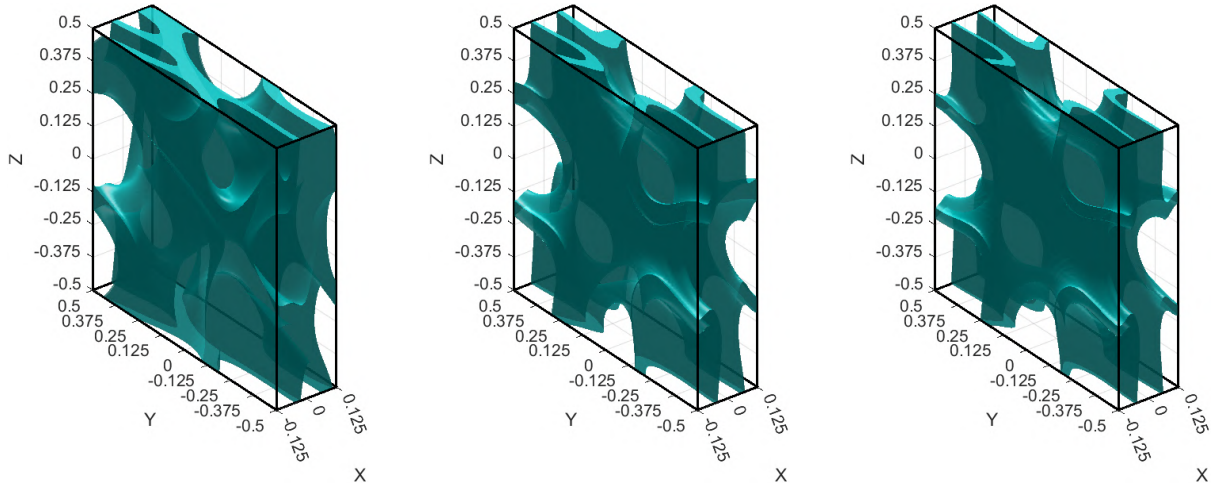


Figure 7.1: Hybrid Gyroid-IWP with $t=0.25$ (left), $t=0.5$ (mid), $t=0.75$ (right).

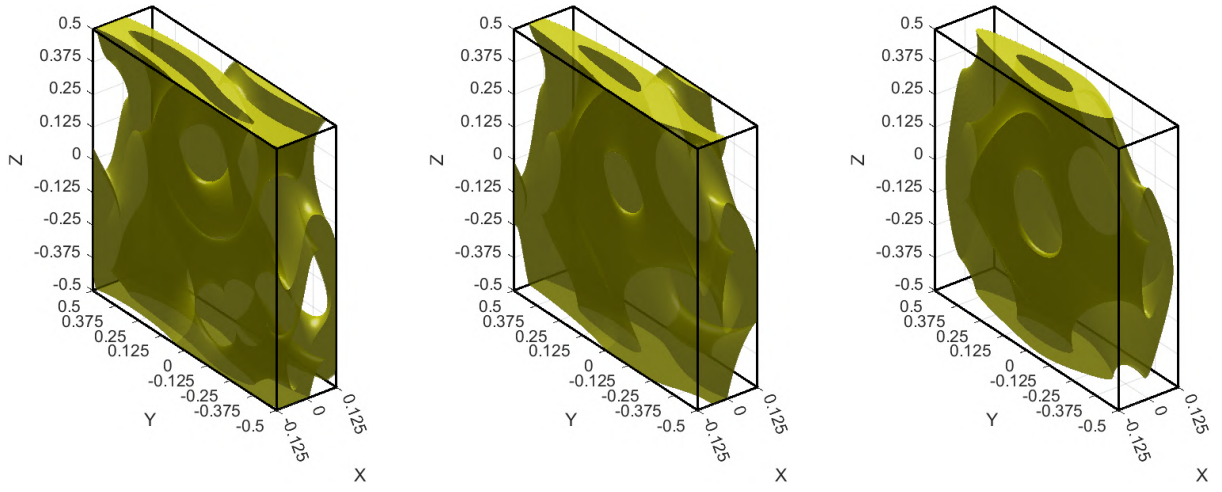


Figure 7.2: Hybrid Gyroid-Primitive with $t=0.25$ (left), $t=0.5$ (mid), $t=0.75$ (right).

which is given by the following equation and figure (7.3):

$$\begin{aligned}
 F(x, y, z, t) = & t \left(2 \left(\sin(2a\pi x) \cos(2b\pi y) + \sin(2b\pi y) \cos(2c\pi z) + \sin(2c\pi z) \cos(2a\pi x) \right) \right. \\
 & \left. - \left(\cos((4a\pi x)) + \cos(4b\pi y) + \cos((4c\pi z)) \right) \right) \\
 & + (1 - t) \left(\cos(2a\pi x) + \cos(2b\pi y) + \cos(2c\pi z) \right) = 0
 \end{aligned} \tag{7.3}$$

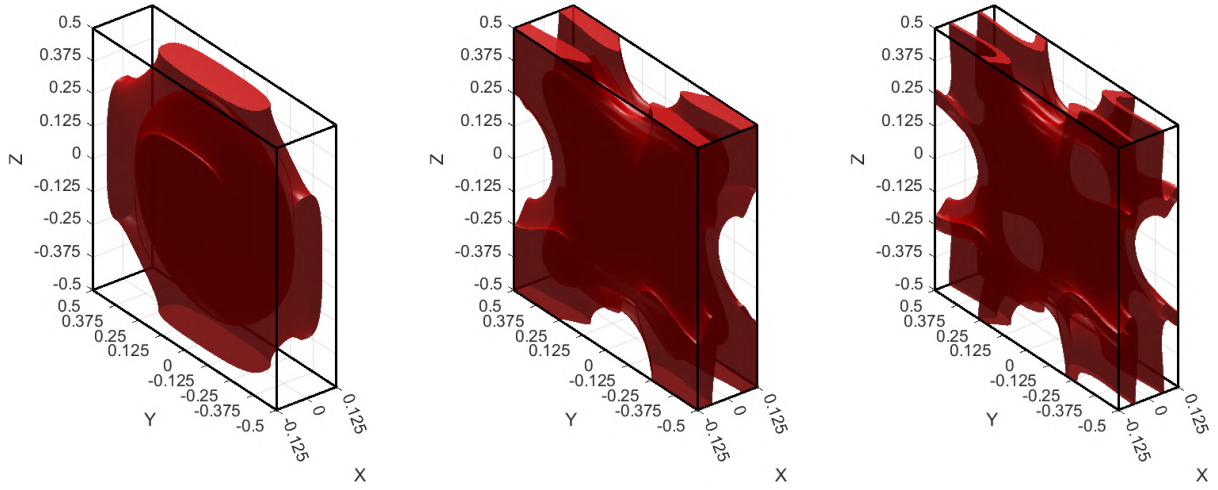


Figure 7.3: Hybrid IWP-Primitive with $t=0.25$ (left), $t=0.5$ (mid), $t=0.75$ (right).

7.1.2 Gradual interpolation

For this specific type of mixing, rather than using the parameter t , the geometry will change gradually from one TPMS to another across the flow axis. To achieve that, the parameter t varies along the Z dimension, which is the flow axis. Furthermore, the function is a third-degree polynomial with zero slope at the boundary values. This polynomial is $P(z) = -2z^3 + 3z^2$. As a result, equations (7.1), (7.2), and (7.3) are transformed into:

$$\begin{aligned}
 F(x, y, z, t) = & (-2z^3 + 3z^2) \left(\sin(2a\pi x) \cos(2b\pi y) + \sin(2b\pi y) \cos(2c\pi z) + \sin(2c\pi z) \cos(2a\pi x) \right) \\
 & + \left(1 - (-2z^3 + 3z^2) \right) \left(2 \left(\sin(2a\pi x) \cos(2b\pi y) + \sin(2b\pi y) \cos(2c\pi z) \right) \right. \\
 & \left. + 2 \sin(2c\pi z) \cos(2a\pi x) - \left(\cos(4a\pi x) + \cos(4b\pi y) + \cos(4c\pi z) \right) \right) = 0.
 \end{aligned} \tag{7.4}$$

$$\begin{aligned}
 F(x, y, z, t) = & (-2z^3 + 3z^2) \left(\sin(2a\pi x) \cos(2b\pi y) + \sin(2b\pi y) \cos(2c\pi z) + \sin(2c\pi z) \cos(2a\pi x) \right) \\
 & + \left(1 - (-2z^3 + 3z^2) \right) \left(\cos(2a\pi x) + \cos(2b\pi y) \right. \\
 & \left. + \cos(2c\pi z) \right) = 0.
 \end{aligned} \tag{7.5}$$

$$\begin{aligned}
 F(x, y, z, t) = & (-2z^3 + 3z^2) \left(2 \left(\sin(2a\pi x) \cos(2b\pi y) + \sin(2b\pi y) \cos(2c\pi z) + \sin(2c\pi z) \cos(2a\pi x) \right) \right. \\
 & \left. - \left(\cos(4a\pi x) + \cos(4b\pi y) + \cos(4c\pi z) \right) \right) \\
 & + \left(1 - (-2z^3 + 3z^2) \right) \left(\cos(2x\pi a) + \cos(2b\pi y) + \cos(2c\pi z) \right) = 0
 \end{aligned} \tag{7.6}$$

Figures (7.4), (7.5), and (7.6) show the geometries generated by equations (7.4), (7.5), (7.6).

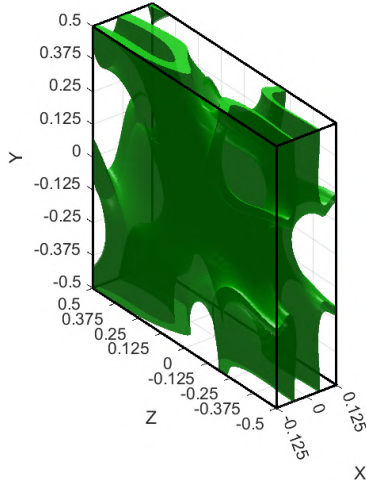


Figure 7.4: Hybrid IWP-Prim.

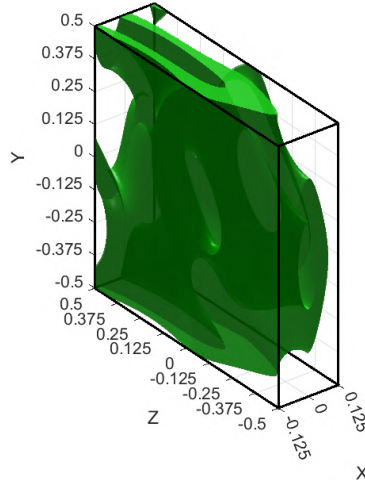


Figure 7.5: Hybrid Primitive-Gyroid.

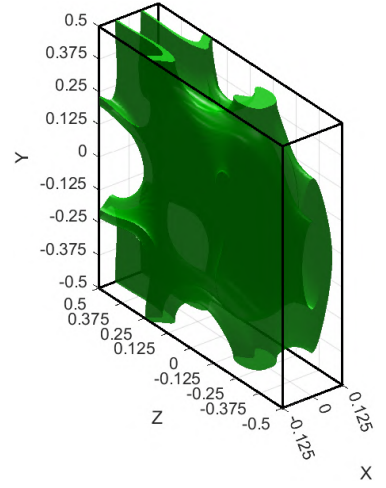


Figure 7.6: Hybrid Primitive-IWP.

7.2 Hybrid Gyroid - IWP

In table (7.1), all the geometries that result from the linear combination of Gyroid and IWP, according to equation (7.1), are presented for different values of t . According to

Case S4a: 75%IWP-25%Gyroid	Case S4b: 50%IWP-50%Gyroid	Case S4c: 25%IWP-75%Gyroid

Table 7.1: Intermediate structures between Gyroid and IWP surfaces.

geometry	S3b	S4a	S4b	S4c	S3a
t	0	0.25	0.5	0.75	1
$\omega_{t,losses}[-]$	0.0412	0.0537	0.0526	0.0543	0.052
$\bar{T}_{outlet}[K]$	321.63	323.41	323.56	325.68	325.72

Table 7.2: Performance metrics of intermediate geometries between Gyroid and IWP.

figure (7.7), the efficiency of intermediate forms between gyroid and IWP is between those of the main corresponding components (Gyroid and IWP). Additionally, these three new cases are completely dominated by the solid network Gyroid geometry. As a result, these solutions cannot be incorporated into the current optimal front.

7.3 Hybrid Primitive-Gyroid

In this case, intermediate geometries between Gyroid and Primitive according to equation 7.2 are examined.

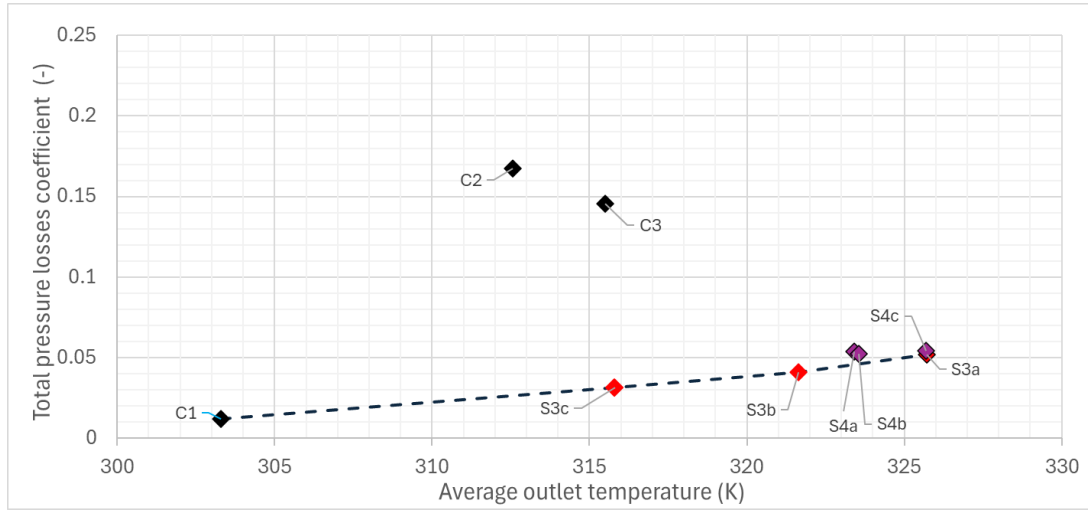


Figure 7.7: Comparison of so-far non-dominated geometries with intermediate geometries between Gyroid and IWP (purple colored).

Case S4d: 75%Primitive-25%Gyroid	Case S4e: 50%Primitive-50%Gyroid	Case S4f: 25%Primitive-75%Gyroid

Table 7.3: Intermediate structures between Gyroid and IWP surfaces..

geometry	S3c	S4f	S4e	S4d	S3a
t	0	0.25	0.5	0.75	1
$\omega_{t,losses}[-]$	0.03315	0.04123	0.04421	0.05857	0.052
$\bar{T}_{outlet}[K]$	315.81	318.22	320.02	327.53	325.72

Table 7.4: Performance metrics of intermediate geometries between Primitive and Gyroid.

Combined Gyroid and Primitive geometries enrich the so-far optimal front with new solutions. First, the combination of 0.25 Primitive - 0.75 Gyroid is not dominated by the simple Solid-Network geometries, and also the combination of 0.75 Gyroid - 0.25 Primitive offers the highest \bar{T}_{out} so far.

7.4 Hybrid Primitive-IWP

The last linear combination of Primitive and IWP follows equation 7.3. Table (7.5) presents all the examined intermediate geometries.

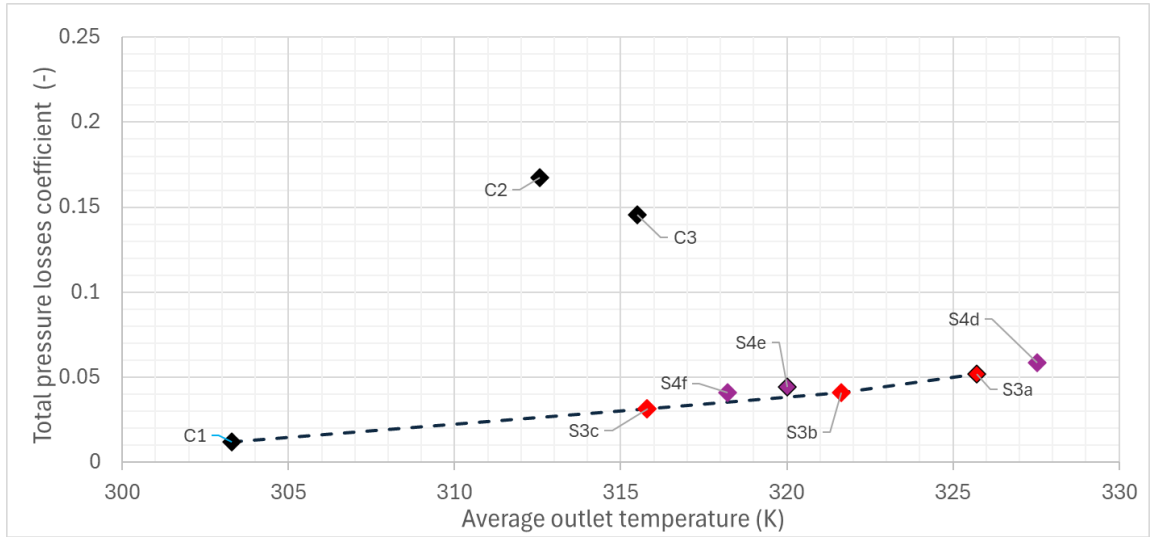


Figure 7.8: Comparison of so-far non-dominated geometries with intermediate geometries between Primitive and IWP (purple colored).

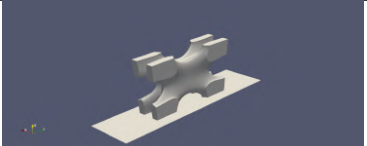
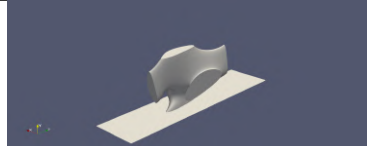
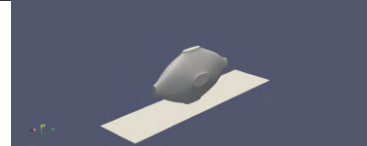
Case S4g: 75%IWP-25%Primitive	Case S4h: 50%IWP-50%Primitive	Case S4i: 25%IWP-75%Primitive
		

Table 7.5: Intermediate structures between Primitive and IWP surfaces.

geometry	S3a	S4g	S4h	S4i	S3b
t	0	0.25	0.5	0.75	1
$\omega_{t,losses}[-]$	0.0315	0.0371	0.04411	0.0524	0.0412
$T_{outlet}[K]$	315.81	316.48	319.79	323.19	321.63

Table 7.6: Performance of intermediate geometries between Primitive and IWP .

Figure (7.9) depicts the performance of these geometries. Only the geometry with $t=0.25$ is added to the current optimal front since the other two are dominated by the Solid-Network Primitive or the Solid-Network IWP.

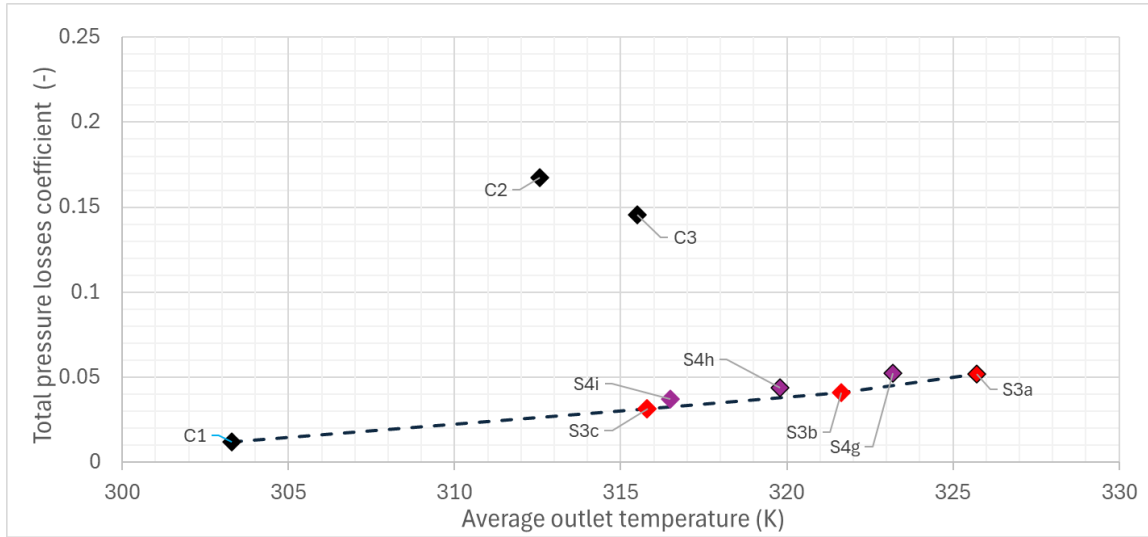


Figure 7.9: Comparison of so-far non-dominated geometries with intermediate geometries between Primitive and IWP (purple colored).

7.5 Gradually transformed geometries

In this case, TPMS will change their shape gradually across the flow axis following equations 7.4, 7.5, 7.6. Table (7.7) displays all these geometries.

Case S5a: IWP-Primitive	Case S5b: Gyroid-Primitive	Case S5c: IWP-Gyroid
		

Table 7.7: Intermediate structures between Primitive and IWP surfaces.

Table (7.7) reveals that the geometry is formulated by a TPMS geometry at the beginning and gradually changes to the other geometry at the end. In figure (7.10), it is clear that this type of geometry does not perform better than the previous solutions because all of these cases have higher total pressure losses without improving thermal efficiency.

geometry	S5a	S5b	S5c
$\omega_{t,losses} [-]$	0.0474	0.0537	0.05698
$T_{outlet} [K]$	320.70	323.7	325.15

Table 7.8: Details of figure (7.10).

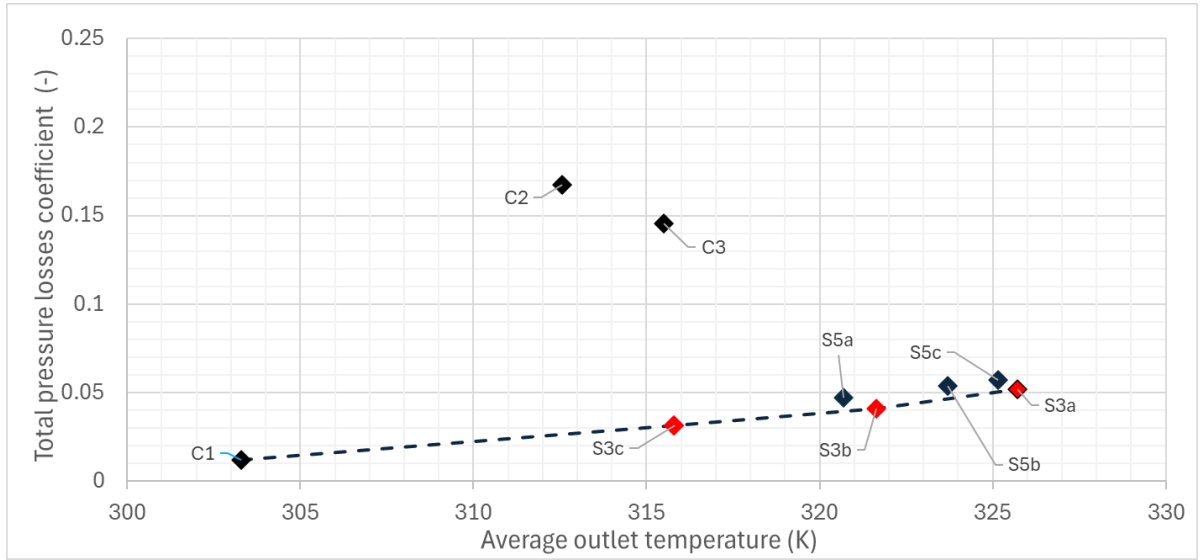


Figure 7.10: Comparison of so-far non-dominated geometries with gradually interpolated geometries (blue colored).

7.6 Analysis of Results

In figure (7.11), all cases tested in this chapter are presented. Non-dominated solutions are connected with a dashed line that form the solution non-dominated front. The procedure of combining TPMS obviously increases all total pressure losses since the transition from one geometry to the other generates non-smooth or asymmetric geometries.

However, there are some cases in which complex geometries would increase the wet

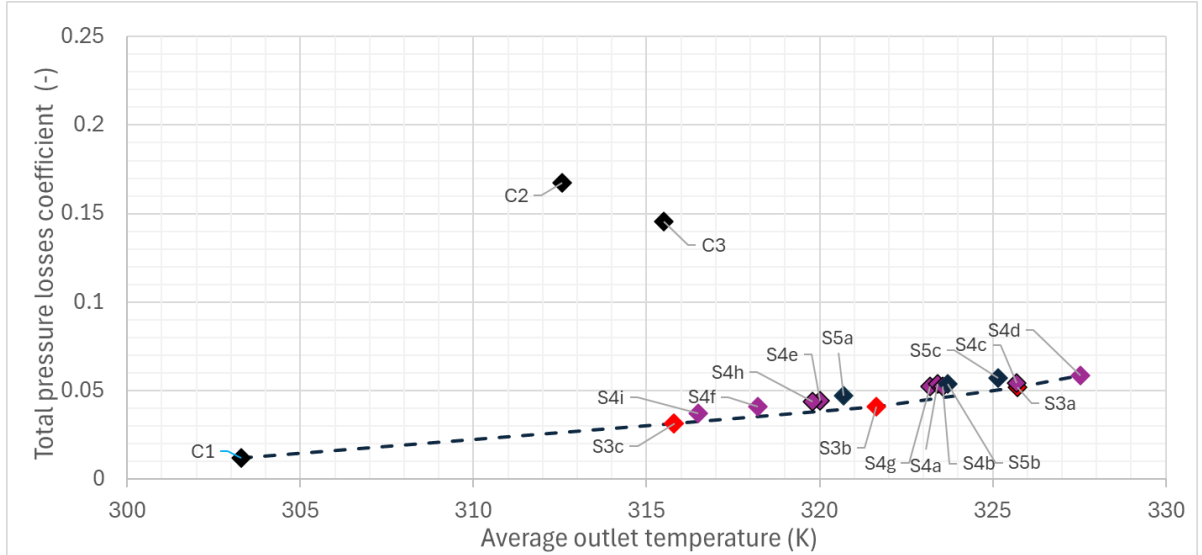


Figure 7.11: Summary results of parametric study of hybrid geometries (purple and blue colored), conventional (black colored), and the third parametric study (red colored).

area and, consequently, \bar{T}_{out}^F . Another observation is that the uniform distribution of parameter t does not mean a uniform distribution of the geometry's performance. Fur-

thermore, in table (7.9), all the solutions are listed in detail.

geometry	C1	S3c	S3b	S3a	S4d
ω_{losses}	0.01215	0.0315	0.04119	0.05204	0.0585
T_{average}	303.304	315.812	321.63	325.721	327.53

Table 7.9: Performance metrics for different structures.

That the gradual interpolation of the cooling geometry from the a TPMS to another can give better results, as it offers solutions that exceed previous non-dominant solution fronts. Considering that combining TPMS geometries is a highly complex topic and there are plenty of methods to do so, the results of the methods that were used before cannot represent the whole concept. Thus, solution S4d has the highest \bar{T}_{out}^F , and is the most preferred one since the temperature profit, from the empty case, is doubled than case C3, and with one third of its total pressure losses.

Chapter 8

Conclusions

In this chapter, a comprehensive summary of all the parametric studies and simulation cases is presented. Tables [8.1],[8.2], and[8.3] show all cases with their performance metrics.

Firstly, it is evident that all the TPMS geometries promoting heat exchange have better performance compared with the traditional heat sinks. The reason is the high surface-to-volume ratio that enhances the heat transfer. Among all the basic TPMS geometries promoting heat exchange, the Gyroid geometry appears to demonstrate higher thermal performance and lower losses than IWP and Primitive geometries.

The case study of the periodicity showed that the duplication of the flow's direction periodic improves the thermal efficiency, since the contact surface with the fluid is increased. However, quadruple-patterned surfaces result in higher total pressure losses without significantly increasing thermal efficiency. As a result, there is an upper bound to the number of times that a TPMS can be repeated.

Thickness variation showed small local improvements in thermal efficiency, but a significant increase in total pressure losses due to more severe recirculation of the fluid flow. Non-uniform thickness does not offer significant improvement in comparison with the basic TPMS geometries because the refinement in \bar{T}_{out} is not enough to offset the total pressure losses.

Using solid network extruded geometries increases thermal efficiency even more and reduces total pressure losses. Among these geometries, the Gyroid still exhibits higher efficiency than IWP and the Primitive geometries.

Finally, the mixture of TPMS further increases the number of possible solutions. Linear interpolation geometries primarily yield new non-dominated solutions that are incorporated into the optimal front. In contrast, geometries promoting heat exchange that gradually change along the flow axis do not offer better solution since their non-symmetric shape increases the total pressure losses significantly.

To sum up, results prove that TPMS have achieved much higher efficiency than traditional heat sinks, especially in the case of solid network extruded geometries. Figure (8.2) presents the front of all cases examined in this thesis.

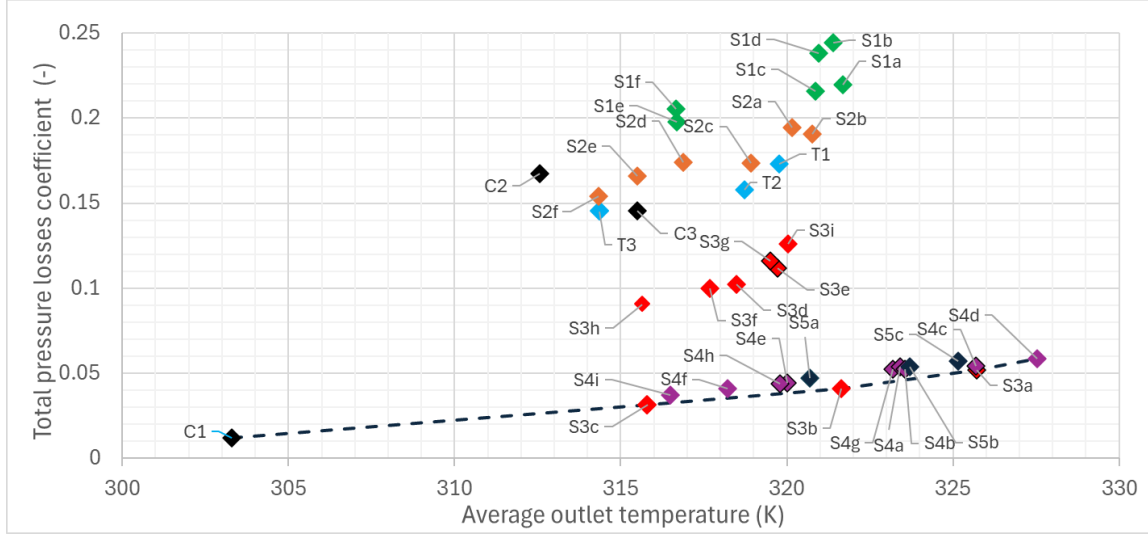


Figure 8.1: Summary solution front. The conventional geometries are displayed with black color, with blue the single TPMS, the patterned geometries with green color, and the non-constant thickness geometries with orange color, solid network extruded geometries with red, linear interpolated geometries with purple, and gradual interpolated geometries with dark blue.

Another interesting parameter that is important to examine is the wet area. This is defined as the area that comes in contact with the fluid. In figures (8.3), it is shown that geometries promoting heat exchange with high wet area tend to have better heat transfer properties. However, another factor that is also important is the surface that connects the heat source and the cooling geometry, because bigger contact surfaces between the heat source and the cooling geometry can spread the heat more easily inside the geometry. In figure (8.4), the contact surface is shown along with \bar{T}_{out}^F . In table (8.4) the wet and the contact area between the heat transfer geometry and the heat source are provided.


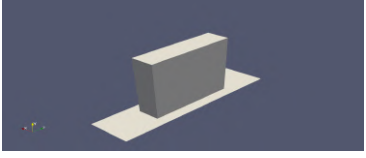
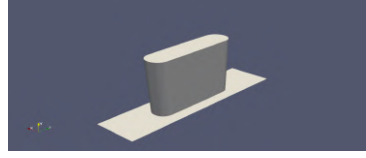
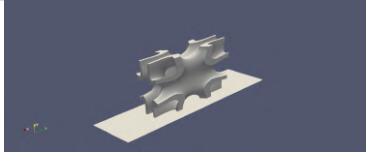
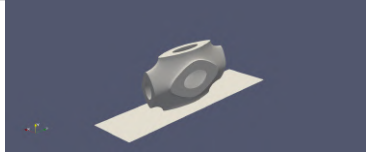
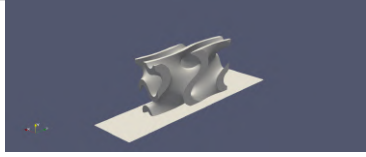
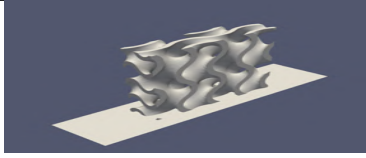
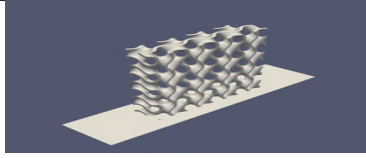
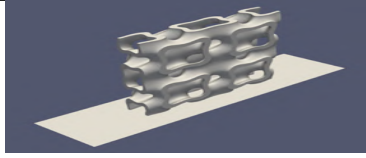
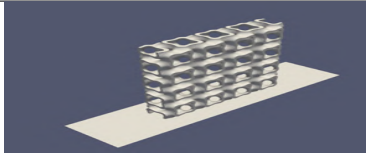
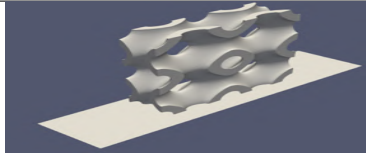
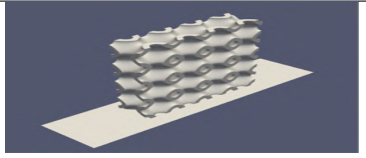
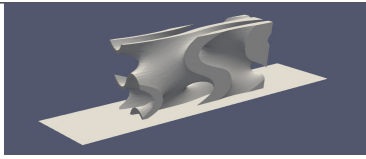
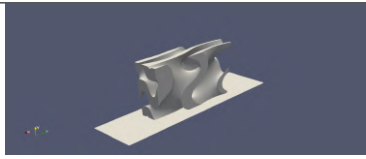
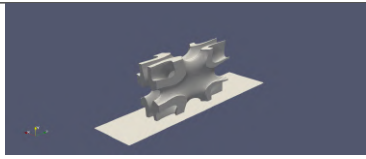
Case C1: empty case		Case C2: Parallelepiped fin		Case C3: Rounded Fin	
					
$\omega_{t,losses}[-]$	0.01215	$\omega_{t,losses}[-]$	0.1675	$\omega_{t,losses}[-]$	0.146
$T_{outlet}[K]$	303.3	$T_{outlet}[K]$	312.57	$T_{outlet}[K]$	315.49
Case T1: IWP		Case T2: Primitive		Case T3: Gyroid	
					
$\omega_{t,losses}[-]$	0.17318	$\omega_{t,losses}[-]$	0.1578	$\omega_{t,losses}[-]$	0.1453
$T_{outlet}[K]$	319.78	$T_{outlet}[K]$	318.74	$T_{outlet}[K]$	314.37
Case S1a: Dual Gyroid		Case S1b: Quadruple Gyroid		Case S1c: Dual IWP	
					
$\omega_{t,losses}[-]$	0.2195	$\omega_{t,losses}[-]$	0.2445	$\omega_{t,losses}[-]$	0.2156
$T_{outlet}[K]$	319.78	$T_{outlet}[K]$	321.39	$T_{outlet}[K]$	320.96
Case S1d: Quadruple IWP		Case S1e: Dual Primitive		Case S1f: Quadruple Primitive	
					
$\omega_{t,losses}[-]$	0.2384	$\omega_{t,losses}[-]$	0.198	$\omega_{t,losses}[-]$	0.2053
$T_{outlet}[K]$	320.96	$T_{outlet}[K]$	316.70	$T_{outlet}[K]$	316.67
Case S2a: Increasing Thickness Gyroid		Case S2b: Decreasing Thickness Gyroid		Case S2c: Increasing Thickness IWP	
					
$\omega_{t,losses}[-]$	0.1943	$\omega_{t,losses}[-]$	0.1907	$\omega_{t,losses}[-]$	0.17381
$T_{outlet}[K]$	320.15	$T_{outlet}[K]$	319.78	$T_{outlet}[K]$	318.92

Table 8.1: Summary table part 1.

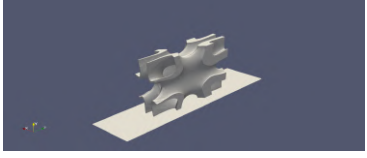
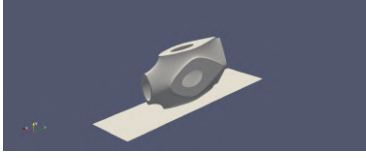
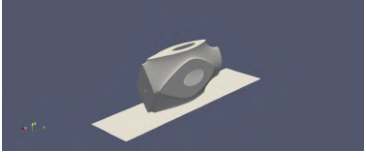
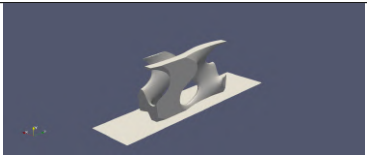
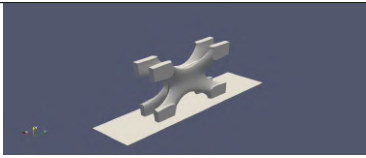
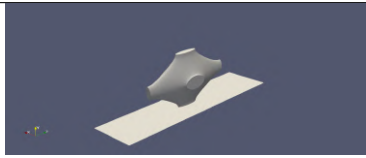
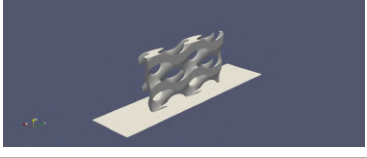
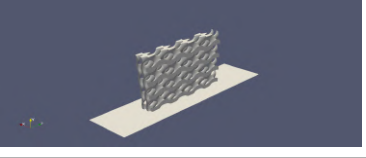
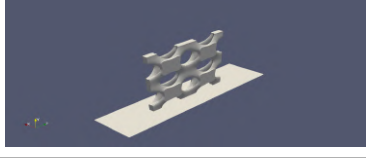
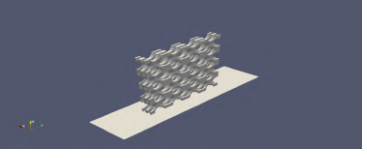
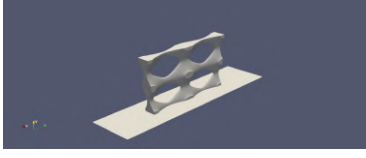
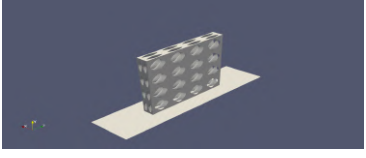
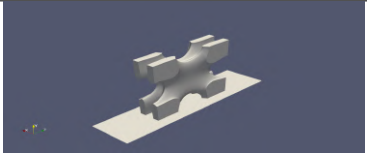


Case S2d: Decreasing Thickness IWP	Case S2e: Increasing Thickness Primitive	Case S2f: Decreasing Thickness Primitive
		
$\omega_{t,losses}[-]$ 0.17429	$\omega_{t,losses}[-]$ 0.166	$\omega_{t,losses}[-]$ 0.1541
$T_{outlet}[K]$ 316.87	$T_{outlet}[K]$ 315.51	$T_{outlet}[K]$ 314.34
Case S3a: Solid Network Gyroid	Case S3b: Solid IWP	Case S3c: Solid Primitive
		
$\omega_{t,losses}[-]$ 0.0315	$\omega_{t,losses}[-]$ 0.0412	$\omega_{t,losses}[-]$ 0.052
$T_{outlet}[K]$ 315.81	$T_{outlet}[K]$ 321.63	$T_{outlet}[K]$ 325.72
Case S3d: Dual Solid Network Gyroid	Case S3e: Quadruple Solid Network Gyroid	Case S3f: Dual Solid IWP
		
$\omega_{t,losses}[-]$ 0.102	$\omega_{t,losses}[-]$ 0.112	$\omega_{t,losses}[-]$ 0.0999
$T_{outlet}[K]$ 318.48	$T_{outlet}[K]$ 319.71	$T_{outlet}[K]$ 317.69
Case S3g: Quadruple Solid IWP	Case S3h: Dual Solid Primitive	Case S3i: Quadruple Solid Primitive
		
$\omega_{t,losses}[-]$ 0.1161	$\omega_{t,losses}[-]$ 0.0906	$\omega_{t,losses}[-]$ 0.1262
$T_{outlet}[K]$ 319.51	$T_{outlet}[K]$ 315.65	$T_{outlet}[K]$ 320.04
Case S4a: 75%IWP-25%Gyroid	Case S4b: 50%IWP-50%Gyroid	Case S4c: 25%IWP-75%Gyroid
		
$\omega_{t,losses}[-]$ 0.0537	$\omega_{t,losses}[-]$ 0.0526	$\omega_{t,losses}[-]$ 0.0543
$T_{outlet}[K]$ 323.41	$T_{outlet}[K]$ 323.56	$T_{outlet}[K]$ 325.68

Table 8.2: Summary table part 2.

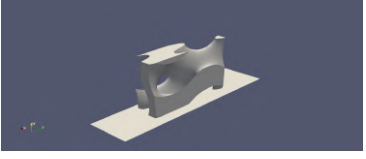
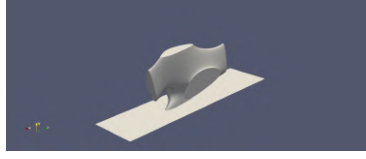
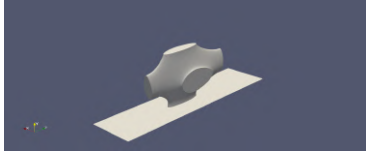
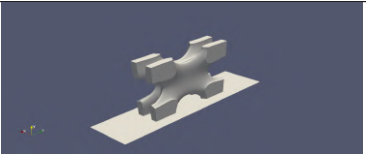
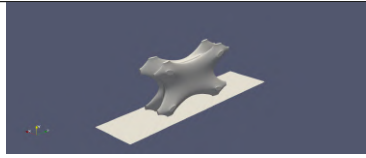
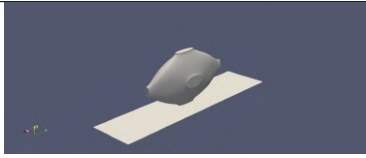
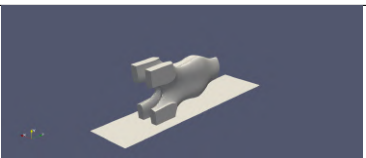
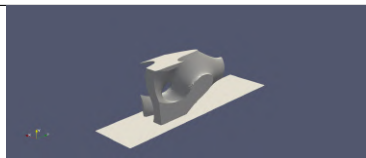
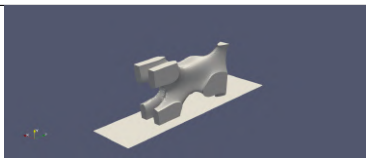
Case S4d: 25%Primitive-75%Gyroid		Case S4e: 50%Primitive-50%Gyroid		Case S4f: 75%Primitive-25%Gyroid	
					
$\omega_{t,losses}[-]$	0.04123	$\omega_{t,losses}[-]$	0.04421	$\omega_{t,losses}[-]$	0.05857
$T_{outlet}[K]$	318.22	$T_{outlet}[K]$	320.02	$T_{outlet}[K]$	327.53
Case S4g: 25%Primitive-75%IWP		Case S4h: 50%Primitive-50%IWP		Case S4i: 75%Primitive-25%IWP	
					
$\omega_{t,losses}[-]$	0.0371	$\omega_{t,losses}[-]$	0.04411	$\omega_{t,losses}[-]$	0.0524
$T_{outlet}[K]$	316.48	$T_{outlet}[K]$	319.79	$T_{outlet}[K]$	323.19
Case S5a: IWP-Primitive		Case S5b: Gyroid-Primitive		Case S5c: IWP-Gyroid	
					
$\omega_{t,losses}[-]$	0.0474	$\omega_{t,losses}[-]$	0.0537	$\omega_{t,losses}[-]$	0.05698
$T_{outlet}[K]$	320.70	$T_{outlet}[K]$	323.7	$T_{outlet}[K]$	325.15

Table 8.3: Summary table part 3.

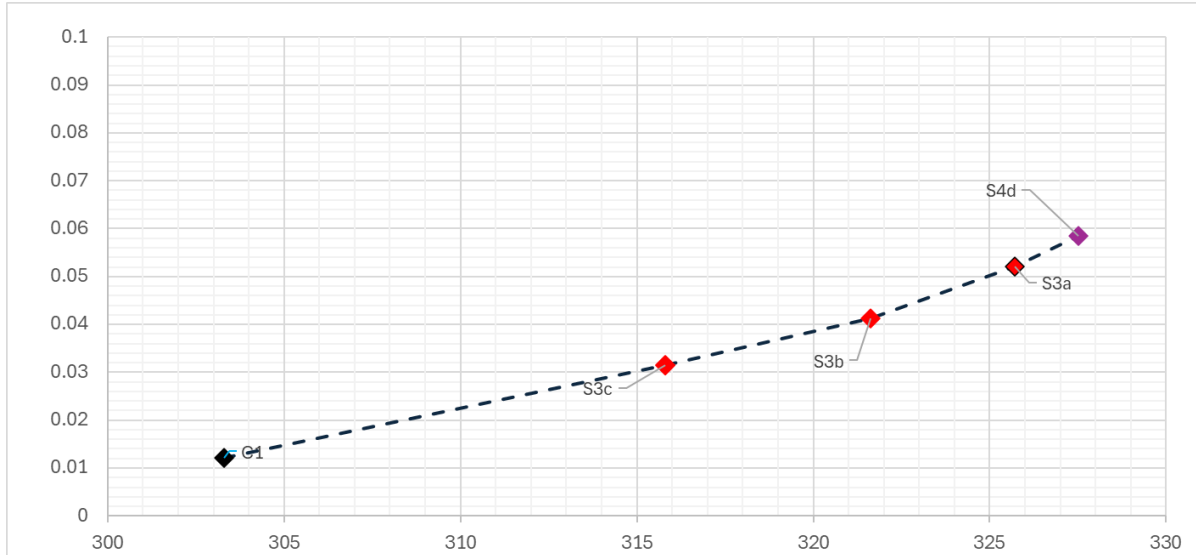


Figure 8.2: Optimal non-dominant solution front.

In conclusion, the study of TPMS examines three geometries (Gyroid, IWP, and Primi-

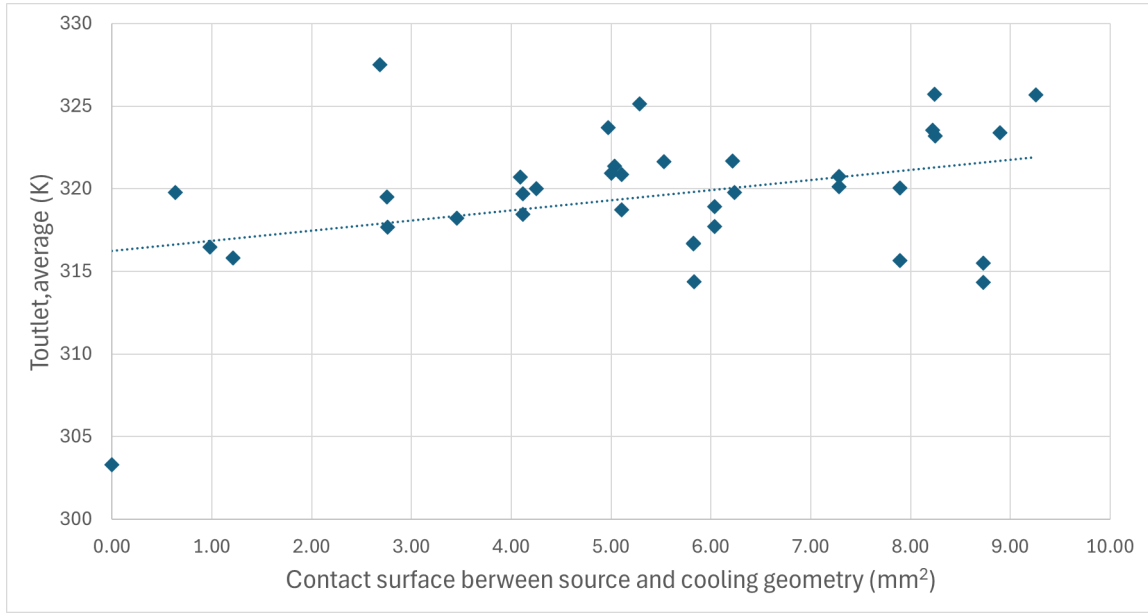


Figure 8.3: Relation between wet surface and average exit temperature. Non-constant line is a linear extrapolation with the least squares method.

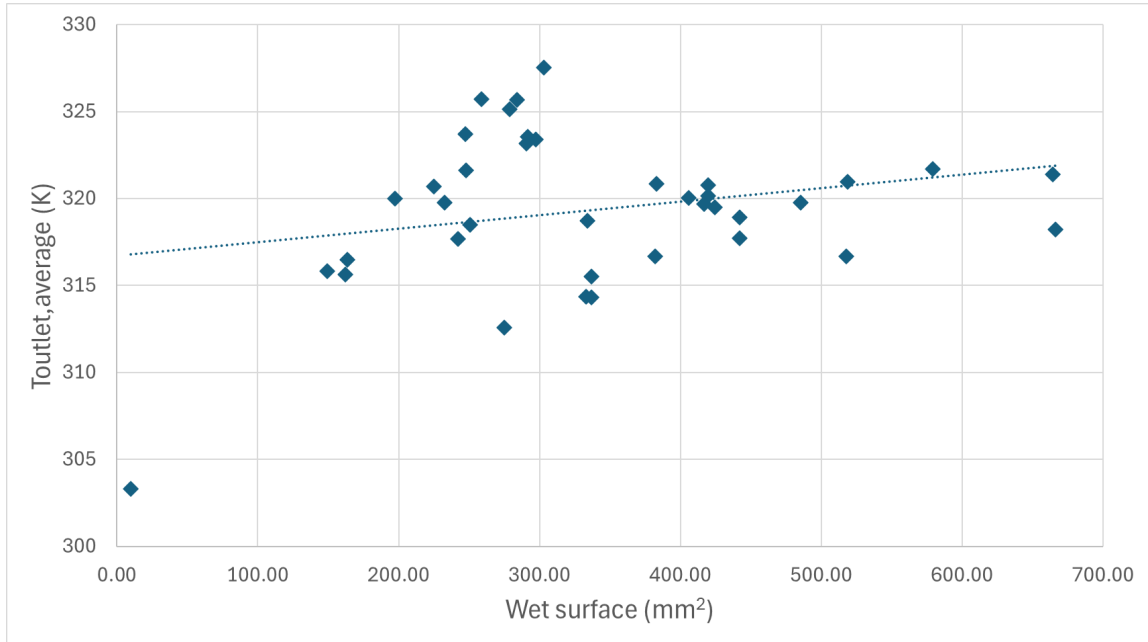


Figure 8.4: Relation between contact surface and average exit temperature. Non-constant line is a linear extrapolation with the least squares method.

tive) for heat exchange applications, using the traditional heat sink as a reference case. First, the theoretical background for generating these surfaces was explained, followed by a description of the methodology used to extrude them into 3D geometries. Furthermore, performance metrics, such as the total pressure loss coefficient and the average outlet temperature of the working fluid were used to evaluate and compare the solutions through two-dimensional diagrams. For all these simulations, the OpenFOAM solver cht-MultiRegionSimpleFoam was used. Performance was evaluated by minimizing the total pressure-loss coefficient and maximizing \bar{T}_{out}^F of the working fluid.

Case	$T_{out}[K]$	wet area [mm^2]	contact area [mm^2]
Case c1	303.30	10.00	0.00
Case c2	312.57	275	10.00
Case T1	321.69	485.53	6.23
Case T2	318.74	333.867	5.105
Case T3	314.37	333.139	5.833
Case S1a	321.69	579.332	6.215
Case S1b	321.39	664.541	5.035
Case S1c	320.87	382.941	5.103
Case S1d	320.97	518.515	5.000
Case 1e	316.70	382.218	5.827
Case 1f	316.67	517.688	5.827
Case S2a	320.77	419.600	7.284
Case S2b	320.15	419.601	7.284
Case S2c	318.92	442.252	7.284
Case S2d	317.74	442.252	8.731
Case S2e	315.51	336.873	8.731
Case S2f	314.34	336.873	6.039
Case S3a	325.72	258.784	6.039
Case S3b	318.48	250.562	8.237
Case S3c	319.71	416.997	4.118
Case S3d	321.63	247.774	4.118
Case S3e	317.69	241.957	5.531
Case S3f	319.51	424.500	2.758
Case S3g	315.81	149.074	2.753
Case S3h	315.65	162.371	1.212
Case S3i	320.04	405.959	7.892
Case S4a	323.41	297.087	7.893
Case S4b	323.56	197.154	8.898
Case S4c	325.68	666.120	8.221
Case S4d	327.53	302.933	9.254
Case S4e	320.02	197.154	2.69
Case S4f	318.22	666.120	4.25
Case S4g	323.19	290.553	3.45
Case S4h	319.79	232.387	8.243
Case S4I	316.48	163.792	0.63
Case 5a	320.70	225.162	0.98
Case S5B	323.7	247.139	4.09
Case S5C	325.1	278.65	4.97

Table 8.4: Results of all cases: \bar{T}_{out}^F , wet area, and contact area.

In table (8.5), all non-dominated solutions are presented. All these geometries have some common attributes like single periodicity, uniform thickness distribution, and they have been extruded with the solid network method. In detail, variable thickness sig-

nificantly increased losses compared to \bar{T}_{out}^F while repeatedTPMS improved \bar{T}_{out}^F as the number of single TPMS was increased, with a temperature peak because repeatedTPMS also reduced the contact area between the heat transfer geometry and the heat source. Even though, the majority of hybrid TPMS does not offer non-dominated solutions, S4d geometry offered the solution with the highest \bar{T}_{out}^F of all. It underlined that hybrid TPMS is a wide chapter and can offer better solutions with further investigation.

For further investigation, all these parametric studies, non-dominated solutions can be used as initializations to topology optimization algorithms. In addition, there are more TPMS that can be examined, such as Diamond and Neovious [31]. Additionally, all these geometries can be examined in other scientific fields, such as structural mechanics or aerodynamics.

	Type	Pattern	Thickness	Extrusion
S3a	Gyroid	1	Constant	Solid network
S3b	IWP	1	Constant	Solid network
S3c	Primitive	1	Constant	Solid network
S4d	75%Gyroid–25%Primitive	1	Constant	Solid network

Table 8.5: Non-dominated geometries properties.

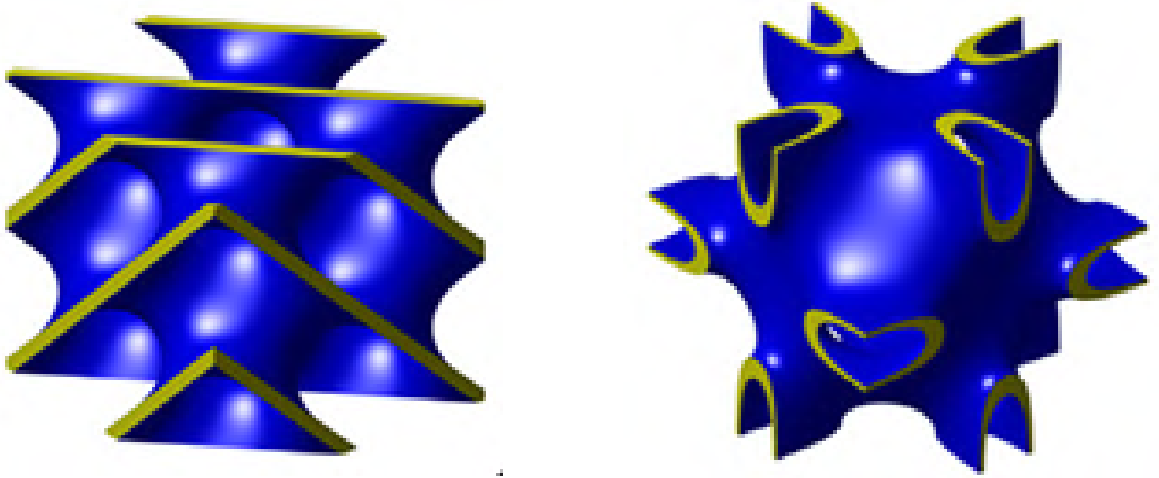


Figure 8.5: Alternative TPMS for further investigation. Diamond (left) and Neovious (right) from reference [31].

Bibliography

- [1] K.Ersoy. Review of electronic cooling and thermal management in space and aerospace applications. *Engineering Proceedings*, 2025.
- [2] A.Arsalan L.Timilsina P. K. Chamarthi B. Papari G.Ozkan C. S. Edrington I.Rahman, A.Moghassemi. Emerging trends and challenges in thermal management of power electronic converters: A state of the art review. *IEEE Access*, 2024.
- [3] T. O. Ale and K. J. Rotipin. Cooling effects on photovoltaic module performance in the tropical region. *Nigerian Journal of Technology (NIJOTECH)*, 2019.
- [4] S.Cai and Z.Gou. Towards energy-efficient data centers: A comprehensive review of passive and active cooling strategies. *Energy and Built Environment*, 2024.
- [5] Ö. Özdiilli. Materials today sustainability. *Elsevier*, 2025.
- [6] Wang Fengwen Hong Jun Sigmund Ole Yan, Suna. Topology optimization of microchannel heat sinks using a two-layer model. *International Journal of Heat and Mass Transfer*, 2019.
- [7] M.Ismail. Experimental and numerical analysis of heat sink using cylindrical pin-fins. *Case Studies in Thermal Engineering*, 2024.
- [8] D.Nikolaidis. Applications of topology optimization in the design of microchannel heat sinks. Diploma thesis, National Technical University of Athens, Athens, 2025.
- [9] Babu Sunith Gupta, Arpit. Triply periodic minimal surfaces: An overview of their features, failure mechanisms, and applications. *Journal of Mines, Metals and Fuels*.
- [10] Rehman Tauseef-ur Ali Mubasher Park C.Woo Yan Wei-Mon Sajjad, Uzair. Manufacturing and potential applications of lattice structures in thermal systems: A comprehensive review of recent advances. *International Journal of Heat and Mass Transfer*, 2022.
- [11] Martin-Nicolas P. Ferney, Paul A. Implementation of triply periodic minimal surfaces (tpms) as surface objects in openmc. *Annals of Nuclear Energy*, 224, 2025.
- [12] W. Saleem B.Ziaie, X. Velay. Exploring the optimal mechanical properties of triply periodic minimal surface structures for biomedical applications: A numerical analysis. *Journal of the Mechanical Behavior of Biomedical Materials*, 2024.

- [13] J. Maszybrocka P.J. Jodłowski M. Iwaniszyn, K. Sinder. 3d-printed triply periodic minimal surface (tpms) structures as catalyst carriers. *Chemical Engineering Research and Design*, 2019.
- [14] L.Zhang S. Fuh J. Y. Hsi L. W. Feng Vijayavenkataraman, S.Zhang. Triply periodic minimal surfaces sheet scaffolds for tissue engineering applications: An optimization approach toward biomimetic scaffold design. *ACS Applied Bio Materials*.
- [15] Q.Gao H.Yang R.Bao S.Xiong X.Du, Z.Wang. Study on novel battery thermal management using triply periodic minimal surface porous structures liquid cooling channel. *Applied Thermal Engineering*, 2024.
- [16] D.Katmeridis. Incorporation of gyroid structures in the design of a static mixing device. Diploma thesis, National Technical University of Athens, Athens, 2024.
- [17] M. Darwish F. Moukalled, L. Mangani. *The Finite Volume Method in Computational Fluid Dynamics: An Advanced Introduction with OpenFOAM® and Matlab®*. 2015.
- [18] The OpenFOAM Foundation. Openfoam – official site. <https://openfoam.org>, 2025. Accessed: 2025-08-29.
- [19] M. el Abbassia, D. J. P. Lahaye, and C. Vuik. Modelling turbulent combustion coupled with conjugate heat transfer in OpenFOAM. In *Proceedings of MCS 10, Naples, Italy*, 2017. MCS 10, Naples, Italy, September 17–21, 2017.
- [20] Pairetti I. Cesar Venier M. Cesar M.Damian Santiago Nigro-M.Norberto Aguerre, J.Horacio. An oscillation-free flow solver based on flux reconstruction. *Journal of Computational Physics*, 2018.
- [21] M.Darwish F.Moukalled, L.Mangani. *The Finite Volume Method in Computational Fluid Dynamics: An Advanced Introduction with OpenFOAM*. Fluid Mechanics and Its Applications. 2016.
- [22] F.Moukalled M.Darwish. A unified formulation of the segregated class of algorithms for fluid flow at all speeds. *Numerical Heat Transfer, Part B: Fundamentals*, 2000.
- [23] D.Lee H.Ramos H.Alabdouli M.Alteneiji Z.Guan W. Cantwell M.Alves S.AlMahri, R.Santiago. Evaluation of the dynamic response of triply periodic minimal surfaces subjected to high-strain-rate compression. *Additive Manufacturing*, 2021.
- [24] H.Ghahramanzadeh D.Karaman. The effects of sheet and network solid structures of similar tpms scaffold architectures on permeability, wall shear stress, and velocity. *Medical Engineering and Physics*, 2023.
- [25] Rowshan Reza Abu Al-Rub Rashid K. Al-Ketan, Oraib. Mslattice: Multiscale lattice structures with graded and multi-morphology designs. *Elsevier*, 2021.
- [26] T.T.Bui T.D.Nguyen, A.V.Vo. Design modeling and CFD simulation of parallel plate-fin heat sink under natural convection. *Makara Journal of Technology*, 2024.

- [27] M.Guzej E.Bartuli P.Kotrbacek J.Kominek, M.Zachar. Influence of ambient temperature on radiative and convective heat dissipation ratio in polymer heat sinks. *Polymers*, 2021.
- [28] K.Giannakoglou. *Viscous Flows in Thermal Turbomachinery Course Handouts*. Laboratory of Thermal Turbomachines, NTUA, Athens, Greece, 1997.
- [29] Philippe R. Spalart and Steven R. Allmaras. A one-equation turbulence model for aerodynamic flows. In *Recherche Aéronautique*, 1992.
- [30] K.Giannakoglou. *Optimization Methods in Aerodynamics Course Handouts*. NTUA, 2006.
- [31] Xie Yi Min Wu Xian-Wang Zhe Li Qing-Zhou Shiwei Chen, Zeyao. On hybrid cellular materials based on triply periodic minimal surfaces with extreme mechanical properties. *Elsevier*, 2019.



Εθνικό Μετσόβιο Πολυτεχνείο
Σχολή Μηχανολόγων Μηχανικών
Τομέας Ρευστών
Μονάδα Παράλληλης Υπολογιστικής Ρευστοδυναμικής
Βελτιστοποίησης

Μελέτες Μεταφοράς Θερμότητας σε Ηλεκτροικά
Ισχύος με χρήση Τριπλά Περιοδικών Ελάχιστων
Επιφανειών

Διπλωματική Εργασία
(Εκτενής Περίληψη στην Ελληνική)

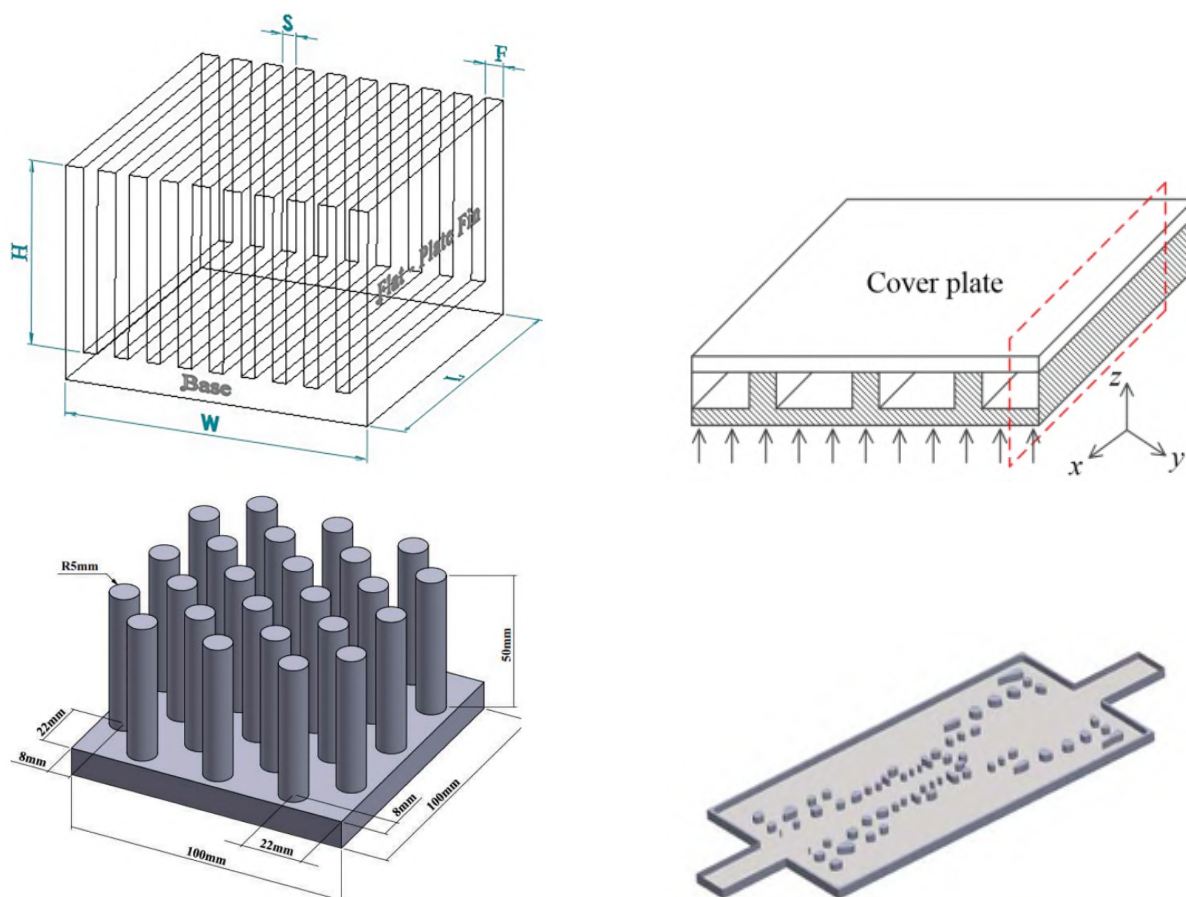
Κατσαρέλος Αθανάσιος

Επιβλέπων: Κυριάκος Χ. Γιαννάκογλου, Καθηγητής ΕΜΠ

Αθήνα 2025

Εισαγωγή

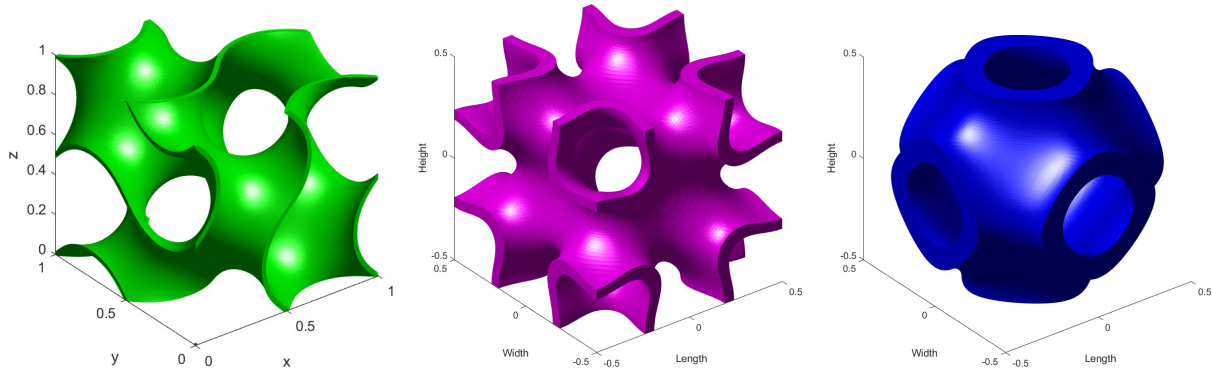
Στη σημερινή εποχή οι απαιτήσεις των συστημάτων σε διάφορα πεδία απαιτούν όλο και περισσότερη ισχύς με αποτέλεσμα να καθίσταται απαραίτητη η χρήση μηχανισμών ψύξης ή, γενικότερα, συναλλαγής θερμότητας. Παραδείγματα από συνήθεις μηχανισμούς συναλλαγής θερμότητας αποτελούν οι ψύκτρες από παραλληλεπίπεδα πτερύγια, μικροκανάλια, κυλινδρικού σχήματος ιδίου μεγέθους ή και διαφορετικού με ακανόνιστες διαστάσεις (σχήμα 1).



Σχήμα 1: Παραδοσιακές γεωμετρίες ψηκτρών. Παραλληλεπίπεδα πτερύγια (πάνω αριστερά), μικροκανάλια (πάνω δεξιά), κυλινδρικού σχήματος ιδίου μεγέθους(κάτω αριστερά) και κυλινδρικού σχήματος διαφορετικού μεγέθους με ακανόνιστες διαστάσεις (κάτω δεξιά).

Παρατηρείται ότι όλες οι γεωμετρίες σχεδιάζονται με στόχο να έχουν μεγάλη επιφάνεια επαφής με το εργαζόμενο μέσο-ρευστό σε σχέση με τον όγκο τους. Ένα χαρακτηριστικό παράδειγμα τέτοιων επιφανειών είναι οι Τριπλά Περιοδικές Ελάχιστες Επιφάνειες (ΤΠΕΕ). Οι ΤΠΕΕ είναι επιφάνειες οι οποίες μπορούν να επαναληφθούν μέσα στο χώρο και στις τρεις διαστάσεις και παράλληλα έχουν μηδενική μέση καμπυλότητα. Οι ΤΠΕΕ οι οποίες επιλέχθηκαν για τη διπλωματική εργασία ονομάζονται Gyroid, I – graphWrappedPackage(IWP), και Primitive ΤΠΕΕ (σχήμα 2).

Για να μελετηθεί κατάλληλα η συνεισφορά της γεωμετρίας στη μεταφορά θερμότητας πρέπει να οριστούν οι αντίστοιχες ποσότητες ενδιαφέροντος. Οι ποσότητες αυτές είναι ο συντελεστής απωλειών ολικής πίεσης (min) και η μέση θερμοκρασία εξόδου (\bar{T}_{out}^F) (max) του



Σχήμα 2: Βασικές Τριπλές Περιοδικές Ελάχιστες Επιφάνειες *Gyroid* (αριστερά) *IWP* (μέση) *Primitive* (δεξιά).

εργαζόμενου μέσου.

Η παραπάνω αξιολόγηση θα πραγματοποιηθεί με τη χρήση λογισμικών συζευγμένης μεταφοράς θερμότητας (*CHT*). Το λογισμικό *OpenFOAM* παρέχει ανοικτούς κώδικες που χρησιμοποιούν *CHT* αλγόριθμους βασισμένους στη μέθοδο των πεπερασμένων όγκων.

Ο στόχος της διπλωματικής εργασίας είναι η χρήση *TΠΕΕ* σε προβλήματα μεταφοράς θερμότητας σε σύγκριση με τις παραδοσιακές γεωμετρίες που χρησιμοποιούνται για τον σκοπό αυτό. Έπειτα πραγματοποιούνται δυο σειρές παραμετρικών μελετών οι οποίες επηρεάζουν τη γεωμετρία των *TΠΕΕ*. Η πρώτη κατηγορία μελετά τις παραμέτρους κατανομής πάχους των γεωμετριών και του πλήθους των επαναλήψεων των μοναδιαίων επιφανειών (μιας περιόδου). Η δεύτερη κατηγορία παρεμβάλλει δύο *TΠΕΕ* σε μια, δημιουργώντας υβριδικές *TΠΕΕ*.

Τριπλά Περιοδικές Ελάχιστες Επιφάνειες

Οι *TΠΕΕ* χαρακτηρίζονται από τις παρακάτω εξισώσεις:

$$f(x, y, z) = \sin(2\pi x) \cos(2\pi y) + \sin(2\pi y) \cos(2\pi z) + \sin(2\pi z) \cos(2\pi x) = 0 \quad (1)$$

$$f(x, y, z) = 2(\sin(2\pi x) \cos(2\pi y) + \sin(2\pi y) \cos(2\pi z) + \sin(2\pi z) \cos(2\pi x)) - (\cos(4\pi x) + \cos(4\pi y) + \cos(4\pi z)) = 0 \quad (2)$$

$$f(x, y, z) = \cos(2\pi x) + \cos(2\pi y) + \cos(2\pi z) = 0 \quad (3)$$

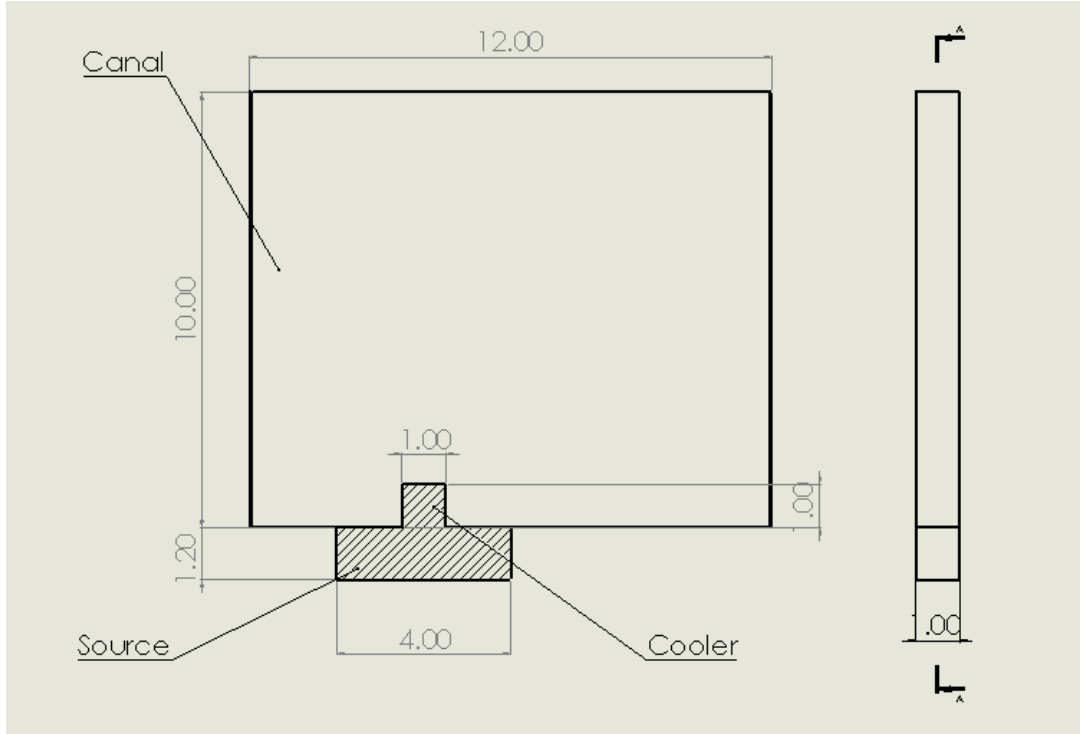
Για να μετατραπεί μία επιφάνεια σε ένα γεωμετρικό στερεό πρέπει να του προσδοθεί πάχος. Η διαδικασία αυτή μπορεί να επιτευχθεί μέσω δύο μεθόδων. Η μέθοδος *Sheet Solid* (εξίσωση 4) η οποία προσδίδει κάθετα το πάχος και από τις δύο πλευρές της επιφάνειας (κατά $T/2$) ενώ η μέθοδος *Network Solid* (εξίσωση 5) προσδίδει το πάχος T μόνο από τη μια πλευρά. Οι μέθοδοι αυτοί εκφράζονται από τις παρακάτω ανισο-ισότητες:

$$-\frac{t}{2} \leq f(x, y, z) \leq \frac{t}{2} \quad (4)$$

$$f(x, y, z) \leq t \quad (5)$$

Σχεδιασμός συστήματος συναλλαγής θερμότητας

Το σύστημα προσομοίωσης αποτελείται από τη θερμική πηγή, το κανάλι ροής και την πρόσθετη γεωμετρία που στοχεύει στην ενίσχυση της συναλλαγής θερμότητας. Το κανάλι έχει διαστάσεις $x=1$ εκ, $y=1.2$ εκ, $z=4$ εκ, το κανάλι $x=1$ εκ, $y=10$ εκ, $z=12$ εκ και η γεωμετρία ψύξης σχεδιάζεται πάντα μέσα σε ένα παραλληλεπίπεδο διαστάσεων $0.25 \times 1 \times 1 \text{ cm}^3$ (σχήμα 3).



Σχήμα 3: Διάταξη συστήματος ψύξης.

Μοντελοποίηση CHT

Οι εξισώσεις με τις οποίες θα χρησιμοποιηθούν για την επίλυση του προβλήματος είναι οι Reynolds – Averaged Navier – Stokes (RANS) για το ρευστό και η εξίσωση μεταφοράς θερμότητας με αγωγή για το στερεό, οι οποίες είναι οι εξής:

$$R^p = -\frac{\partial u_i}{\partial x_i} = 0 \quad (6)$$

$$R_i^p = u_j \frac{\partial u_i}{\partial x_j} + \frac{1}{\rho^F} \frac{\partial p}{\partial x_i} - \frac{\partial \tau_{ij}}{\partial x_j} = 0 \quad (7)$$

$$R_F^T = u_j C_p \frac{\partial T^F}{\partial x_j} + \frac{u_j}{2} \frac{\partial u_k^2}{\partial x_j} - \frac{\partial}{\partial x_j} \left(\frac{k^F}{\rho^F} \frac{\partial T^F}{\partial x_j} \right) = 0 \quad (8)$$

$$R_S^T = -\frac{\partial}{\partial x_i} \left(k^S \frac{\partial T^S}{\partial x_i} \right) = 0 \quad (9)$$

Επιπρόσθετα, για τη μοντελοποίηση της τύρβης χρησιμοποιείται το μοντέλο τύρβης των

Περιοχή	Ταχύτητας	Πίεση	Θερμοκρασία
Είσοδος	<i>Dirichlet</i>	<i>Zero Neumann</i>	<i>Dirichlet</i>
Έξοδος	<i>Zero Neumann</i>	<i>Dirichlet</i>	<i>Zero Neumann</i>
Εσωτερικοί τοίχοι	Μη ολίσθηση	<i>Zero Neumann</i>	<i>Zero Neumann</i>
Εξωτερικοί τοίχοι	Μη ολίσθηση	<i>Zero Neumann</i>	<i>Zero Neumann</i> ¹

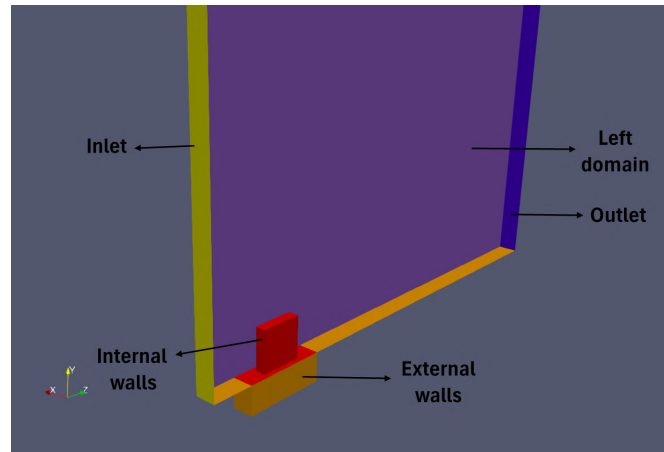
Πίνακας 1: Ιδιότητες ρευστού και στερεού.

Spalart – Allmaras με την ακόλουθη εξίσωση:

$$R^{\tilde{\nu}} = u_j \frac{\partial \tilde{\nu}}{\partial x_j} - C_{b1} (1 - f_{t2}) \tilde{S} \tilde{\nu} + \left(C_{w1} f_w + \frac{C_{b1}}{\kappa^2} f_{t2} \right) \left(\frac{\tilde{\nu}}{d} \right)^2 - \frac{1}{\sigma} \left[\frac{\partial}{\partial x_j} \left[(\nu + \tilde{\nu}) \frac{\partial \tilde{\nu}}{\partial x_j} \right] + C_{b2} \frac{\partial^2 \tilde{\nu}}{\partial x_i^2} \right] = 0 \quad (10)$$

Για τις επακόλουθες προσομοιώσεις επιβάλλονται οι οριακές συνθήκες που παρουσιάζονται στον πίνακα (1).

Στους πίνακες (2) και (3) δίνονται οι ιδιότητες του στερεού και του ρευστού που χρη-



Σχήμα 4: Πεδίο ροής με τη θερμική πηγή.

σιμοποιείται αλλά και οι βασικές ρυθμίσεις του επιλύτη. Οι ποσότητες ενδιαφέροντος που αξιολογούν τη μεταφορά θερμότητας είναι οι εξής:

$$\omega_{\text{total, losses}} = \frac{\int_{A_{\text{outlet}}} \left(p + \frac{1}{2} \rho u_i^2 \right) dA - \int_{A_{\text{inlet}}} \left(p + \frac{1}{2} \rho u_i^2 \right) dA}{\frac{A_{\text{inlet}} \rho v_{\text{inlet}}^2}{2}} \quad (11)$$

$$\bar{T}_{\text{out}}^F = \frac{\int_{A_{\text{outlet}}} T u_z dA}{\int_{A_{\text{outlet}}} u_z dA} \quad (12)$$

Αποτελέσματα

Τα αποτελέσματα παρουσιάζονται αναλυτικά στους πίνακες (5), (6) και (7). Γίνεται αντιληπτό ότι όλες οι TΠΕΕ τείνουν να αυξάνουν τη \bar{T}_{out}^F εις βάρος των απωλειών. Όμως δίνεται ιδιαίτερη σημασία στη μέθοδο Network extrusion η οποία μειώνει σημαντικά τις απώλειες πίεσης αλλά και αυξάνει τη \bar{T}_{out}^F στην έξοδο του ρευστού. Επιπρόσθετα, η αλλαγή του πάχους κατά μήκος της γεωμετρίας αύξησε τις απώλειες χωρίς να υπάρξει σημαντική

¹Για την κάτω επιφάνεια της θερμικής πηγής η οριακή συνθήκη τύπου *Dirichlet*.

Μέγεθος	Τιμή	Μονάδες
Πυκνότητα στερεού	2719	kg/m^3
Θερμική αγωγιμότητα στερεού	202.4	$W/(m \cdot K)$
Ειδική θερμοχωρητικότητα στερεού (C_p)	871	$J/(kg \cdot K)$
Πυκνότητα αέρα	1.225	kg/m^3
Ειδική θερμότητα αέρα (C_p)	1006.43	$J/(kg \cdot K)$
Δυναμική συνεκτικότητα αέρα	1.846×10^{-5}	$Pa \cdot s$
Υδραυλική διάμετρος	0.0182	m
Αριθμός <i>Reynolds</i>	2420	-
Αριθμός <i>Prandtl</i>	0.726414	-

Πίνακας 2: Ιδιότητες ρευστού και στερεού.

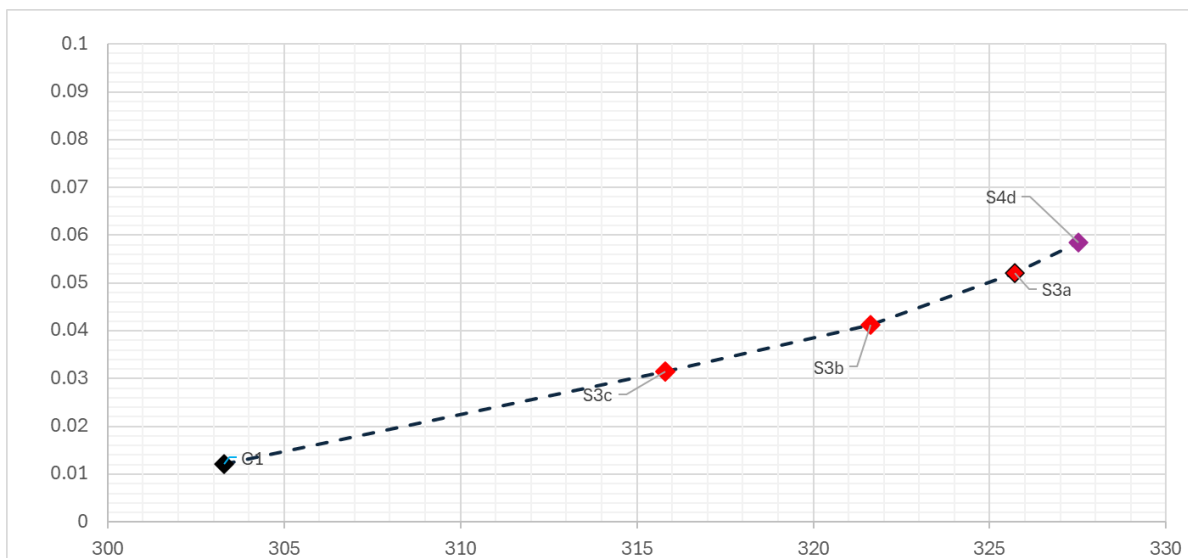
Παράμετρος	Τιμή
Μέγιστος αριθμός επαναλήψεων	3000
Χαλάρωση ταχύτητας	0.5
Χαλάρωση πίεσης	0.5
Χαλάρωση ενεργειακής εξίσωσης ρευστού	0.7
Χαλάρωση ενεργειακής εξίσωσης στερεού	0.9
Χαλάρωση $\bar{\nu}$	0.5

Πίνακας 3: Ρυθμίσεις επιλύτη.

αύξηση στη \bar{T}_{out}^F . Επίσης, οι γεωμετρίες που αποτελούνται από επαναλαμβανόμενες ΤΠΕΕ μπορεί να αποφέρει βελτίωση στη \bar{T}_{out}^F αλλά παρουσιάζεται ένα μέγιστο διότι μειώνεται η επιφάνεια επαφής της γεωμετρίας με τη θερμική πηγή. Όσον αφορά τις υβριδικές γεωμετρίες, απέδωσαν τη λύση με τη μεγαλύτερη \bar{T}_{out}^F αλλά πρέπει να υπογραμμιστεί ότι ο συνδυασμός γεωμετριών είναι ένα ευρύ κεφάλαιο και μπορεί να αποφέρει ακόμα καλύτερες λύσεις.

Σύμφωνα με τον πίνακα (4) όλες οι μη-κυριαρχούμενες γεωμετρίες έχουν ως κοινά χαρακτηριστικά τη μη-επανάληψη μοτίβων, τη σταθερή κατανομή πάχους και τη μέθοδο απόδοσης πάχους τη *Solid Network*.


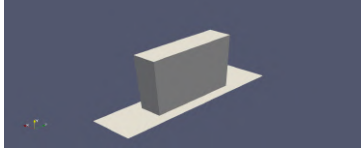
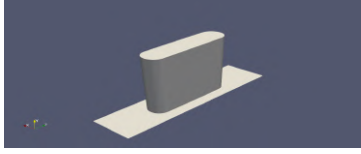
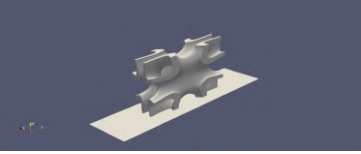
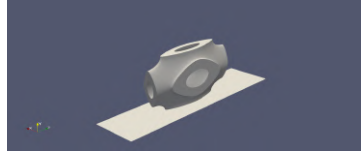
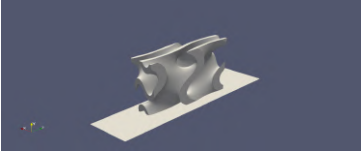
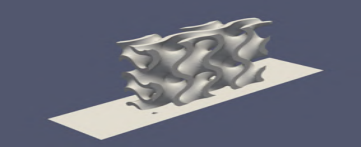
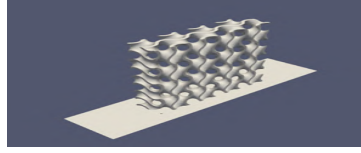
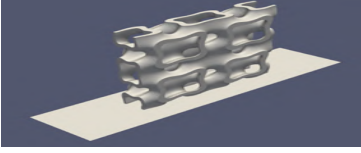
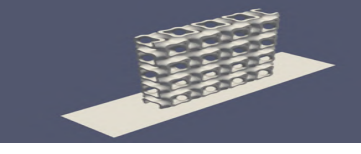
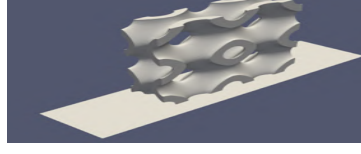
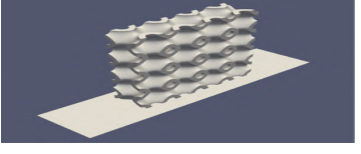
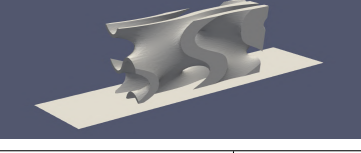
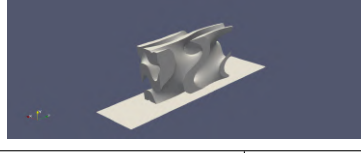
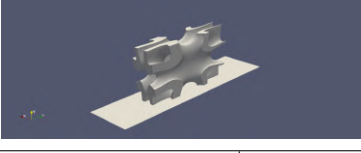
Σύμφωνα με το σχήμα (5) και τις επιδόσεις των παραδοσιακών ψηκτρών παρατηρείται ότι οι απώλειες ολικής πίεσης έχουν μειωθεί στο $\frac{1}{3}$ και η \bar{T}_{out}^F έφτασε μέχρι τους 327 K. Οι λύσεις αυτές προσφέρουν καλύτερους μηχανισμούς συναλλαγής θερμότητας με πολύ μικρότερες απώλειες λόγω της μεγάλης τους 'βρεχόμενης' επιφάνειας που ενισχύει τη μεταφορά θερμότητας.



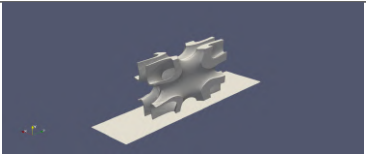
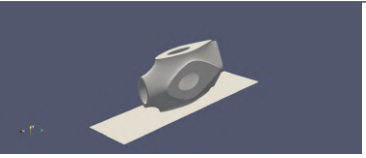
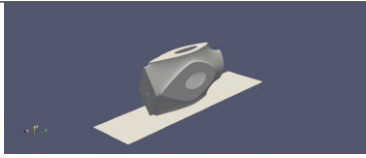
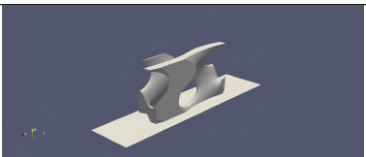

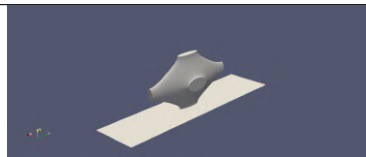
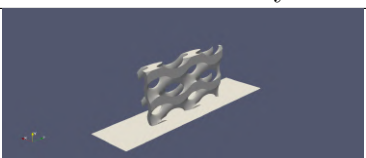
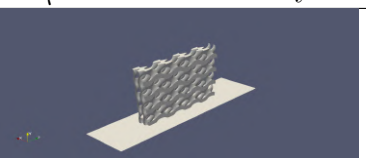
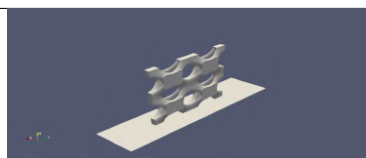
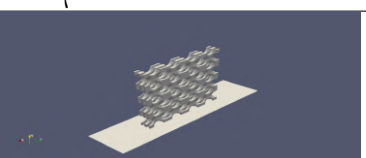
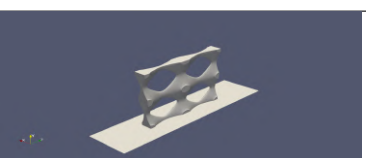
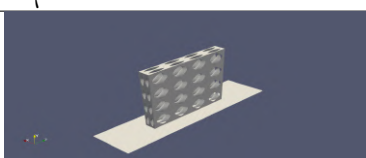
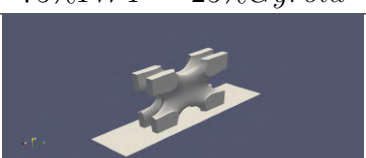
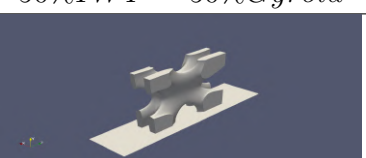
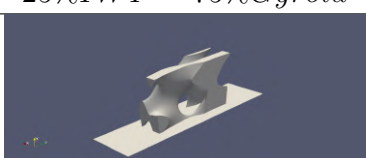
Σχήμα 5: Μέτωπο βέλτιστων λύσεων.

	Τύπος	Πολλαπλότητα	Πάχος	Πρόσδοση πάχους
<i>S3a</i>	<i>Gyroid</i>	1	Σταθερό	<i>Solid network</i>
<i>S3b</i>	<i>IWP</i>	1	Σταθερό	<i>Solid network</i>
<i>S3c</i>	<i>Primitive</i>	1	Σταθερό	<i>Solid network</i>
<i>S4d</i>	<i>75%Gyroid – 25%Primitive</i>	1	Σταθερό	<i>Solid network</i>

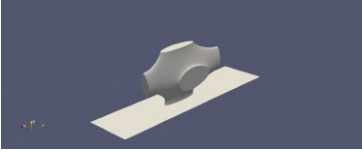
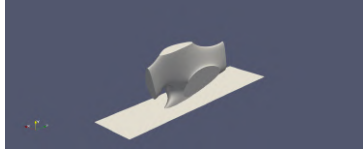
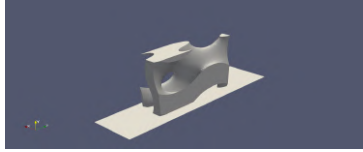
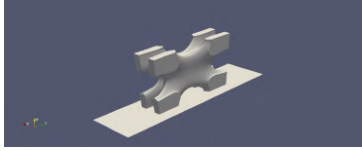
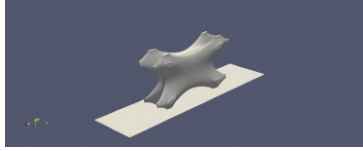
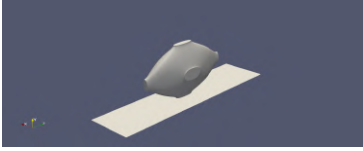
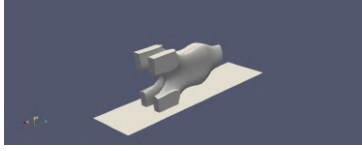
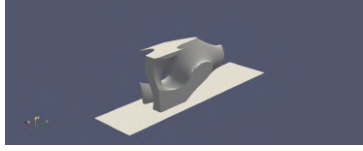
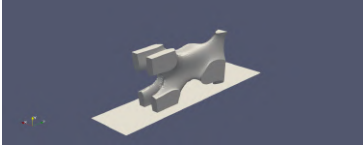
Πίνακας 4: Συγκριτικός πίνακας με γεωμετρίες *Gyroid*, *IWP*, *Primitive* και την υβριδική *75%Gyroid – 25%Primitive*.

Περίπτωση C1: Χωρίς γεωμετρία		Περίπτωση C2: Παραλληλεπίπεδο Πτερύγιο		Περίπτωση C3: Στρογγυλεμένο Πτερύγιο	
					
$w_{ολικων\ απωλειων} [-]$	0.01215	$w_{ολικων\ απωλειων} [-]$	0.1675	$w_{ολικων\ απωλειων} [-]$	0.146
$T_{εξόδου} [K]$	303.3	$T_{εξόδου} [K]$	312.57	$T_{εξόδου} [K]$	315.49
Περίπτωση T1: IWP		Περίπτωση T2: Primitive		Περίπτωση T3: Gyroid	
					
$w_{ολικων\ απωλειων} [-]$	0.17318	$w_{ολικων\ απωλειων} [-]$	0.1578	$w_{ολικων\ απωλειων} [-]$	0.1453
$T_{εξόδου} [K]$	319.78	$T_{εξόδου} [K]$	318.74	$T_{εξόδου} [K]$	314.37
Περίπτωση S1a: Διπλό Gyroid		Περίπτωση S1b: Τετραπλό Gyroid		Περίπτωση S1c: Διπλό IWP	
					
$w_{ολικων\ απωλειων} [-]$	0.2195	$w_{ολικων\ απωλειων} [-]$	0.2445	$w_{ολικων\ απωλειων} [-]$	0.2156
$T_{εξόδου} [K]$	319.78	$T_{εξόδου} [K]$	321.39	$T_{εξόδου} [K]$	320.96
Περίπτωση S1d: Τετραπλό IWP		Περίπτωση S1e: Διπλό Primitive		Περίπτωση S1f: Τετραπλό Primitive	
					
$w_{ολικων\ απωλειων} [-]$	0.2384	$w_{ολικων\ απωλειων} [-]$	0.198	$w_{ολικων\ απωλειων}$	0.2053
$T_{εξόδου} [K]$	320.96	$T_{εξόδου} [K]$	316.70	$T_{εξόδου} [K]$	316.67
Περίπτωση S2a: Gyroid αυξανόμενου πάχους		Περίπτωση S2b: Gyroid μειωμένου πάχους		Περίπτωση S2c: IWP αυξανόμενου πάχους	
					
$w_{ολικων\ απωλειων} [-]$	0.1943	$w_{ολικων\ απωλειων} [-]$	0.1907	$w_{ολικων\ απωλειων}$	0.17381
$T_{εξόδου} [K]$	320.15	$T_{εξόδου} [K]$	319.78	$T_{εξόδου} [K]$	318.92

Πίνακας 5: Συγκεντρωτικός πίνακας μέρος 1.

Περίπτωση $S2d$: IWP μειωμένου πάχους		Περίπτωση $S2e$: Primitive αυξανόμενου πάχους		Περίπτωση $S2f$: Primitive μειωμένου πάχους	
					
$\omega_{t,λοσσες} [-]$	0.17429	$w_{ολικων\ απωλειων} [-]$	0.166	$w_{ολικων\ απωλειων} [-]$	0.1541
$T_{εξόδου} [K]$	316.87	$T_{εξόδου} [K]$	315.51	$T_{εξόδου} [K]$	314.34
Περίπτωση $S3a$: Network Gyroid		Περίπτωση $S3b$: Network IWP		Περίπτωση $S3c$: Network Primitive	
					
$w_{ολικων\ απωλειων} [-]$	0.0315	$w_{ολικων\ απωλειων} [-]$	0.0412	$w_{ολικων\ απωλειων}$	0.052
$T_{εξόδου} [K]$	315.812	$T_{εξόδου} [K]$	321.63	$T_{εξόδου} [K]$	325.72
Περίπτωση $S3d$: Διπλό Network Gyroid		Περίπτωση $S3e$: Τετραπλό Network Gyroid		Περίπτωση $S3f$: Διπλό Network IWP	
					
$w_{ολικων\ απωλειων} [-]$	0.102	$w_{ολικων\ απωλειων} [-]$	0.112	$w_{ολικων\ απωλειων}$	0.0999
$T_{εξόδου} [K]$	318.48	$T_{εξόδου} [K]$	319.71	$T_{εξόδου} [K]$	317.69
Περίπτωση $S3g$: Τετραπλό Network IWP		Περίπτωση $S3h$: Διπλό Network Primitive		Περίπτωση $S3i$: Τετραπλό Network Primitive	
					
$w_{ολικων\ απωλειων} [-]$	0.1161	$w_{ολικων\ απωλειων} [-]$	0.0906	$w_{ολικων\ απωλειων}$	0.1262
$T_{εξόδου} [K]$	319.51	$T_{εξόδου} [K]$	315.65	$T_{εξόδου} [K]$	320.04
Περίπτωση $S4a$: 75%IWP – 25%Gyroid		Περίπτωση $S4b$: 50%IWP – 50%Gyroid		Περίπτωση $S4c$: 25%IWP – 75%Gyroid	
					
$w_{ολικων\ απωλειων} [-]$	0.0537	$w_{ολικων\ απωλειων} [-]$	0.0526	$w_{ολικων\ απωλειων}$	0.0543
$T_{εξόδου} [K]$	323.41	$T_{εξόδου} [K]$	323.56	$T_{εξόδου} [K]$	325.68

Πίνακας 6: Συγκεντρωτικός πίνακας μέρος 2.

Περίπτωση $S4d$: $75\%Primitive - 25\%Gyroid$		Περίπτωση $S4e$: $50\%Primitive - 50\%Gyroid$		Περίπτωση $S4f$: $25\%Primitive - 75\%Gyroid$	
					
$w_{ολιχών\ απωλειών} [-]$	0.05857	$w_{ολιχών\ απωλειών} [-]$	0.04421	$w_{ολιχών\ απωλειών} [-]$	0.04123
$T_{εξόδου} [K]$	327.53	$T_{εξόδου} [K]$	320.02	$T_{εξόδου} [K]$	318.215
Περίπτωση $S4g$: $25\%Primitive - 75\%IWP$		Περίπτωση $S4h$: $50\%Primitive - 50\%IWP$		Περίπτωση $S4i$: $75\%Primitive - 25\%IWP$	
					
$w_{ολιχών\ απωλειών} [-]$	0.0371	$w_{ολιχών\ απωλειών} [-]$	0.04411	$w_{ολιχών\ απωλειών} [-]$	0.0524
$T_{εξόδου} [K]$	316.48	$T_{εξόδου} [K]$	319.79	$T_{εξόδου} [K]$	323.19
Περίπτωση $S5a$: $IWP - Primitive$		Περίπτωση $S5b$: $Gyroid - Primitive$		Περίπτωση $S5c$: $IWP - Gyroid$	
					
$w_{ολιχών\ απωλειών} [-]$	0.0474	$w_{ολιχών\ απωλειών} [-]$	0.0537	$w_{ολιχών\ απωλειών} [-]$	0.05698
$T_{εξόδου} [K]$	320.70	$T_{εξόδου} [K]$	323.7	$T_{εξόδου} [K]$	325.15

Πίνακας 7: Συγκεντρωτικός πίνακας μέρος 3.